

**Functional and Structural Characterization of
Androgen Receptor Variant 7 (ARV7) in
Prostate Cancer**

by

Zeynep Kaya

A Dissertation Submitted to the
Graduate School of Science and Engineering
in Partial Fulfillment of the Requirements for
the Degree of

Master of Science

in

Molecular Biology and Genetics



**KOÇ
UNIVERSITY**

June 24, 2016

Functional and Structural Characterization of Androgen Receptor Variant 7 (ARV7) in Prostate Cancer

Koç University

Graduate School of Sciences and Engineering

This is to certify that I have examined this copy of a master's thesis by

Zeynep Kaya

and have found that it is complete and satisfactory in all respects,
and that any and all revisions required by the final
examining committee have been made.

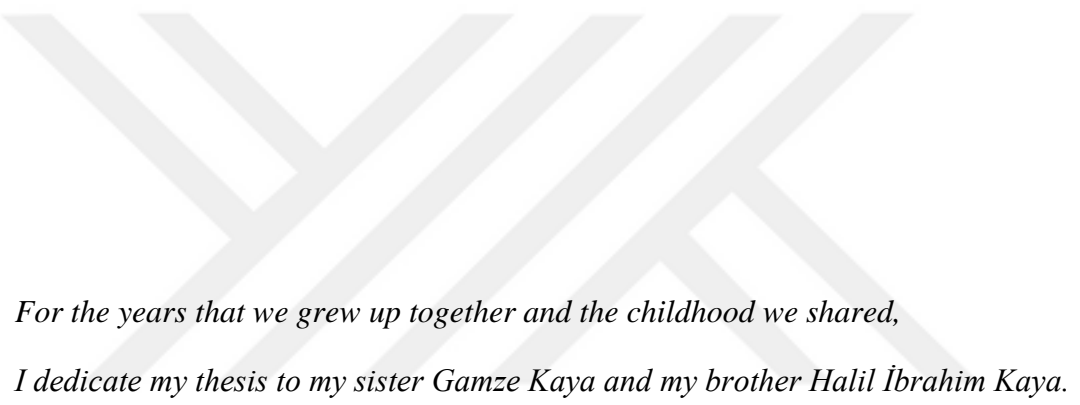
Committee Members:

Asst. Prof. NATHAN A. LACK

Asst. Prof. HALIL BAYRAKTAR

Prof. MESUT MUYAN

Date:



*For the years that we grew up together and the childhood we shared,
I dedicate my thesis to my sister Gamze Kaya and my brother Halil İbrahim Kaya.*

ABSTRACT

The androgen receptor (AR) is critical at all stages of prostate cancer. Interestingly, Androgen Receptor Variants (ARVs) have been shown to occur in late-stage prostate cancer patients by alternative splicing of the AR. Lacking a ligand binding domain (LBD) these constitutive active variants are intrinsically resistant to all clinically approved AR antagonists. Understanding the mechanism of ARV7 activation is critical to better treating late-stage prostate cancer patients.

Upon ligand binding, the AR rapidly undergoes an allosteric modification that allows the N terminal domain and LBD to form an N-C intramolecular interaction. Following nuclear localization, the AR then forms homodimers via intermolecular interactions. Given that ARV7 lack a LBD, it is unclear if the variants undergo a similar homodimerization or they in fact heterodimerize with the AR^{full-length}. To clarify this, the project aims to study ARV7 interactions using both cell biology and biophysics.

Utilizing a commonly observed variant (ARV7) and using a Tet-inducible ARV7 model in LNCaP cells we were able to study the impact of ARV7 on cell cycle progression and AR signaling. Surprisingly, in single cell clones we found that overexpression of ARV7 causes marked cellular senescence and the degree of senescence was dependent on the expression of ARV7. This was independent of AR^{full-length} and was mediated by an activation of the p53 pathway. This phenotype was also observed in several androgen responsive prostate cancer cell lines. Our results indicate that constitutive activity of ARV7 was dependent on the presence of androgen receptor and a shift from androgen receptor mediated growth to ARV7 mediated growth is not tolerated in AR dependent cells. Interestingly, we were able to identify several clones that were resistant to ARV7 expression mimicking what is clinically observed.

We also studied the predicted inter- or intramolecular interaction between ARV7 and AR^{full-length} with live cell imaging FRET microscopy. Using custom analysis software that can track and quantify the FRET signal in living cells we observed inter- and intramolecular interactions of AR^{full-length} upon stimulation with its ligand in temporal manner. Using this methodology our results suggest that AR^{full-length} and ARV7 form a C-C interaction. The experimental design we used enabled spatiotemporal identification of the interactions and revealed different conformational changes happening throughout androgen stimulation.

ÖZETÇE

Androjen reseptörü (AR) prostat kanserinin tüm aşamalarında önemlidir. İlginç bir şekilde, ileri seviye prostat kanseri hastalarında androjen reseptörünün alternative splicing (alternatif kırılma) ile androjen reseptör varyantlarının (ARVs) ortaya çıktığı gösterilmiştir. Ligand bağlama bölümü (LBD) bulunmayan bu sürekli aktif varyantları doğal olarak klinikte onaylanmış tüm androjen reseptörü antagonistlerine dirençlidir. ARV7 aktivasyon mekanizmasının anlaşılması daha geç evre prostat kanseri hastalarının tedavisi için büyük önem taşımaktadır.

Ligand bağlanması ile birlikte, androjen reseptörü N-terminal bölümü (NTD) ve ligand bağlama bölgesini molekül içi etkileşimi meydana getirecek şekilde hızlı bir yapısal değişikliğe uğramaktadır. Daha sonra AR hücre çekirdeğine geçerek burada birbirlerine bağlanır ve dimer yapılar oluştururlar. Ligand bağlama bölgesi eksikliği göz önünde bulundurulduğunda androjen reseptörü varyantlarının benzer bir şekilde homodimerize olup olmadığı ya da androjen reseptörü ile heterodimerize olup olmadığı bilinmemektedir. Bu proje hücre biyolojisi ve biyofizik kullanarak androjen reseptörü varyantlarının olası homodimerizasyon ya da androjen reseptörü ile heterodimerizasyonunu açıklığa kavuşturmayı amaçladık.

Sıkça rastlanan AR varyasyonu olan ARV7 kullanarak LNCaP hücrelerinde Tetrasiklin-indüklenebilir ARV7 modeli ile ARV7'nin hücre döngüsü ilerlemesi ve AR'nin sebep olduğu gen transkripsiyonunu üzerine etkisini inceledik. Şaşırtıcı bir şekilde, LNCaP hücre hattının dilüsyon serileri kullanılarak elde edilen tek hücre kolonilerinde ARV7 ekspresyonunun belirgin bir şekilde erken hücre yaşlanmasına neden olduğunu ve yaşlanma derecesinin ARV7 sentezlenmesine bağlı olduğunu bulduk. Ayrıca bu değişimin androjen reseptörü seviyesinden bağımsız olduğunu ve p53 yolağının aktivasyonu aracılığı ile gerçekleştiğini gözlemledik. Bu fenotipi aynı zamanda androjene duyarlı farklı prostat kanseri hücre hatlarında da gözlemledik. Sonuçlarımız ARV7'nin sürekli aktifliğinin androjen reseptörünün varlığına bağlı olduğunu ve androjene duyarlı hücrelerin AR bağımlı büyümeden ARV7 bağımlı büyümeye değişime tolere etmediğini göstermiştir. Ayrıca klinikte gözlemlenen duruma benzer olarak ARV7 ekspresyonuna dirençli olan birkaç farklı tek hücre kolonileri tespit ettik.

Aynı zamanda canlı hücre görüntüleme Förster rezonans enerji transferi (FRET) mikroskopi tekniğini kullanarak ARV7 ve AR arasında olduğu tahmin edilen moleküller arası

etkileşimlerini çalıştık. Canlı hücrelerdeki FRET sinyalini hesaplayan ve hücreleri takip eden özel analiz yazılımını kullanarak, androjen reseptörünün ligandı ile uyarılması sonucu ortaya çıkan etkileşimleri zamansal bir şekilde gözlemledik. Bu yöntemi kullanılarak elde ettiğimiz sonuçlar androjen reseptörü ve ARV7'nin etkileşimde olduğunu göstermiştir. Kullandığımız deneysel tasarım androjen uyarımı ile oluşan etkileşimleri, zaman mekânsal bir şekilde tespit etmeyi ve farklı yapısal değişiklikleri gözlemlemeyi sağlamıştır.



ACKNOWLEDGEMENTS

Firstly, I would like to express my sincere gratitude to my advisor Asst. Prof. Nathan A. Lack for the continuous support of my MSc study and related research, for his patience, motivation, and guidance. His guidance helped me in all the time of research and writing of this thesis. He set an example of perfection to me as an advisor and lab-manager, and I will carry the traits I learned from him with me, all the way through my academic career.

Besides my advisor, I would like to thank the rest of my thesis committee for their time and insightful comments. I separately thank to Prof. Dr. Mesut Muyan for coming and representing my previous school METU, which I will always be connected to. I would like to thank to Asst. Prof. Dr. Halil Bayraktar together with my advisor for showing me a good example of collaboration.

I am thankful to Dr. Tuğba Bağcı Önder and Dr. Tamer Önder for being available whenever I knock their doors and for all the ideas, guidance, and both academic and personal support.

I thank sincerely and wholeheartedly Başak Kale for the support, advice and general guidance she has given to me for my PhD.

I thank Koç University and Foundation for providing me this productive scientific environment and research facilities and GSHS and GSSE office members for their assistance in all paperwork.

I would like to thank all the people, whom I benefit from and contributed to; I learned a lot from the work we performed together. I would like to thank past and present Lack Lab members for our early morning meetings, sleepless nights we were working together before deadlines, and for all the fun we have had in the last three years. I thank undergraduate students especially Abdullah Salih Budan and Elif Demirtaş who have worked with me and contributed to this research for their interest and enthusiasm. I also thank to Selen Manioğlu for all the experiments we did together and image analyses she did, and to Mohammad Haroon Qureshi for supporting each other's research and for being peaceful while arranging the bookings for the microscope.

In the past three years, many friends have contributed to color my life. I have to acknowledge all my colleagues in Koç University School of Medicine. I would like to thank to Fatma Özgün and Fidan Şeker for sharing the home and life with me. I would also like to thank Gülben Gürhan for being as sincere as Kadıköy and Ayyub Ebrahimi for all the songs we have sing together while doing experiments right next to each other.

I would like to thank Can Aztekin for simply enjoying my company. I feel like my worldline have changed with a significant destination with his presence and my master's degree has become more memorable with all the fruitful scientific discussions and simple daily conversations we had and all the steps and obstacles we overcome together. Separately, I thank him for always being honest and telling me the truth. So long and thanks for all the fish!

I am very grateful to Naile Kahya who knows and understands all the past and up-to-date details in my life (except the content of this thesis) for her presence in my life both in Ankara and in İstanbul since we met and having done everything together since then. Thank you for being there through good times and bad, for always making time for me and for the invaluable friendship. I look forward to sharing many more of life's lovely moments with you.

My deepest gratitude goes to my parents, Lütfiye Kaya and Mehmet Kaya for raising me up the way I am and for unconditional support and encouragement to pursue my interests, even when the interests went beyond boundaries of field and geography; my sister and first friend Gamze Kaya for listening to my complaints and frustrations, and for believing in me; and my brother Halil İbrahim Kaya, for talking to me like a big brother and supporting me. This accomplishment would not have been possible without them. Thank you.

TABLE OF CONTENTS

ABSTRACT	iv
ÖZETÇE	v
ACKNOWLEDGEMENTS	vii
TABLE OF CONTENTS	viii
LIST OF TABLES	xi
TABLE OF FIGURES	xii
NOMENCLATURE	xvi
Chapter 1: Introduction	1
1.1 Overview	1
1.1.1 Androgen Receptor.....	1
1.1.2 Androgens and the Androgen Receptor in Normal Prostate	3
1.1.3 Castration Resistant Prostate Cancer	5
1.1.4 Mechanisms of castrate resistance.....	5
1.1.5 Androgen Receptor Variants	6
1.1.6 Androgen Receptor Variant 7 (AR3)	8
1.2 Cellular senescence	9
1.2.1 Features that define senescent cells.....	10
1.2.2 Common stimuli in cells leading to cellular senescence	10
1.2.2.1 Stress induced senescence	11
1.2.2.2 Oncogene driven cellular senescence	11
1.2.2.3 DNA damage	11
1.2.2.4 Misregulation of CDKN2A locus.....	12
1.2.3 Senescence in prostate cancer	12
1.3 Aims of this work	13
Chapter 2: Materials and methods	14
2.1 Materials	14
2.1.1 Chemicals and reagents	14
2.1.2 Bacterial strains and cell lines	14
2.1.3 Bacterial growth media	14
2.1.4 Plasmids	15
2.1.4.1 Plasmids used for Functional Characterization of ARV7	15
2.1.4.1.1 TetO-FUW-EGFP	15
2.1.4.1.2 pLIX 402	16
2.1.4.1.3 pLIX_402-ARV7 plasmid	17
2.1.4.2 Plasmids used for structural interactions of ARV7	18
2.1.4.2.1 Plasmids used in FRET experiments.....	18
2.1.4.2.2 Plasmids used in Mammalian Two-Hybrid System (MTHS)	23
2.1.5 Primers	26
2.1.6 Antibodies	30

2.2	Methods	31
2.2.1	Bacterial growth	31
2.2.1.1	Culture conditions of E. coli.....	31
2.2.1.2	Antibiotics used and their concentration	31
2.2.1.3	Production and storage of bacterial glycerol stocks	31
2.2.2	Molecular biology	31
2.2.2.1	Sequences	31
2.2.2.2	Polymerase chain reaction.....	31
2.2.2.3	DNA isolation.....	32
2.2.2.4	Quantification of DNA concentration	33
2.2.2.5	Agarose gel electrophoresis.....	33
2.2.2.6	Restriction endonucleases	33
2.2.2.7	Cloning procedures.....	33
2.2.2.7.1	Cloning using PCR products	33
2.2.2.7.2	Subcloning.....	34
2.2.2.7.3	Oligonucleotide cloning	34
2.2.2.7.4	Gateway cloning with LR reaction.....	34
2.2.2.7.5	Site-directed mutagenesis.....	34
2.2.2.7.6	TOPO-TA Cloning.....	35
2.2.2.8	Heat shock transformation.....	35
2.2.3	Protein characterization.....	35
2.2.3.1	SDS-PAGE	35
2.2.3.2	Western Blots	35
2.2.4	Cell culture	36
2.2.4.1	Culture conditions	36
2.2.4.2	Production of lentiviruses.....	36
2.2.4.3	Stable transduction of the cells.....	37
2.2.4.4	Determination of viral packaging efficiency	37
2.2.4.5	Transient transfection of the cells.....	38
2.2.4.6	Single cell generations.....	38
2.2.4.7	Live cell imaging experiment for cell proliferation.....	38
2.2.4.8	X-gal staining	38
2.2.4.9	Cell cycle analysis using BD-Accuri-Flow Cytometer	39
2.2.4.10	Luciferase Assay	39
2.2.4.11	qRT-PCR	39
2.2.4.12	Cell viability assay (MTS).....	39
2.2.5	FRET experiments.....	40
2.2.5.1	Ratiometric FRET using live cell imaging	40
2.2.5.2	Acceptor Photobleaching FRET	41
Chapter 3:	Functional Characterization of Androgen Receptor Variant ARV7	43
3.1	Introduction	43
3.2	Results.....	44
3.1.1	Generation of inducible ARV7 expressing LNCaP cell lines using TetO-FUW backbone	44
3.2.1.1	Cloning of ARV7 gene into TetO-FUW plasmid.....	44
3.2.1.2	Lentiviral Packaging of TetO-FUW-ARV7	44
3.2.1.3	Transduction of LNCaP cells	45
3.2.2	Generation of inducible ARV7 expressing LNCaP cell lines using pLIX_402 backbone	47
3.2.2.1	Cloning of ARV7 into pLIX_402 backbone	47
3.2.2.2	Transduction of wtLNCaP cells with pLIX_402-ARV7 lentiviruses.....	48
3.2.2.3	Single cell clones of ARV7	49
3.2.2.4	Live cell imaging of the change in morphology of SCC7	51
3.2.2.5	Autophagy marker in SCC7 cells	52
3.2.2.6	EMT markers in ARV7 expressing LNCaP cells.....	53

3.2.2.7	Unfolded protein response genes in ARV7 expressing cells.....	54
3.2.2.8	ARV7 expression and cellular senescence	55
3.2.2.9	G ₀ /G ₁ arrest at cell cycle is permanent	58
3.2.2.10	Senescence is not due to decrease in expression of AR ^{full-length}	60
3.2.2.11	Activation of tumor suppressor networks in ARV7 expressing LNCaP cells	62
3.2.2.12	Assessment of DNA Double-Strand-Breaks (DSB) in ARV7 expressing cells	63
3.2.2.13	Generation of DNA Binding Mutant of pLIX402 ARV7.....	66
3.2.2.14	Generation of ARV7-DBD expressing single cells of LNCaP cells.	67
3.2.2.15	Testing ARV7 resistant single cell clones	68
3.2.3	Characterization of effect of ARV7 on other prostate cancer cell lines	71
3.2.3.1	ARV7 expression in PC3 cells	72
3.2.3.2	ARV7 expression in RWPE1 cells	73
3.2.3.3	ARV7 expression in BPH1 cells	74
3.2.3.4	ARV7 expression in LNAI cells.....	75
3.2.3.5	ARV7 expression in 22RV1 cells.....	76
3.2.3.6	ARV7 expression in LNCaP-Abl cells.....	77
3.3	Discussion.....	79
Chapter 4: Structural Interaction of Androgen Receptor and Androgen Receptor Variant ARV7..... 82		
4.1	Introduction	82
4.2	Results.....	83
4.2.1	Cloning of AR ^{full-length} and ARV7 fusion constructs with Cerulean and Venus FRET pair ..	83
4.2.1.1	Cloning of Cerulean-AR-Venus and Cerulean-ARV7-Venus.....	83
4.2.2	Cloning of constructs for studying intermolecular interactions among AR and ARV7	83
4.2.3	Expression of FRET constructs in 293T cells	84
4.2.4	Measuring FRET intensity using live cell- imaging microscopy	86
4.2.5	Measurement of intramolecular and intermolecular AR ^{full-length}	86
4.2.6	Intermolecular Interactions of Androgen Receptor	90
4.2.6.1	Transfection of the constructs in different ratios.....	91
4.2.6.2	Changing linker size in FRET constructs	92
4.2.6.3	Changing the linker composition in the fusion proteins.....	94
4.2.7	Androgen Receptor intermolecular and intramolecular interactions using Acceptor Photobleaching	95
4.2.8	Studying interactions of AR and ARV7 using CFP-YFP as FRET pair	97
4.2.9	Transcriptional activity of FRET constructs	98
4.2.9.1	Intermolecular interactions of AR ^{full-length} using YFP-AR-CFP fusion protein.....	99
4.2.9.2	The interactions of DNA-binding domain mutated AR	100
4.2.9.3	The interactions of AR ^{full-length} and ARV7	101
4.2.10	Testing AR and ARV7 interactions using mammalian two hybrid system.....	103
4.3	Discussion.....	105
Chapter 5: Conclusions and Future Work 109		
5.1	Final Conclusions	109
5.2	Future work	111
Chapter 6: Bibliography 113		

LIST OF TABLES

Table 1: <i>E. coli</i> strains used for maintenance and cloning of all plasmids.	14
Table 2: Media used for growth of bacteria in this study.	14
Table 3: Oligonucleotides used for sequencing of FRET constructs.	26
Table 4: Oligonucleotides used for generation of constructs.	27
Table 5: Primers used to clone ARV7 into TetO-FUW plasmids.	27
Table 6: Oligonucleotides used in site-directed mutagenesis and oligonucleotide clonings.	28
Table 7: Primers used for qRT-PCR.	29
Table 8: Antibodies used throughout this work.	30
Table 9: Concentration of commonly used antibiotics.	31
Table 10: Thermocycling conditions for Phusion DNA polymerase.	32
Table 11: Thermocycling conditions for Taq DNA polymerase.	32
Table 12: PCR conditions for site directed mutagenesis of ARV7.	32
Table 13: Fluorescence channels used in ratiometric FRET experiments.	40
Table 14: Transduction of LNCaP cells with TetO-FUW plasmids and rTTA.	45
Table 15: Properties of common prostate cancer cell lines used in this study.	71

TABLE OF FIGURES

Figure 1-1: Genomic organization of the androgen receptor gene.	1
Figure 1-2: mRNA structure of AR ^{full-length} .	1
Figure 1-3: Crystal structure of <i>Rattus norvegicus</i> AR DBD bound to a direct repeat response element.	2
Figure 1-4: Crystal structure of Androgen Receptor LBD in complex with DHT.	3
Figure 1-5: Schematic representation of the spatiotemporal organization of domain interactions in AR function.	4
Figure 1-6: Alternatively spliced AR-Vs in prostate cancer.	7
Figure 2-1: TetO-FUW-EGFP plasmid map.	15
Figure 2-2: pLIX_402 plasmid map.	16
Figure 2-3: pLIX_402-ARV7 plasmid map.	17
Figure 2-4: pC17V plasmid map.	18
Figure 2-5: mCerulean N1 plasmid map.	19
Figure 2-6: mCerulean C1 plasmid map.	20
Figure 2-7: mVenus N1 plasmid map.	21
Figure 2-8: mVenus C1 plasmid map.	22
Figure 2-9: pACT plasmid map.	23
Figure 2-10: pBIND plasmid map.	24
Figure 2-11: pG5luc plasmid map.	25
Figure 2-12: GFP expression in 293 T cells transduced with different amount of CMV-EGFP virus.	37
Figure 3-1: Cloning strategy used to generate TetO-FUW-ARV7.	44
Figure 3-2: Outline for lentiviral packaging.	45
Figure 3-3: LNCaP cells transduced with TetO-FUW-eGFP and rTTA viruses.	46
Figure 3-4: Single cell clones of TetO-FUW-ARV7.	46
Figure 3-5: Tet-On system summary.	47
Figure 3-6: ARV7 expression in LNCaP cells transduced with pLIX_402-ARV7.	48
Figure 3-7: PSA levels in wtLNCaP and ARV7 expressing LNCaP cells with change in Dox.	48
Figure 3-8: ARV7 expressing single cell clones of LNCaP cells.	49
Figure 3-9: Quantification of the levels of AR ^{full-length} and ARV7 in single cell clones.	50

Figure 3-10: ARV7 expression in SSC7.	50
Figure 3-11: Live cell imaging of morphology of SCC7 cells.	51
Figure 3-12: Autophagy marker in doxycycline-treated wtLNCaP and SCC7.	52
Figure 3-13: Epithelial-mesenchymal transition (EMT) gene expression in doxycycline-treated wtLNCaP and SCC7 cells.	53
Figure 3-14: ER stress markers with UPR inducing chemicals.	54
Figure 3-15: ER stress markers in doxycycline treated wtLNCaP and SCC7 cells.	55
Figure 3-16: Senescence-associated β -galactosidase staining in ARV7 expressing LNCaP cells.	56
Figure 3-17: Quantification of proliferative and senescent cells.	56
Figure 3-18: Cell cycle distribution of ARV7 expressing LNCaP cells.	57
Figure 3-19: Cell viability in ARV7 expressing LNCaP cells.	57
Figure 3-20: ARV7 expression correlates to percentage of senescent cells.	58
Figure 3-21: Recovery of AR and ARV7 protein levels after Dox removal.	59
Figure 3-22: SA β -gal staining in SCC7 after Dox removal.	59
Figure 3-23: Viability of wtLNCaP and SCC7 cells after dox removal.	60
Figure 3-24: Protein levels of AR ^{full-length} and ARV7 after co-transduction of Tet-on AR & Tet-on ARV7.	60
Figure 3-25: mRNA quantification of AR and ARV7 levels with RT-PCR in wtLNCaP, SCC7 and SCC7 cells expressing inducible AR ^{full-length} .	61
Figure 3-26: Viability of treated cells measured by the MTS assay.	61
Figure 3-27: Cell cycle distribution of AR recovered cells.	61
Figure 3-28: mRNA expression levels of tumor suppressors in wtLNCaP and SCC7 cells with Dox and DHT treatment.	62
Figure 3-29: mRNA expression levels of genes controlling G ₁ /S transition.	62
Figure 3-30: The levels of phosphorylated Rb protein upon ARV7 expression.	63
Figure 3-31: DNA double-strand break (DSB) foci detected via H2AX/53BP1 co-staining.	64
Figure 3-32: DNA double-strand break (DSB) foci detected via H2AX/53BP1 co-staining.	65
Figure 3-33: AR and ARV7 expression in transduced 293T cells.	66
Figure 3-34: Transcriptional activity of pLIX constructs shown by luciferase assay.	67
Figure 3-35: ARV7 and ARV7-DBD expression in LNCaP cells.	67
Figure 3-36: Single cell clones of ARV7-DBD expressing LNCaP cells.	68
Figure 3-37: Cell viability (A) and SA- β -gal staining (B).	68
Figure 3-38: Characterization of SCC22 and SCC23.	69

Figure 3-39: Protein levels of AR and ARV7 in transduced PC3 cells.	72
Figure 3-40: Viability of PC3 cells that express ARV7 upon Doxycycline treatment.	72
Figure 3-41: The percentage of senescent cells in PC3 cells.	72
Figure 3-42: Protein levels of AR and ARV7 in transduced RWPE1 cells.	73
Figure 3-43: Viability of RWPE cells that express ARV7 upon Doxycycline treatment.	73
Figure 3-44: The percentage of senescent cells in RWPE1 cells.	73
Figure 3-45: Protein levels of AR and ARV7 in transduced BPH1 cells.	74
Figure 3-46: Viability of BPH1 cells that express ARV7 upon Doxycycline treatment.	74
Figure 3-47: The percentage of senescent cells in BPH1 cells.	74
Figure 3-48: Protein levels of AR and ARV7 in transduced LNAI cells.	75
Figure 3-49: Viability of LNAI cells that express ARV7 upon Doxycycline treatment.	75
Figure 3-50: The percentage of senescent cells in LNAI cells.	75
Figure 3-51: Protein levels of AR and ARV7 in transduced 22RV1 cells.	76
Figure 3-52: Viability of 22RV1 cells that express ARV7 upon Doxycycline treatment.	76
Figure 3-53: The percentage of senescent cells in 22RV1 cells.	76
Figure 3-54: Protein levels of AR and ARV7 in transduced LNCaP-Abl cells.	77
Figure 3-55: Viability of LNCaP-Abl cells that express ARV7 upon Doxycycline treatment.	77
Figure 3-56: The percentage of senescent cells in LNCaP-Abl cells.	77
Figure 4-1: Cerulean and Venus fusion proteins used in this project.	82
Figure 4-2: Expression of FRET constructs in 293T cells.	84
Figure 4-3: Transcriptional activity of Venus fusion constructs.	85
Figure 4-4: Transcriptional activity of Cerulean constructs.	85
Figure 4-5: 293T cells transfected with pC17V plasmid.	86
Figure 4-6: Single cell tracking steps of Cer-AR-Ven interaction.	88
Figure 4-7: AR dimerization and NTD-to-LBD intramolecular interactions by FRET microscopy.	89
Figure 4-8: FRET analysis of Cerulean-AR-Venus constructs in 6 h.	89
Figure 4-9: Intermolecular interactions of AR.	90
Figure 4-10: The correlation between donor and acceptor intensities in different transfection ratios.	92
Figure 4-11: Linker size between fluorescence protein in Cerulean and Venus fusion proteins.	92
Figure 4-12: Expression of all AR constructs.	93

Figure 4-13: Expression level in the construct with shortened linker.	93
Figure 4-14: The linker composition in the constructs used in acceptor photobleaching FRET.	94
Figure 4-15: Expression of AR constructs with 6(GA) repeats.	94
Figure 4-16: AR and ARV7 constructs with 6(GA) linker.	95
Figure 4-17: AR and ARV7 interactions using acceptor photobleaching.	95
Figure 4-18: Temporary bleaching of Cerulean in acceptor photobleaching.	96
Figure 4-19: The effect of zooming on relative intensity of CFP.	96
Figure 4-20: Expression of ARV7-CFP and YFP-ARV7 constructs.	97
Figure 4-21: Transcriptional activity of constructs with equal expression.	98
Figure 4-22: Interactions of Androgen Receptor shown by FRET.	99
Figure 4-23: The NFRET histograms of C17V, YFP-AR-CFP, YFP-AR(DBD-mutant)-CFP.	100
Figure 4-24: The NFRET histograms of intermolecular AR ^{full-length} interactions.	102
Figure 4-25: The NFRET histograms of interactions of AR ^{full-length} and ARV7.	103
Figure 4-26: Interactions of AR and ARV7 studied by mammalian two hybrid system.	104

NOMENCLATURE

AR	Androgen Receptor
ADT	Androgen Deprivation Therapy
AREs	Androgen Response Elements
ARVs	Androgen Receptor Variants
CDK	The Cyclin-Dependent Kinase
CRPC	Castrate-Resistant Prostate Cancer
DBD	DNA-Binding Domain
DHT	Dihydrotestosterone
DSB	Double-Strand-Breaks
EMCCD	Electron Multiplying Charge Coupled Device
EMT	Epithelial-Mesenchymal Transition
FRET	Förster Resonance Energy Transfer
GnRH	Gonadotropin-Releasing Hormone
IGF1	Insulin-Like Growth Factor 1
LBD	Ligand Binding Domain
LH	Luteinizing Hormone
MTHS	Mammalian Two-Hybrid System
NFRET	Normalized FRET
NTD	N-Terminal Domain
ORF	Open Reading Frame
SA β -gal	Senescence Associated β -Galactosidase
SAHF	Senescence Associated Heterochromatic Foci
SASP	Senescence-Associated Secretory Phenotype
SCC	Single Cell Clone
SHBG	Sex Hormone-Binding Globulin
Skp2	S-Phase Kinase-Associated Protein 2
TGF β	Transforming Growth Factor-B
TRE	Tet Response Element
UPR	Unfolded Protein Response

Chapter 1: Introduction

1.1 Overview

1.1.1 Androgen Receptor

The androgen receptor (AR) is a steroid-hormone activated transcription factor, which plays a critical role in male sexual differentiation and the growth and survival of prostate tissue under both normal and cancer conditions [1]. The gene encoding AR is located on the X chromosome (q11-12) (**Figure 1-1**), and consists of eight exons which code for a protein made up of 919 amino acids with a mass of 110 kDa (**Figure 1-2**) [2]. The gene spans >80 kb region and the mature transcript spanning 1-8 exons (10.6 kb) yields 2.7 kb open reading frame (ORF).

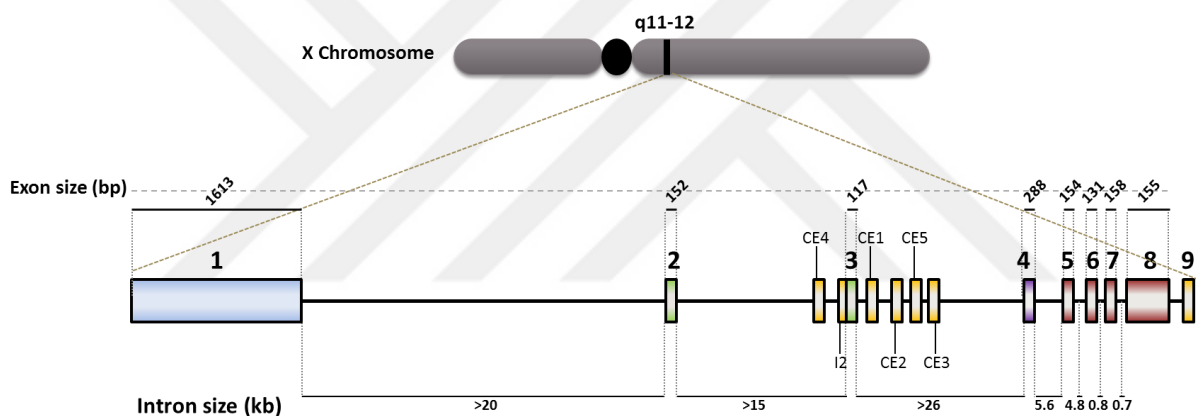


Figure 1-1: Genomic organization of the androgen receptor gene. Figure adapted from [1, 3].

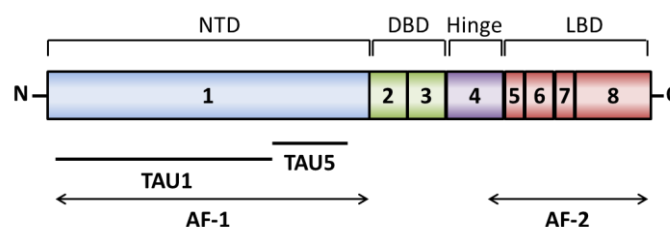


Figure 1-2: mRNA structure of AR^{full-length}.

The diagram of the mature mRNA indicating the organization of the exons in the AR^{full-length}. The discrete functional regions are indicated N-terminal domain (NTD) (blue), DNA-binding domain (DBD) (green), hinge region (purple) and ligand binding domain (LBD) (red). Figure adapted from [3].

Similar to other nuclear receptors including estrogen receptor and progesterone receptor, AR has a modular structure comprised of a DNA-binding domain (DBD), ligand-binding domain (LBD), and the amino-terminal domain (NTD) (**Figure 1-2**) [4]. Exon 1 of the AR encodes the N-terminal domain. This is the largest domain, constituting more than half of the receptor. The N-terminal domain contains (CAG) and (GGN) repeats that encode polyglutamine (Q) and polyglycine (G) tracts, respectively [5, 6]. The NTD is primarily responsible for transactivation of androgen receptor via TAU1 and TAU5 [7, 8]. The second and third exons of androgen receptor gene encode for a highly conserved DNA binding domain (DBD) (**Figure 1-3**). Located at the center of AR it contains two zinc-finger motifs. The first zinc-finger recognizes DNA and interacts with the major groove residues of androgen response elements, while the second one mediates dimerization of AR in the neighboring AREs [9].

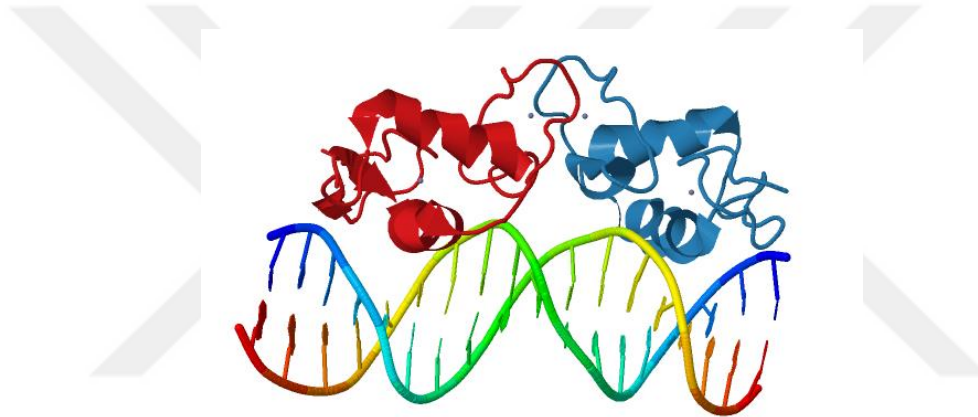


Figure 1-3: Crystal structure of *Rattus norvegicus* AR DBD bound to a direct repeat response element.

The sequence alignment of androgen receptor DNA-binding domain of *Rattus norvegicus* to *Homo sapiens* is 100% homologous [10].

A short flexible hinge region encoded by the fourth exon of AR gene connects the DBD and ligand binding domain (LBD) [2]. The nuclear localization signal of AR is a bipartite motif within exons 3 and 4 [11]. The LBD of the AR is encoded by exon 5-8 and mediates the regulation of activation by androgens. The structure of LBD has been crystallographically solved and was found to contain 12 helices (**Figure 1-4**) [12]. Helices 3, 4, 5, 7, 11, 12 and β -sheet preceding helix 6 form the ligand binding pocket.

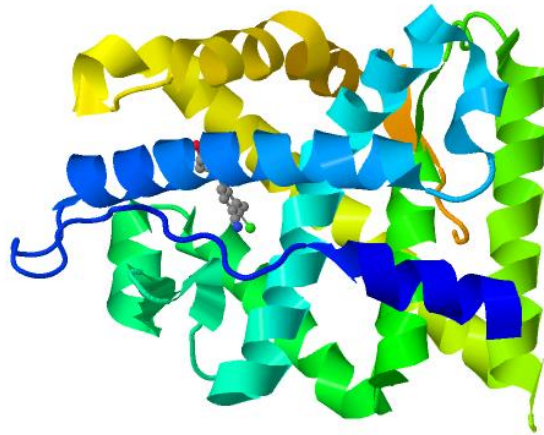


Figure 1-4: Crystal structure of Androgen Receptor LBD in complex with DHT. Crystal structure of Androgen Receptor in complex with DHT (*Homo sapiens*). The structure was determined by X-ray diffraction to a resolution of 2.1 Å [13].

1.1.2 Androgens and the Androgen Receptor in Normal Prostate

The normal growth and development of the human prostate is dependent on androgen-mediated activation. Androgen production is controlled by the hypothalamic–pituitary–gonadal axis. The secretion of gonadotropin-releasing hormone (GnRH) from the hypothalamus occurs in 90–120 minutes and stimulates the luteinizing hormone (LH) from the pituitary gland. LH binds to the luteinizing hormone/choriogonadotropin receptor leading to the production of androgen in the testis [14]. Testosterone is the primary circulating androgen in men. While the major source of circulating testosterone is the Leydig cells in the testis, a small portion (5%) is secreted from adrenal gland. Whichever the source, the gamma-5 metabolic pathway is the main pathway for androgen production [15]. Circulating testosterone is typically bound by sex hormone-binding globulin (SHBG) thereby regulating the amount of free testosterone available to target tissues. Once entered into the cells, testosterone is usually converted to DHT by 5 α -reductase [16]. Both testosterone and DHT can bind to AR, though the latter has higher affinity for AR [17]. Upon binding to DHT the AR is activated and it binds to coactivators to control the expression of genes related to growth and development of prostate [14, 18].

The inactive AR is found in cytoplasm bound to heat-shock proteins [19, 20]. In this state, AR does not interact with coactivators and thus cannot induce gene transcription. When an androgen binds to the ligand binding site in the LDB the AR undergoes a conformation change whereby helix 12 is folded over the pocket exposing the AF2 site [21]. This allows the NTD to form an N-C intramolecular interaction via an FxxLF/WxxLF motif on TAU5 [22].

This N/C interaction is critical for both stabilizing the androgen in the ligand binding pocket and also exposing the bipartite nuclear localization signal which is located downstream of DNA binding domain and hinge region [23]. The conformational change in AR that happens upon binding of androgens has been extensively studied using quantitative imaging techniques. Studies found that ligand binding causes an initial cytoplasmic intramolecular interaction between N and C terminus in the androgen receptor which is followed by nuclear localization of the receptor. Once in the nucleus the AR dimerizes via D-box residues, forming a head-to-tail interaction that supports the interaction between two androgen receptors [24]. The formed homodimers then bind to androgen response elements (AREs) in promoter and enhancer elements of target genes and initiates transcriptional regulation [9, 25, 26].

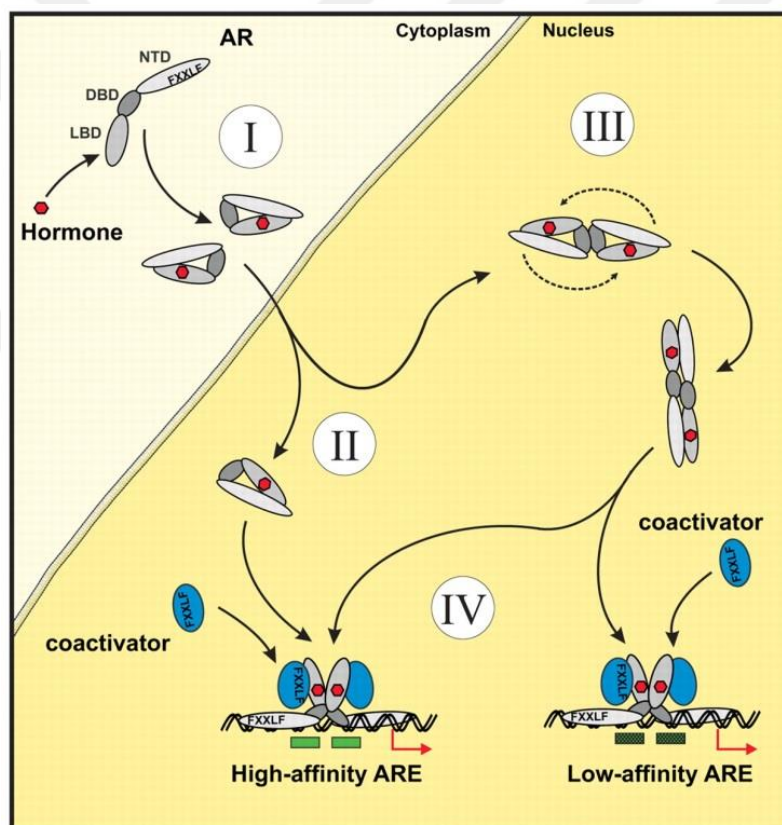


Figure 1-5: Schematic representation of the spatiotemporal organization of domain interactions in AR function. Figure from [24].

1.1.3 Castration Resistant Prostate Cancer

As the prostate is an AR-dependent tissue, prostate cancer cells continue to show dependence on both androgen and AR following neoplastic transformation [27]. In almost all patients the growth and progression of prostate cancer is dependent on AR signaling [28]. The AR has been widely studied for its oncogenic role including support of proliferation and inhibition of apoptosis in tumor cells [29–32]. As the normal development and growth of prostate tissue depends on functional androgen receptor signaling, androgen deprivation therapy (ADT) is the first line therapy for the prostate cancer patients with locally advanced and metastatic types of the disease [33, 34]. ADT includes surgical castration (orchiectomy), pharmacologic castration, or treatment with chemicals that bind to androgen receptor and inhibit its nuclear localization are different ways of ADT [27]. Although ADT initially slows the progression of the disease, the cancer almost always relapses, progressing to an advanced state called castrate-resistant prostate cancer (CRPC). This is the major cause of PCa death with CRPC patients having a median survival of 13.6 months [35, 36]. The progression of the disease from a treatable, androgen-dependent state to a lethal, castration-resistant form is focus of intense investigation [37].

1.1.4 Mechanisms of castrate resistance

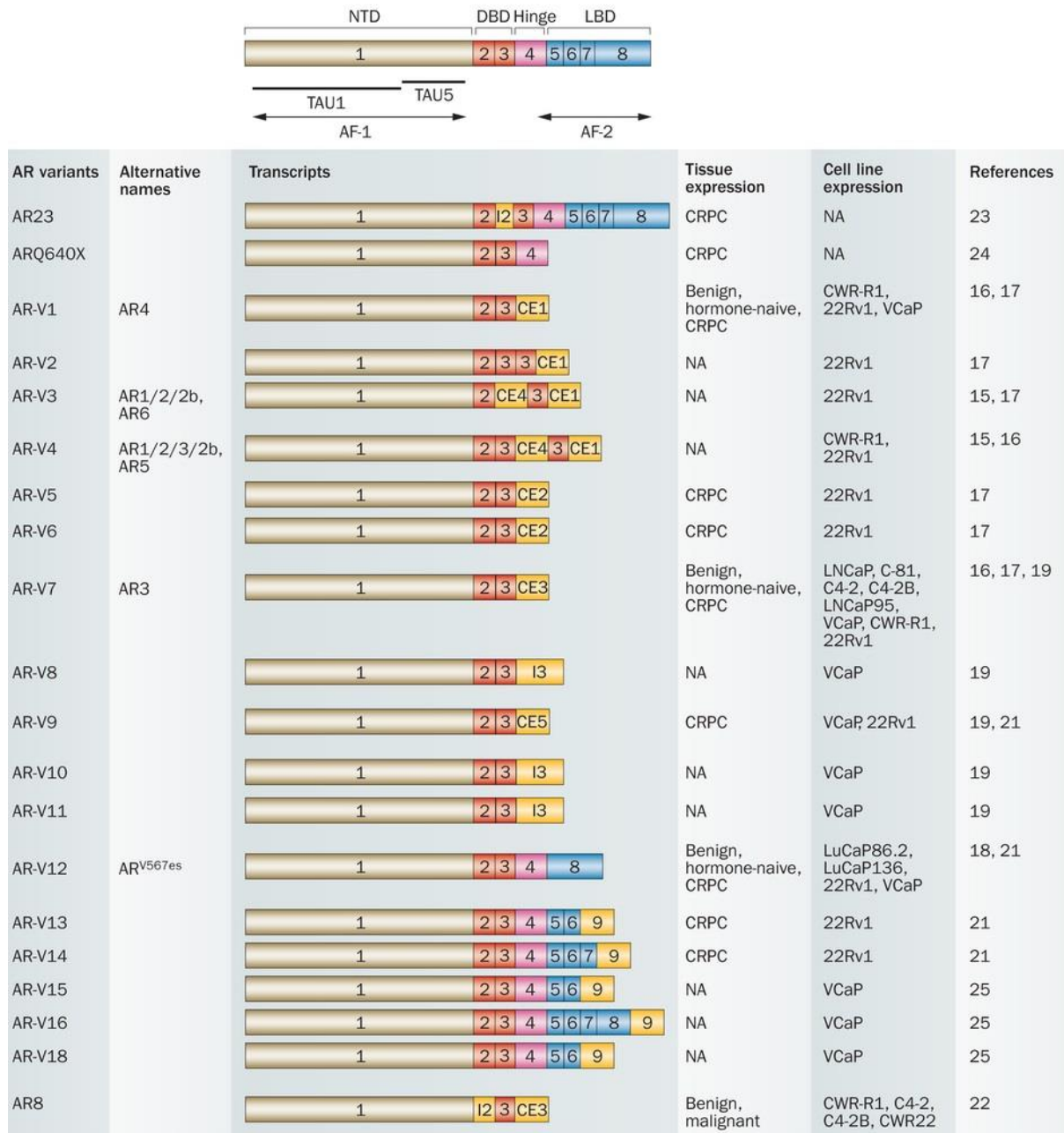
Interestingly, despite castrate levels of androgen, the AR still remains active in CRPC [38]. There are several proposed mechanisms of AR activation under castrate conditions. First, the cancer can synthesize intratumoral androgens to allow AR signaling even in the castrate levels of androgens [39]. It has been previously shown that the level of testosterone in prostate tumor is close to the level of testosterone in non-castrate patients [40]. Androgen synthesis in the prostate cancer cells is due to an increase in the enzymes involved in the synthesis of testosterone [41, 42]. More commonly, increased AR copy number can cause androgen receptor signaling at very low levels of androgen [43, 44]. Third, mutations on androgen receptor can lead to activation of AR by non-androgenic but common steroids [45]. Mutations of the LBD of the androgen receptor can result in decreased specificity of the receptor for binding to androgen [46–49]. Alternatively, mutations on the LBD, specifically in the antiandrogen binding sites may prevent the antiandrogen activity and actually cause the antiandrogen to act as an agonist [50–52]. Further, the activity of androgen receptor can increase in CRPC due to alternative activation of such pathways as tyrosine-kinase receptor activation, Wnt- β -catenin signaling, epithelial growth factor and insulin-like growth factor signaling [53–59]. Another proposed mechanism for castrate resistance is the increased

activity of coactivators of androgen receptor [60]. The increased expression or increased phosphorylation of coactivators of androgen receptor were previously shown to increase androgen receptor transcriptional activity [61, 62]. Moreover, epigenetic alterations are also proposed to be important for androgen independent growth in castration resistant prostate cancer. For example, (EZH2) which is subunit of Polycomb repressive complex 2 (PRC2) has been shown to have oncogenic activity in supporting androgen independent growth [63]. Finally, the presence of constitutively active isoforms of androgen receptor have been suggested to be important in CRPC progression [64].

1.1.5 Androgen Receptor Variants

In several studies involving AR, a lower molecular weight form of the AR in addition to wild type AR (110 kDa) has been detected by antibodies against N-terminal region [65]. The first evidence for these variants found in the 22RV1 cell line [66]. A similar variant has been reported in the western blot of the samples collected from benign and malignant prostate tissue, demonstrating that these variants are present in clinical samples [67]. Although it was previously unclear whether the isoforms are functionally important in prostate cancer, later studies demonstrated that these C-terminally truncated variants are constitutively active. Further characterization revealed that these variants had N-terminal domain and DNA binding domain, but not ligand binding domain and it was constitutively found in nucleus where it can bind to DNA independent of presence of androgens (**Figure 1-6**). These variants lack ligand binding domain and thus, their activation does not depend on binding of the androgen. Importantly, they cannot be inhibited by any clinically approved antiandrogens.

These AR variants were proposed to occur due the following: (i) alternative splicing, (ii) alternative transcription start site, (iii) occurrence of premature stop codon, and (iv) proteolytic cleavage [67–72]. Evidence for the alternative splicing came from siRNA studies where different siRNAs depleted different isoforms in 22RV1 cells [70]. In this study, siRNA targeting NTD of AR resulted in disappearance of all isoforms while targeting ligand binding domain only decreased the full length AR but not the truncated isoform.



Nature Reviews | Urology

Figure 1-6: Alternatively spliced AR-Vs in prostate cancer.

The structure of mRNA structure of AR^{full-length} is depicted at top. The exons encoding the domains are color coded: NTD (brown) DNA-binding domain (red), hinge region (pink) and ligand binding domain (blue). Alternatively spliced isoforms of androgen receptor are shown at bottom. Cryptic exons present in these are colored in yellow. (AF, activation function; AR, androgen receptor; AR-FL, full-length androgen receptor; AR-V, androgen receptor variant; CE, cryptic exon; CRPC, castration-resistant prostate cancer; DBD, DNA-binding domain; I, intron; LBD, ligand-binding domain; NTD, N-terminal domain; TAU, transcription activation unit.) Figure was taken from [73].

Numerous AR variants have been identified by 3' rapid amplification of cDNA ends technique. These alternatively spliced isoforms are emerging from cryptic exons present in exon 2 and exon 3 of the androgen receptor (**Figure 1-6**). Most of them have exons 1, 2, and 3 which encode NTD and DBD, some has exon 4 which encodes hinge region, but they usually lack exons 5, 6, 7 encoding the ligand binding domain.

Among these, AR isoform AR^{1/2/2b} and AR^{1/2/3/2b} were the isoforms identified in 22RV1 cells isolated from a CWR22 xenograft that relapsed during androgen ablation [70]. Therefore, these isoforms have the exon 1, 2, and cryptic exon 2b; while the latter one had also exon 3 in the mature mRNA transcript. They are C-terminally truncated and mediate androgen-independent transcriptional activation of AR target genes including PSA, TMPRSS2. Three other isoforms named as AR3, AR4 and AR5, have been identified in androgen independent prostate cancer cells (the LNCaP derivative C-81, CWR-R1, and 22RV1 cells), and these included exons 1, 2 and 3 in common. AR3 contains exon 3b, AR4 contains exon 3a and AR5 contains exon 3b [71]. Another study revealed the presence of AR splice variants in LuCaP xenografts cells which were derived from metastases obtained from men with CRPC [74]. The isoform identified in this study was AR^{v567es} and it was found to be devoid of exons 5, 6, and 7. Both the transcription and transcriptional activity of AR was increased by constitutively active AR^{v567es} in PCa cell lines and presence of the isoform contributed to cancer progression in human cancer xenograft model in castrated mice. Further, using RNA as source to identify different isoforms of AR and using sequence analysis of the cDNA derived from these RNAs, seven AR variant transcripts were also identified that are devoid of ligand-binding domain [72]. In addition to the expression in prostate cancer cells, xenografts and patient samples; AR variants have also been shown to be expressed in breast (MFM223, MDA-MB-453, MDA-MB-231, ZR75.1, MCF-7, T47D) and liver (HepG2) cancer cell lines and human embryonic kidney cell line (HEK293) [75]. In this study, four different ARVs with the cryptic exon 9 (CE9) were identified in MDA-MB-453 and VCaP cells.

1.1.6 Androgen Receptor Variant 7 (AR3)

The constitutively active splice variant ARV7 is the most studied member of ARVs [76, 77]. ARV7 was reported to be upregulated in prostate cancer tissue samples and its expression level was correlated with tumor relapse after prostatectomy [71]. It also was involved in androgen-independent growth of prostate cancer cells. Specific targeting of this isoform in cells resulted in slowed growth of androgen dependent cells in androgen depleted condition

suggesting an important role for ARV7 in androgen-depleted conditions in prostate cancer cells. An additional study comparing bone metastasis samples from of hormone naïve and hormone resistant prostate cancer patients revealed that ARV7 expression was markedly higher in resistant patients who had a worse clinical outcome [78]. Further, it was reported that androgen deprivation induces ARV7 expression but it is also noted that the level of increase was not enough for the restoration of AR activity [79].

Despite the increase in expression in CRPC patients, many questions still remain about the role of ARV7 in cancer progression. For example, a study demonstrated that increased expression of ARV7 results in resistance to therapies targeting androgen receptor [80]. On the other hand, ARV7 was shown to confer castration resistance in animal models but could not do so alone and required the AR^{full-length} [81]. The tumorigenic role of ARV7 has been supported by a study indicating that ARV7 expression in LNCaP cells increased the expression of mesenchymal marker genes N-cadherin, Vimentin, Snail and ZEB1 as compared to cells expressing exogenous AR^{full-length} [82]. These findings were confirmed in a separate study that showed that CDH2, VIM, Snai1 and TWIST, genes associated with epithelial-to-mesenchymal transition were upregulated in ARV7 expressing transgenic mouse model. In this study, insulin-like growth factor 1 and transforming growth factor β 2 which are tumor-associated autocrine and paracrine growth factors were also upregulated. Overall, these studies proposed that ARV7 expression was associated with EMT [83]. On the other hand, a recent study involving detection of ARV7 in circulating tumor cells of prostate cancer patients has shown that ARV7 positive patients did not show significant resistance to taxane treatment while the efficacy of taxane was more in ARV7 positive patients [84]. A study has associated the paclitaxel resistance in PCa to epithelial to mesenchymal transition, and the results related to ARV7 regarding taxol and increase in mesenchymal markers does not hold in this case [85].

Therefore, a better understanding of the effect of ARV7 in prostate cancer and the mechanism through which ARV7 maintains constitutive activity is needed to understand the basic biology of CRPC and then find novel drugs to successfully treat this disease.

1.2 Cellular senescence

Cellular senescence was first described by Leonard Hayflick and Paul Moorhead as the limited capacity of cells to divide [86]. Once in senescent state, the cells have permanently exited from cell cycle yet still remain metabolically active [87, 88]. Later work demonstrated

that cellular senescence can occur due to the natural shortening of telomeres which occurs with each cell division. However, senescence can also be induced by different stimuli. This is defined as premature senescence as the exit from cell cycle happens at a stage that would otherwise be induced by telomere shortening. Upon induction with stimuli cells enter into premature senescence and they differ from other cells by gaining different features.

1.2.1 Features that define senescent cells

Several features and markers have been widely used to characterize senescent cells [89]. First, upon entering senescence, cells gain an enlarged, flat, vacuolized and sometimes multinucleated morphology [90]. Senescent cells also demonstrate a marked increase in β -galactosidase activity. This has led to senescence-associated β -galactosidase (SA β -gal) being one of the most commonly used biomarkers for senescence. The assay detects the increased lysosomal β -D-galactosidase (encoded by GLB1 gene) activity at suboptimal pH (6.0) which is suboptimal for the activity of the enzyme that normally is happening in the highly acidified lysosomes [91]. In addition, as senescence is related to proliferation senescent cells show a decrease in proliferation [92]. This affects the cell cycle distribution in the population, typically leading to an increase in G_0/G_1 [93]. Senescent cells also have increased levels of p16, ARF, p53, p21, p15, p27 and hypophosphorylated RB [91]. In addition, the presence of heterochromatin, known as senescence-associated heterochromatic foci (SAHF), can be used as a marker of senescence in some cases, particularly in oncogene-driven senescence [94, 95]. Finally, senescent cells acquire senescence-associated secretory phenotype (SASP) turning them into proinflammatory cells that have the ability to promote tumor progression. Certain secreted extracellular factors or receptors are increased in senescent cells [96, 97]. These factors include inflammatory cytokines and chemokines, transforming growth factor- β (TGF β), insulin-like growth factor 1 (IGF1)-binding proteins, plasminogen activator inhibitor 1 (PAI1), decoy receptor 2 (DCR2) and DEC1 [96, 98, 99].

1.2.2 Common stimuli in cells leading to cellular senescence

There are a number of mechanisms proposed to induce premature senescence. These include DNA damage, oncogene induction, and stress, including ROS. Premature senescence is mainly regulated by p53 and p16/Rb pathways, which then result in activation of the cyclin-dependent kinase (CDK) inhibitors p16 (also known as INK4A; encoded by CDKN2A), p15 (also known as INK4B; encoded by CDKN2B), p21 (also known as WAF1; encoded by

CDKN1A) and p27 (encoded by CDKN1B) [100, 101]. Activation of CDK inhibitors result in inhibition of cyclin dependent kinases and eventually leading to hypophosphorylation of Rb [102].

1.2.2.1 Stress induced senescence

Cells can enter premature senescence when taken from an organism and cultured *in vitro*. This has been proposed to be due to insufficient culturing conditions such as deficiency in required growth factors, absence of surrounding cells, different extracellular matrix composition or inadequate O₂ levels can cause stress in cells and result in premature senescence [103]. Oxidative stress can also lead to premature senescence in cells grown *in vitro*. Levels of reactive oxygen species increases due to chemotherapeutic drugs, DNA damage and oncogene activation and this then increase the levels of p38 MAPK through RAS–RAF–MEK–ERK cascade [104, 105]. Senescence caused by increase in reactive oxygen species can be prevented by treatment with antioxidants [106].

1.2.2.2 Oncogene driven cellular senescence

Oncogenes are defined as genes that have the potential to induce neoplastic transformation. It has been demonstrated that cells enter senescence upon expression of oncogenes as they are sensitive to oncogenic activation [107]. For example exogenous expression of H-RAS^{G12V} in normal fibroblast initiated senescence, independent of telomere shortening [108]. Oncogenic RAS activates p16 and results in formation of senescence associated heterochromatic foci [95]. Similarly, overexpression of c-myc, TGFβ and deregulation of PTEN, were also correlated with oncogene driven cellular senescence in one-week period [109, 110]. In addition to the common pathways including S-phase kinase-associated protein 2 (Skp2) can also promote senescence by inactivation of PTEN or oncogene Ras. Skp2, an E3 ligase degrades p27^{Kip1} and other targets and it is downregulated in prostate cancer leading to decreased cellular proliferation [111–113].

1.2.2.3 DNA damage

DNA damage triggers a DNA-damage response mediated by ATM, ATR, CHK1 and CHK2 that can lead to cellular senescence [93]. Following DNA damage, these proteins activate several regulatory proteins including p53. p53 in turn increases expression of p21, which then inhibit cyclin-CDK complexes [114]. Senescence caused by telomere shortening is also mediated by this pathway [115, 116]. These senescence cells can often be differentiated from others by the formation of SAHF.

1.2.2.4 Misregulation of CDKN2A locus

CDKN2A locus encodes two essential tumor suppressors, p16 and ARF which are inhibitors of CDK4 and CDK6; and regulators of p53 stability, respectively [117, 118]. Normally this locus is expressed at low levels but in aging cells the expression increases [119, 120]. Some cells have increased expression of p16 and activate tumor suppressor pRb, leading to the formation of SAHF and de-regulation of pro-proliferative genes [95, 121, 122].

1.2.3 Senescence in prostate cancer

Cellular senescence is proposed as potential mechanism to suppress tumors in cancer cells. However, while senescent cells are not actively dividing they still remain metabolically active and can gain tumor promoting capabilities. These cells can gain senescence resistant adaptations or they can support proliferation of neighboring cells by secreting senescence associated factors.

Androgen deprivation therapy is the first line of treatment option for most of the prostate cancers. In a study, prostate cancer cells treated ADT has been shown to facilitate cellular senescence and induces senescence associated secretion [96, 97]. Examples to these secreted factors include interleukins, chemokines, growth factor regulators, proteases or regulators, etc. [107]. It was also suggested that down-regulation of Skp2 by androgen depletion induced irreversible senescence in prostate cancer cells and the expression of members of senescence associated secretory phenotype was increased leading to neuroendocrine differentiation. Another study demonstrated that androgen deprivation promotes survival mechanisms in androgen responsive prostate cancer cells LNCaP and LAPC4 [123] and repeated exposure to androgen deprivation induced senescence promote the formation of senescence resistant cells in the population which show androgen resistant characteristics. A recent study indicated that treatment of LNCaP cells with naturally occurring androgen receptor antagonist atraric acid (AA) causes Rb-hypophosphorylation and increases of p16 expression, leading to cellular senescence. In addition to the studies delineating the link between androgen deprivation and cellular senescence. Interestingly, it has also been reported that supraphysiological levels of androgen can induce cellular senescence by increasing ROS [124–127]. Supportive to these findings, another study demonstrated that high levels of androgen stimulation also results in cellular senescence through Src-Akt pathway [128]. Taken together, recent studies indicate that senescence can occur in prostate cancer through both AR inhibition and overactivation.

1.3 Aims of this work

The mechanism through which ARV7 maintains constitutive activity is extremely important to understand the basic biology of CRPC and then find novel drugs to successfully treat CRPC patients. Therefore, in this project we proposed to characterize the molecular mechanism of ARV7 activation. The overall aims of this work presented in this study are as follows:

Functional characterization of ARV7(Chapter 3)

- To generate a “tunable” system that can allow us to modulate the level of ARV7 or AR^{full-length} activity through chemical agents.
- To characterize the impact of ARV7 on gene expression, proliferation, cell cycle. This model will also be used to further validate various pharmacological treatments to determine how to best inhibit ARV7 mediated proliferation.

Structural interaction of androgen receptor and ARV7 (Chapter 4)

- To quantify both the intra- and intermolecular interactions using fluorescently labeled ARV7 with live-imaging FRET.
- To quantify both the type and kinetics of interactions that are required for DNA binding and activation.
- To determine if the ARV7 forms dimers with other variants (homodimerization) or if they require an ARfull length (heterodimerization).

Chapter 2: Materials and methods

2.1 Materials

2.1.1 Chemicals and reagents

All chemicals were purchased from Sigma-Aldrich or Merck unless otherwise stated. Molecular biology reagents were obtained from Biorad, Promega, Invitrogen, Thermo Fisher Scientific, Macherey-Nagel, Roche, and New England Biolab. Cell culture reagents were purchased from Gibco, Invitrogen, or Lonza. Bacterial growth media was purchased from BD and antibiotics were purchased from Gold BioTechnology or Sigma.

2.1.2 Bacterial strains and cell lines

E. coli strains used for maintenance and cloning of all plasmids are described in **Table 1**.

Table 1: <i>E. coli</i> strains used for maintenance and cloning of all plasmids.	
<i>E. coli</i> strains	Chromosomal markers
DH5α	<i>dlacZ</i> , Δ M15, Δ (<i>lacZYA-argF</i>) U169, <i>recA1</i> , <i>endA1</i> , <i>hsdR17</i> (rK-mK+), <i>supE44</i> , <i>thi-1</i> , <i>gyrA96</i> , <i>relA1</i> [129]
STBL3	F, <i>mcrB</i> , <i>mrrhsdS20</i> (r _B ⁻ , m _B ⁻), <i>recA13</i> , <i>supE44</i> , <i>ara-14</i> , <i>galK2</i> , <i>lacY1</i> , <i>proA2</i> , <i>rpsL20</i> (Str ^R), <i>xyl-5</i> , λ <i>leumtl-1</i>

2.1.3 Bacterial growth media

The media used to grow *E. coli* are described in **Table 2**. All media was sterilized by autoclaving for 30 min at 121 °C.

Table 2: Media used for growth of bacteria in this study.	
Media	Components
244620 - BD Difco™ LB Broth, Miller (Luria-Bertani)	25 g/L medium contains, 10.0 g Tryptone, 5.0 g Yeast Extract, 10.0 g Sodium Chloride
244520 - BD Difco™ LB Agar, Miller (Luria-Bertani)	40 g/L medium contains, 10.0 g Tryptone, 5.0 g Yeast Extract, 10.0 g Sodium Chloride, 15.0 g Agar

2.1.4 Plasmids

2.1.4.1 Plasmids used for Functional Characterization of ARV7

2.1.4.1.1 TetO-FUW-EGFP

The plasmid is used as lentiviral transfer vector for doxycycline-inducible expression of EGFP (**Figure 2-1**) (Addgene plasmid # 30130) [130].

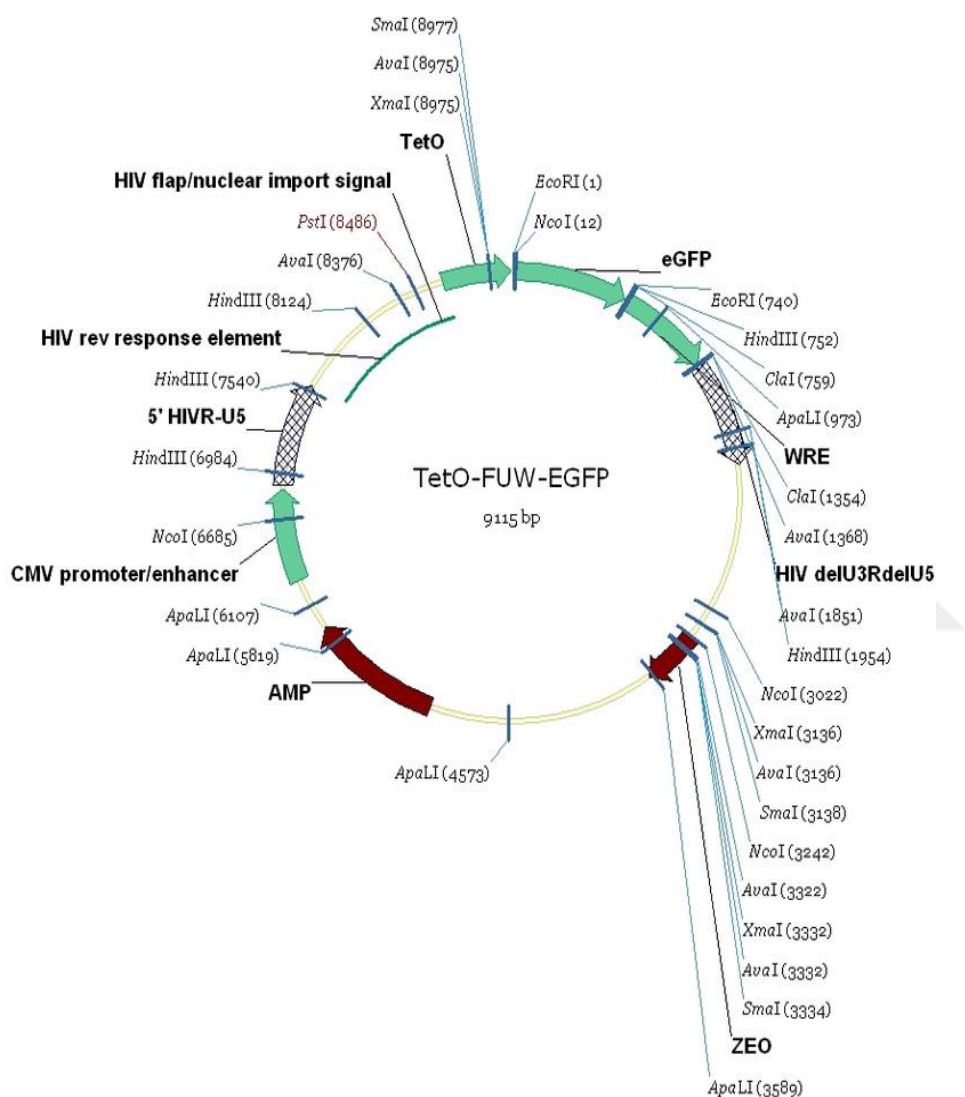


Figure 2-1: TetO-FUW-EGFP plasmid map.

2.1.4.1.2 pLIX 402

The plasmid is a gateway-compatible destination lentiviral vector, used for Tet-ON - doxycycline-inducible gene expression with the Tet Response Element (TRE) promoter (**Figure 2-2**). It has rtTA-VP16-2A-puro expression under the control of PGK promoter, thus, can be considered an 'all-in-one' inducible system (Addgene Plasmid #41394).

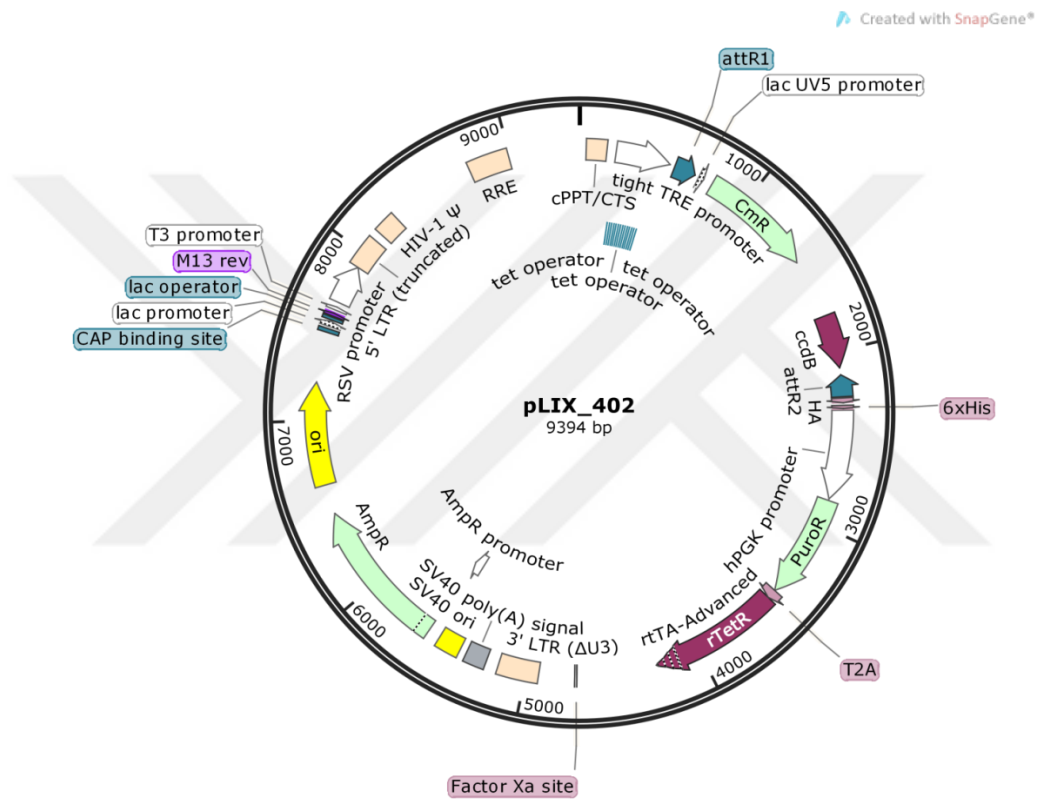


Figure 2-2: pLIX_402 plasmid map.

2.1.4.1.3 pLIX_402-ARV7 plasmid

The plasmid was generated by inserting ARV7 cDNA into pLIX_402 plasmid by gateway cloning (**Figure 2-3**).

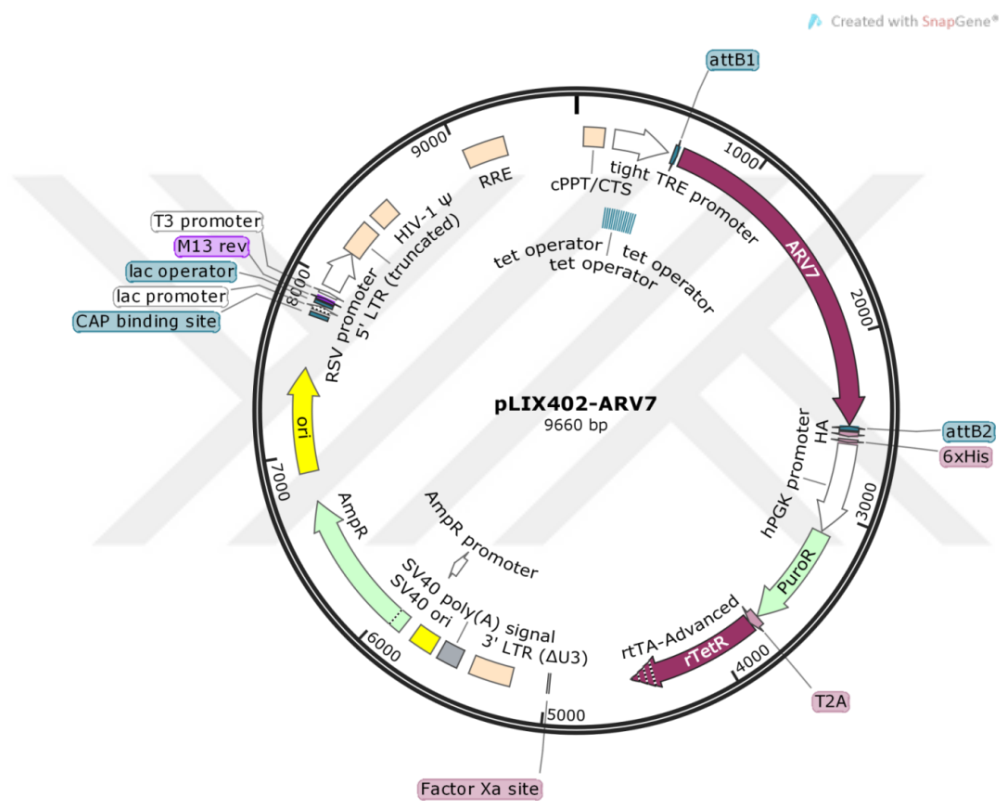


Figure 2-3: pLIX_402-ARV7 plasmid map.

2.1.4.2 Plasmids used for structural interactions of ARV7

2.1.4.2.1 Plasmids used in FRET experiments

2.1.4.2.1.1 pC17V

The plasmid expresses a Cerulean-Venus fusion protein attached via a 17 amino acid linker. It can be used as standard in FRET experiments (**Figure 2-4**).

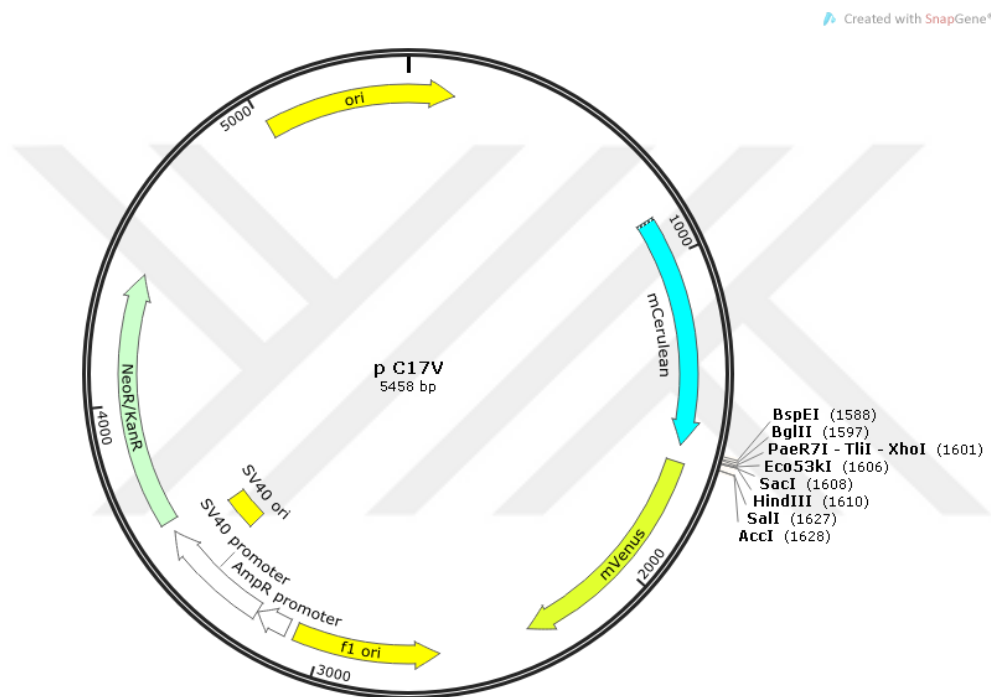


Figure 2-4: pC17V plasmid map.

2.1.4.2.1.2 *mCerulean N1*

The plasmid has a multiple cloning site upstream of a Cerulean gene, enabling the expression of C-terminus Cerulean fusion constructs (**Figure 2-5**) [131]. Cloning requires modification of the stop codon at of the gene of interest so that the fusion construct is successfully translated (Addgene Plasmid #27795).

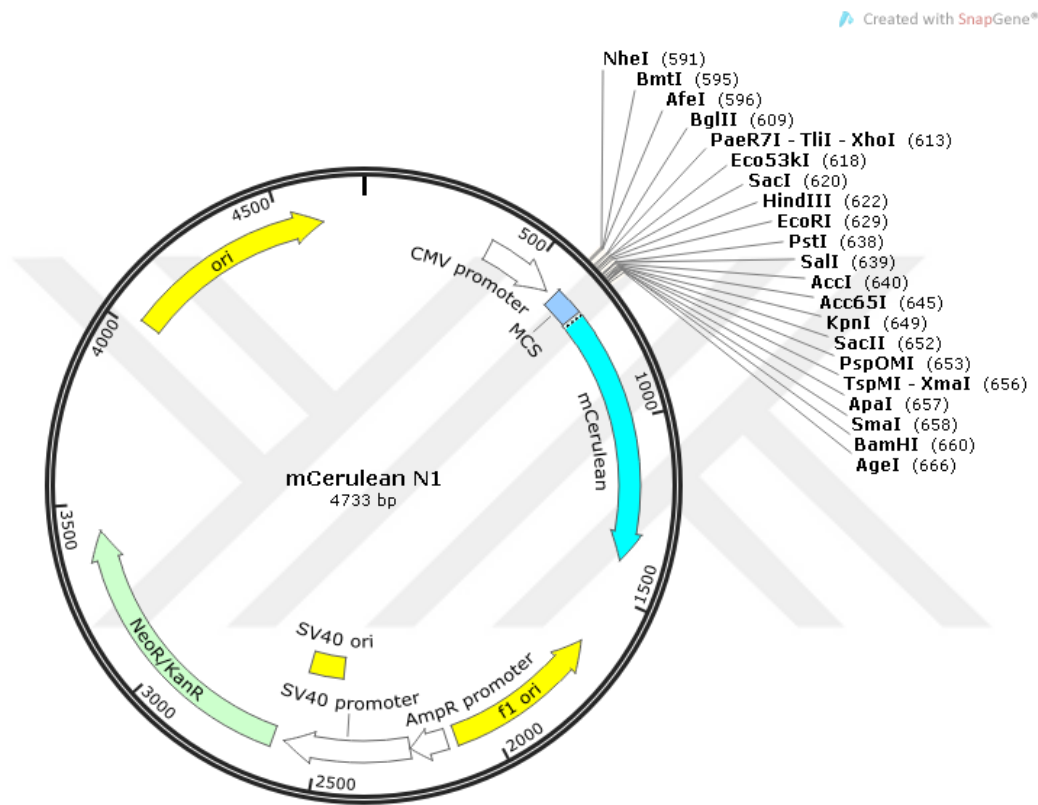


Figure 2-5: mCerulean N1 plasmid map.

2.1.4.2.1.3 *mCerulean C1*

The plasmid contains a multiple cloning site downstream of a Cerulean gene, enabling the expression of N-terminus Cerulean fusion protein (**Figure 2-6**) [129]. The stop codon of the Cerulean is mutated to allow translation of a fusion protein. (Addgene Plasmid #27795)

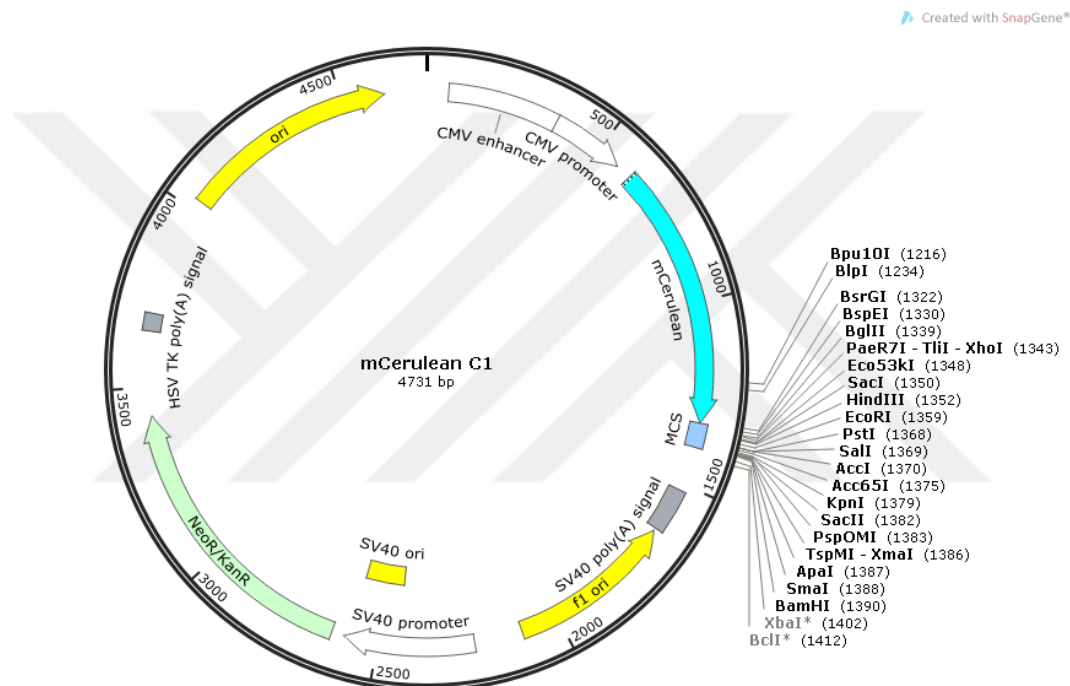


Figure 2-6: mCerulean C1 plasmid map.

2.1.4.2.1.4 *mVenus N1*

The plasmid has a multiple cloning site upstream of a Venus gene, allowing the expression of C-terminus Venus fusion constructs (**Figure 2-7**) [131]. Cloning requires modification of the stop codon at of the gene of interest so that the fusion construct is successfully translated. (Addgene Plasmid #27793)

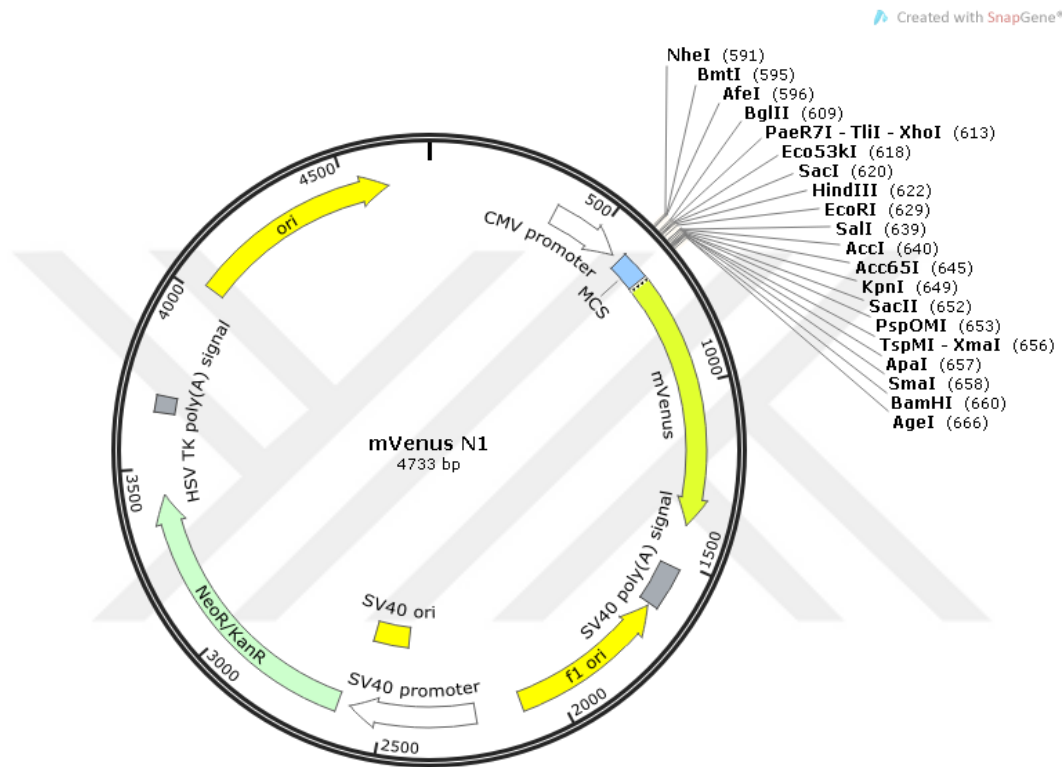


Figure 2-7: mVenus N1 plasmid map.

2.1.4.2.1.5 *mVenus C1*

The plasmid contains a multiple cloning site downstream of a Venus gene, enabling expression of a N-terminus Venus fusion protein (**Figure 2-8**). The stop codon of the Venus was deleted for generation of a single transcript for the generation of fusion protein. (Addgene Plasmid #27794)

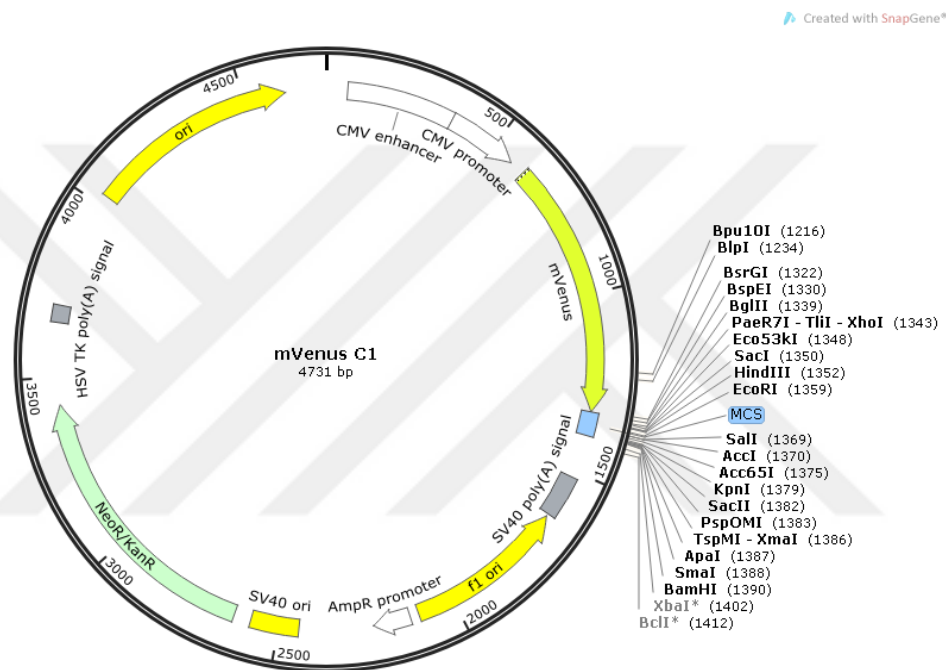


Figure 2-8: mVenus C1 plasmid map.

2.1.4.2.2 Plasmids used in Mammalian Two-Hybrid System (MTHS)

Empty pACT and pBIND plasmids were kindly provided by Prof. Halil Kavaklı (Koç University).

2.1.4.2.2.1 pACT

This high-copy plasmid is used to generate a herpes simplex virus VP16 activation domain (amino acids 411–456)-fusion protein for MTHS (**Figure 2-9**). Expression of the VP16-gene fusion is driven by a human cytomegalovirus (CMV) immediate early promoter. The cDNA clones of interest are cloned into the multiple cloning site, and the expression of cDNA is increased due to the presence of the chimeric intron, CMV promoter, and polyadenylation signal.

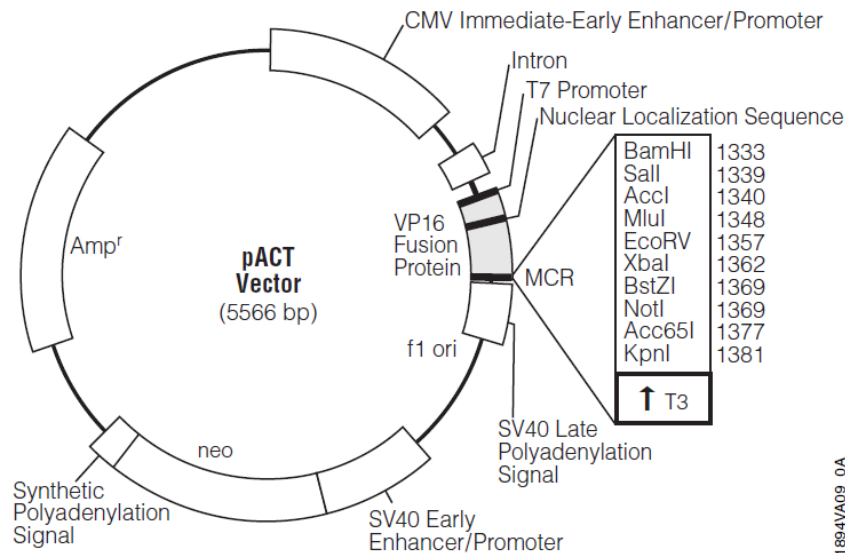


Figure 2-9: pACT plasmid map.

2.1.4.2.2.2 *pBIND*

This high-copy plasmid is used to generate a yeast GAL4-fusion protein for MTHS (**Figure 2-10**). The vector has CMV immediate early promoter-chimeric intron-GAL4 fusion protein and multiple cloning site in 5'-3' direction. The vector also constitutively expresses a renilla luciferase gene for transfection normalization.

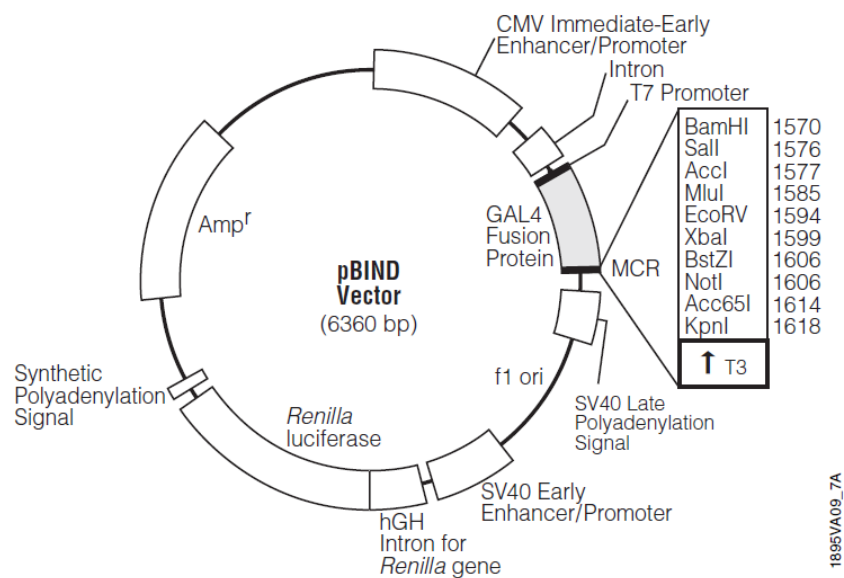


Figure 2-10: pBIND plasmid map.

2.1.5 Primers

Oligonucleotide primers used for cloning, site-directed mutagenesis and qRT-PCR were purchased from Macrogen (Macrogen Europe, Amsterdam, Netherlands). Oligonucleotides used for sequencing of AR and ARV7 constructs for validation of cloning are shown in **Table 3**. Oligonucleotides shown in **Table 4** and **Table 6** were used for generation of constructs used in FRET experiments. The primers used for generation of AR and ARV7 fusion constructs for FRET experiments is described in **Chapter Chapter 4**: . Oligonucleotides used in qRT-PCR are listed in **Table 7**.

Table 3: Oligonucleotides used for sequencing of FRET constructs.		
Oligonucleotide	Orientation	Sequence (5' – 3')
[ARseq_1500]	Sense	CTCATCCTGGCACACTCT
[INtAR2000]	Sense	CCATTTCTGACAACGCCA
[Int_AR_for]	Sense	TTAGGGGGCACTTCG
[IntAR_rev]	Antisense	GAATACTCAGCAGTATCT
[Int_AR_1000]	Sense	CTATGGAGCTCTCACATG
[Int_AR1_Rev]	Antisense	CTAGATCACTGGGTGTGG
[Ext_AR2_rev]	Antisense	CAGAGGTTGATTGTGCGAG
[Int_AR900_for]	Sense	ATTGATAAATTCCGAAGG
[Int700_Seq]	Sense	GGTGTAGTGTGTGCTGGA
[IntAr800_for]	Sense	ACCACCAGCCCCACTGAG
[IntARfull_for]	Sense	GCTTTAAAGGAACCAATT
[ColPCRAR_Rev]	Antisense	CTTCCTGCTGCTGTTGCT
[IntAR1000_for]	Sense	CTATGGAGCTCTCACATG
[ExtAR2_rev]	Antisense	CAGAGGTTGATTGTGCGAG
[Seq_venus_for]	Sense	GCCGCCGGGATCAC
AR_seq_5rev	Antisense	AGGGCCGACTGCGGCTG

Table 4: Oligonucleotides used for generation of constructs.

Construct	Oligonucleotide	Orientation	Expected Product Size	Sequence (5' – 3')
TetO-FUW-ARV7	For Tet ARV7 EcoRI	Sense	1916 nt	GGGGGAATTCCATGGAAGTGCAGTTA
	Rev Tet ARV7 EcoRI	Antisense		AAAAAGAATTCCTACGGGCGGGTCAT
p C-AR-V	For AR XhoI	Sense	2789 nt	AATACTCGAGCCATGGAAGTGCAGTTAG
	Rev wtARDL SalI	Antisense		AATAGTCGACGCACTGGGTGTGGAAA
p C-ARV7-V	For AR XhoI	Sense	1915 nt	AATACTCGAGCCATGGAAGTGCAGTTAG
	Rev ARV7DL SalI	Antisense		AATAGTCGACAAACGGGCGGGTCATTT
p C-AR	For AR XhoI	Sense	2787 nt	AATACTCGAGCCATGGAAGTGCAGTTAG
	Rev WT C-fluoro BamHI	Antisense		AAAAAAGGATCCTCACTGGGTGTGGAAA
p C-ARV7	For AR XhoI	Sense	1917 nt	AATACTCGAGCCATGGAAGTGCAGTTAG
	Rev ARV7 C-fluoro BamHI	Antisense		AAAAAAGGATCCCTACGGGCGGGTCATTT
p AR-V	For AR XhoI	Sense	2798 nt	AATACTCGAGCCATGGAAGTGCAGTTAG
	Rev WT N-fluoro BamHI	Antisense		AAAAAAGGATCCTCTAACTGGGTGTGGAAA
p ARV7-V	For AR XhoI	Sense	1916 nt	AATACTCGAGCCATGGAAGTGCAGTTAG
	Rev ARV7 N-fluoro BamHI	Antisense		AAAAAAGGATCCCTCGGGCGGGTCATTT

Table 5: Primers used to clone ARV7 into TetO-FUW plasmids.

Oligonucleotide	Orientation	Sequence (5' – 3')
For Tet ARV7 EcoRI	Sense	GGGGGAATTCCATGGAAGTGCAGTTA
Rev Tet ARV7 EcoRI	Antisense	AAAAAGAATTCCTACGGGCGGGTCAT

The restriction endonuclease sites for EcoRI enzyme are underlined.

Gene	Forward Primer (5' – 3')	Reverse Primer (5' – 3')
sXBP1	CTGAGTCCGAATCAGGTGCAG	ATCCATGGGGAGATGTTCTGG
usXBP1	CAGCACTCAGACTACGTGCA	ATCCATGGGGAGATGTTCTGG
Total XBP1	TGGCCGGGTCTGCTGAGTCCG	ATCCATGGGGAGATGTTCTGG
ATF4	GTTCTCCAGCGACAAGGCTA	ATCCTGCTTGCTGTTGTTGG
BiP	TGTTCAACCAATTATCAGCAAATC	TTCTGCTGTATCCTCTTCACCAGT
GRP4	GAAACGGATGCCTGGTGG	GCCCCTTCTTCCTGGGTC
GAPDH	AGCCACATCGCTCAGACAC	GCCAATACGACCAAATCC
PSA	GATGCTGTGAAGGTCATGGA	TGGAGGTCCACACACTGAAG
KLK2	AGCCTGCCAAGATCACAGAT	GCAAGAACTCCTCTGGTTCG
FKBP1	TCCCTC GAATGCAACTCTCT	GCCACATCTCTGCAGTCAAA
AR	CCTGGCTCCGCAACTTACAC	GGA CTT GTG CAT TGC GGT ACT CA
ARV7	CCATCTTGTCGTCTTCGGAAATGTTATGAAGC	CTACGGGCGGGTCATTTTCAGATGTTTGCAGT
P14	CCTGGAGGCGGCGAGAAC	CAGCACGAGGGCCACAGC
P16	CTTGCCTGGAAAGATACCG	CCCTCCTCTTTCTTCCTCC
P21	TCGACTTTGTCACCGAGACACCAC	CAGGTCCACATGGTCTTCCTCTG
P53	CCGCAGTCAGATCCTAGCG	AATCATCCATTGCTTGGGACG
E2F	GCAGAGCAGATGGTTATGG	GATCTGAAAGTTCTCCGAAGAG
CycD1	TCAACCTAAGTTCGGTTCGGATG	GTCAGCCTCCACACTCTTGC

2.1.6 Antibodies

The antibodies used in this study are listed below in **Table 8**.

Table 8: Antibodies used throughout this work.				
Source	Antibody	Dilutions	Catalog Number	Description
Santa Cruz	AR Antibody (N-20): sc-816	1:1000	SC-816	Rabbit polyclonal IgG
Santa Cruz	GAPDH Antibody (FL-335): sc-25778	1:4000	SC-25778	Rabbit polyclonal IgG
Novus Biologicals	gamma H2AX [p Ser139] Antibody (2F3)	1:200	nb100-78356	Mouse monoclonal
Invitrogen	Alexa Fluor® 488	1:250	a11008	Goat anti-Rabbit IgG (H+L) Secondary Antibody
Invitrogen	Texas Red-X	1:250	t6390	Goat anti-Mouse IgG (H+L) Secondary Antibody
Santa Cruz	goat anti-rabbit IgG-HRP	1:4000	SC-2054	
Santa Cruz	goat anti-mouse IgG-HRP	1:4000	SC2055	
Novus Biologicals	53BP1 Antibody	1:200	100-304	Rabbit polyclonal antibody
Santa Cruz	Rb Antibody (C-15): sc-50	1:1000	SC-50	rabbit polyclonal IgG
Cell Signaling	Phospho-Rb Antibody (Ser-780)	1:1000	#9307	Rabbit polyclonal
Sigma	LC3B	1:1000	L7543	Rabbit polyclonal

2.2 Methods

2.2.1 Bacterial growth

2.2.1.1 Culture conditions of *E. coli*

Liquid cultures of *E. coli* were grown in LB in either sterile round bottom tubes for small cultures (<5 ml) or in sterile 500 ml erlenmayer flasks with baffled-base for large cultures (>50 ml) at 37 °C with shaking (225 rpm) for 16 hours. Cultures were inoculated with an isolated bacterial colony or from glycerol stocks. After plasmid transformation, *E. coli* strains were grown on solid media, on LB agar at 37 °C.

2.2.1.2 Antibiotics used and their concentration

The final concentrations of commonly used antibiotics are listed in **Table 9**.

Antibiotics	Concentration
Ampicillin	100 µg/mL
Carbenicillin	100 µg/mL
Chloramphenicol	25 µg/mL
Kanamycin	50 µg/mL

2.2.1.3 Production and storage of bacterial glycerol stocks

Strains of *E. coli* were stored at -20 °C as glycerol stocks for long term storage. Stocks were prepared by freezing bacterial cultures with 25% glycerol in a 2 ml cryo-vial.

2.2.2 Molecular biology

2.2.2.1 Sequences

Nucleotide and amino acid sequence alignment and all *in silico* cloning were performed using Serial Cloner software (http://serialbasics.free.fr/Serial_Cloner.html).

2.2.2.2 Polymerase chain reaction

Polymerase chain reaction was done in a total volume of 50 µl using 0.5 µM of forward and reverse primer, 200 µM dNTPs, 500 ng of template DNA, 1X polymerase buffer and 1 unit of

Phusion Polymerase (NEB, # M0530S). Taq DNA polymerase (Fermentas, Dream *Taq* green PCR master mix (2X)) was used for analytical purposes. For GC-rich template DNA, 1M Betaine or 3% DMSO (v/v) was included.

Table 10: Thermocycling conditions for Phusion DNA polymerase.

Step	Temperature	Time
Initial Denaturation	98°C	30 seconds
25-35 Cycles	98°C	5-10 seconds
	45-72°C	10-30 seconds
	72°C	15-30 seconds per kb
Final Extension	72°C	5-10 minutes
Hold	4-10°C	

Table 11: Thermocycling conditions for Taq DNA polymerase.

Step	Temperature	Time
Initial Denaturation	95°C	30 seconds
30 Cycles	95°C	15-30 seconds
	45-68°C	15-60 seconds
	68°C	1 minute/kb
Final Extension	68°C	5 minutes
Hold	4-10°C	

Table 12: PCR conditions for site directed mutagenesis of ARV7.

Step	Temperature	Time
Initial Denaturation	95°C	30 seconds
30 Cycles	95°C	15-30 seconds
	63°C	15-60 seconds
	68°C	1 minute/kb
Final Extension	68°C	5 minutes
Hold	4-10°C	

2.2.2.3 DNA isolation

Plasmid DNA was purified from of *E.coli* using NucleoSpin® Plasmid (MACHEREY-NAGEL) or NucleoBond® Xtra Midi/Maxi (MACHEREY-NAGEL) kits. Plasmid DNA isolation system relied on NaOH/SDS lysis, clearing of the lysate, binding of DNA to silica

resin containing columns and then elution with low-salt buffer. PCR products, enzymatic reactions and DNA from agarose gels were isolated using NucleoSpin® Gel and PCR Clean-up kit (MACHEREY-NAGEL). This system is also based on binding of DNA on silica membrane in the presence of chaotropic salt and then purification with ethanolic buffer.

2.2.2.4 Quantification of DNA concentration

The relative yield of DNA was measured by spectrophotometric analysis at 260 nm (A_{260}) wavelength using Thermo Scientific™ NanoDrop 2000 full-spectrum UV-Vis spectrophotometer.

2.2.2.5 Agarose gel electrophoresis

Agarose gels were prepared by boiling 1% agarose (w/v) in TAE (Tris-acetate-EDTA) buffer (40 mM Tris, 20 mM acetic acid, 1 mM EDTA) (Fermentas, 50X TAE Buffer). DNA samples were mixed in 1:6 ratio with 6X DNA loading dye (10 mM Tris-HCl (pH 7.6) 0.03% bromophenol blue, 0.03% xylene cyanol FF, 60% glycerol 60 mM EDTA) (Thermo-Scientific, #R0611). A 1kb DNA ladder (NEB, # N3232) was run together with the samples to determine the size of the DNA products. Electrophoresis was conducted under constant voltage. Ethidium bromide (0.5 µg/ml) conjugated DNA was visualized with UV.

2.2.2.6 Restriction endonucleases

Purified DNA (1 µg) was digested with 10 U of restriction endonuclease (New England Biolabs) for 1 h according to the manufacturers recommended conditions. Restriction enzyme digestions were carried in total 20 µl volumes.

2.2.2.7 Cloning procedures

2.2.2.7.1 Cloning using PCR products

Purified plasmids were digested with relevant endonucleases, and the desired bands were gel purified as described in section 0. For cloning involving a single restriction endonuclease cut site, the backbone was dephosphorylated with Alkaline Phosphatase, Calf Intestinal (CIP) (NEB, #M0290) to prevent self-ligation. Primers used for PCR were designed to include desired restriction sites to the 5' and 3' ends of PCR product. Amplified PCR products were purified and digested with the enzyme of interest as described in section 2.2.2.6. 50 ng of the digested backbone and the PCR product (insert) were ligated in 1:3 molar ratio (calculated as:

required mass insert (g) = desired insert/vector molar ratio x mass of vector (g) x ratio of insert to vector lengths) by using 1 µl of T4 DNA ligase (NEB, #M0202), and 1 h incubation at room temperature.

2.2.2.7.2 Subcloning

DNA having restriction sites on both 5' and 3' were cloned into destination plasmid that has the same sites in the same orientation. Both plasmids are digested with relevant enzymes the desired portions are gel extracted and ligated with T4 DNA ligase.

2.2.2.7.3 Oligonucleotide cloning

Oligonucleotides were phosphorylated and annealed by mixing 1µl of each oligo (100 µM) with 1µl of 10X T4 ligation buffer and 0.5 1µl of T4 PNK (NEB, M0201S) in total volume of 10 µl. Phosphorylation/annealing reaction was incubated in a thermocycler as follows: 30 min at 37°C, 5 min at 95°C, and then ramp down to 25°C at 5°C/min. The annealed oligos were diluted at a 1:200 dilution into sterile water and 1µl of the diluted oligos were ligated to digested plasmid.

2.2.2.7.4 Gateway cloning with LR reaction

LR gateway cloning was conducted by incubating 75 ng pDONR vector (i.e. pENTR1A-geneX) and 75 ng pDEST vector (i.e. pLENTI CMV-PURO) with 1 µl LR clonase (Invitrogen, 11791-020/ Gateway LR Clonase II) in the presence of TE buffer at a final reaction volume of 5 µl. The reaction mixture is incubated overnight at room temperature. The reaction was then stopped with 0.5 µl of Proteinase K and incubated at 15 min at 37° C before transformation.

2.2.2.7.5 Site-directed mutagenesis

Q5® Site-Directed Mutagenesis Kit (NEB, #E0554S) was used as per the manufacturer's instructions. Primers were designed to include the desired mutation in the target sequence. The plasmid was amplified by PCR using Q5 Hot Start High-Fidelity DNA Polymerase with mutagenic primers to create insertions, deletions and point mutations in the relevant plasmids. Following to PCR, the amplified product was mixed with Kinase-Ligase-DpnI (KLD) enzyme mix for 5 minutes at room temperature and then transformed into chemically competent bacteria.

2.2.2.7.6 TOPO-TA Cloning

For addition of Adenine nucleotide to the ends of PCR product, 0.15-1.5 pmol of purified PCR product was mixed with dATP (final concentration 0.2 mM), PCR buffer with Magnesium (final concentration of MgCl₂: 1.5 mM) and 1 unit of *Taq* polymerase in a final volume of 50 µl and the mixture was incubated at 72 °C for 20 min. Following to Adenine addition, TOPO® TA Cloning Kit (Invitrogen, #450641) was used with protocol as recommended by manufacturer. 3 µl of fresh PCR product mixed with 1 µl of salt solution and 1 µl of TOPO vector in a final volume of 6 µl was incubated for 5 min at room temperature. The TOPO TA cloning mixture was transformed to chemically competent DH5α cells.

2.2.2.8 Heat shock transformation

Chemically competent DH5α and STBL3 strains of *E.coli* were transformed using a standard heat shock protocol. Briefly, 50 ng of ligated cloning mixture was added to 50 µl of chilled competent cells in a 15 ml round bottom tubes and then incubated for 15 min on ice. The mixture was transferred to 42°C water bath for 45 seconds and then put on ice for 2 min. 250 µl of SOC medium (NEB, # B9020S) was added to the mixture and then incubated with shaking (225 rpm) at 37°C for 1h.

2.2.3 Protein characterization

2.2.3.1 SDS-PAGE

Proteins were separated using discontinuous sodium dodecyl sulfate-polyacrylamide gel electrophoresis (SDS-PAGE) system described by Laemmli [132]. 10 % separating gel was composed of 375 mM Tris-HCl (pH 8.8), 10 % (v/v) Acrylamide:Bis 29:1, 0.1 % (w/v) SDS, 0.125 % (w/v) ammonium persulfate (APS) and 0.025 % tetramethylethylenediamine (TEMED). The 6 % stacking gel was composed of 125 mM Tris-HCl (pH 6.8), 6 % (v/v) Acrylamide:Bis 29:1, 0.125 % (w/v) SDS, 0.03 (w/v) APS and 0.004 % TEMED. Gels were cast using Mini-PROTEAN® Tetra Handcast Systems (Biorad).

2.2.3.2 Western Blots

Cells were lysed with 1X passive lysis buffer (NEB, B3321S) and with 1X EDTA-protease inhibitor (Gold Biotechnology, ProBlock™ Gold Mammalian Protease Inhibitor). Protein

concentration was determined using Pierce™ BCA Protein Assay Kit. Protein samples were mixed with 4x Laemmli Sample Buffer (Biorad, 161-0747) containing 10% β-mercaptoethanol and denatured for 10 min at 95 °C. Proteins (5-10 μg) were run on a 10 % SDS-gel at a constant current (25 mA). Proteins were transferred onto PVDF membrane (Immun-Blot® PVDF Membrane, 162-0177) by Trans-Blot® Turbo™ RTA Mini PVDF Transfer Kit (Biorad, #170-4272). The membranes were blocked with 5% non-fat dry milk (Biorad, 170-6404 / Blotting-Grade Blocker_Non-fat dry milk) in TBS-T (20 mM TrisHCl, 150 mM NaCl, 0.1% v/v Tween-20, pH 7.8) at RT for 2 hour. All antibody dilutions are listed in (Table 8). The membranes were incubated with primary antibodies overnight at 4°C; GAPDH (Santa Cruz, (FL-335): sc-25778) was used as loading control. Primary antibodies were washed in TBS-T 6 times for 5 min. The membranes were incubated with secondary antibodies for 1 hour at RT and washed with TBS-T 6 times for 5 min. Membranes were developed using ECL western blotting substrate (Pierce™ ECL Western Blotting Substrate, Cat no: 32106) and CL-XPosure Film (Thermo-Scientific).

2.2.4 Cell culture

2.2.4.1 Culture conditions

LNCaP, LNCaP-Abl, LNAI, BpH-1 cells were grown in RPMI 1640 (Lonza, BE12-702F) medium, supplemented with 1% Penicillin-Streptomycin (Invitrogen, 15070-063) and either 10% fetal bovine serum (Invitrogen)(wtLNCaP and 22Rv1), 10 % Tetracycline free Fetal Bovine Serum (Biowest, S181T-500) (SCC7) or 10% Charcoal Stripped Fetal Bovine Serum (Biowest, S181F-500)(LNCaP-Abl, LNAI and BpH-1). RWPE cells were grown in Keratinocyte Serum-Free Media (Gibco™, cat# 17005042). HEK 293T cells were cultured in Dulbecco's modified Eagle's medium (DMEM; Lonza) supplemented with 10% fetal bovine serum (Invitrogen). All cells were grown in 37⁰ C humidified incubator with 5% CO₂.

2.2.4.2 Production of lentiviruses

Second-generation lentiviruses were packaged according to previously published protocols [133]. 293T cells (2.5x10⁶) were seed in a 10 cm plate and next day 2250 ng of packaging vector (8.2ΔVPR), 250 ng of VSVG envelope vector and 2500 ng of transfer vector were transfected in using 20 μl of Fugene (Promega E2692 / Fugene 6.5 × 1ml). Viruses were collected 48 and 72 hr following transfection. Viral containing media was filtered with a 0.45μm filter, aliquoted and stored at -80°C.

2.2.4.3 Stable transduction of the cells

Cells seeded into 6 well plate (200,000/well) were transduced with lentiviruses in media containing 8 $\mu\text{g/ml}$ of protamine sulfate. Transduced cells were selected with puromycin at killing concentration for 72 hours. The cells were grown one extra day in complete medium for recovery.

2.2.4.4 Determination of viral packaging efficiency

To determine the viral packaging efficiency, 293T cells were seeded in each well of a 6-well (200,000/well) in complete DMEM. One day after seeding, the cells were transduced with 10, 100 and 1000 μl of CMV-EGFP viruses as described in 2.2.4.3. Three days after transduction the cells the expression of green fluorescent protein were checked by inverted fluorescent microscopy.

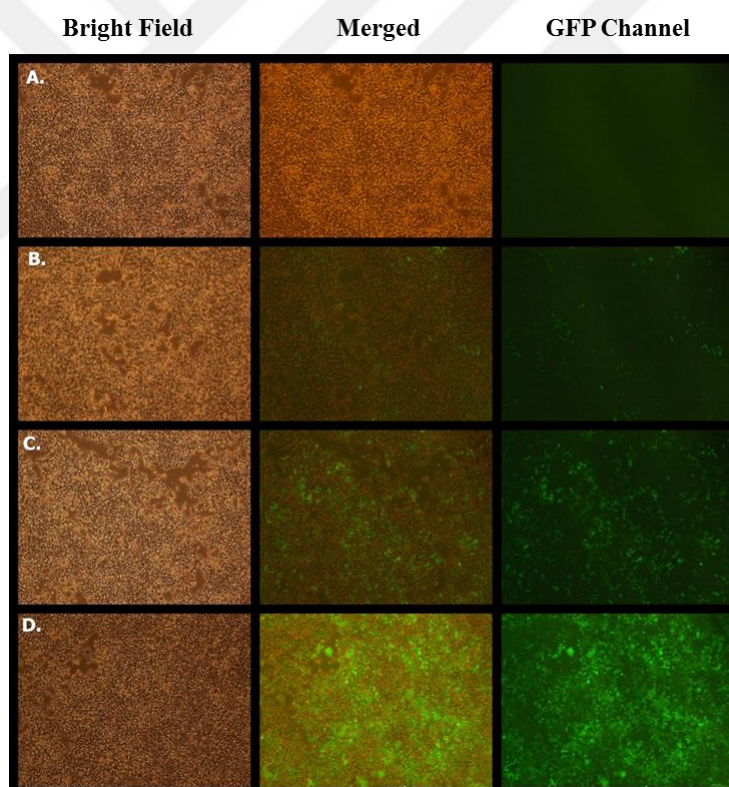


Figure 2-12: GFP expression in 293 T cells transduced with different amount of CMV-EGFP virus.

A representative experiment outlining for determination of viral packaging efficiency. A, no virus; B, 10 μl of virus; C, 100 μl virus, and D, 1000 μl of virus. The pictures were taken at 4X objectives, total 40X magnification. Accordingly, 1000 μl of virus was used to transduce 200,000 cells to ensure that all the cells in the well-plate have been infected by the virus of interest.

2.2.4.5 Transient transfection of the cells

As indicated, 1 µg of plasmid DNA was used to transfect 200,000 cells using Fugene (Promega E2692 / Fugene 6, 5 × 1ml) following the protocol provided by manufacturer. DNA amount was changed if less or more cells were to be transfected.

2.2.4.6 Single cell generations

1000 cells were seeded into first column of a 96-well plate and serially diluted by half till the last column. The wells at the edges of the plate were filled with PBS to prevent drying of the cells. Single cells that were able to form colonies were further grown and expanded in separate wells.

2.2.4.7 Live cell imaging experiment for cell proliferation

200,000 cells were seeded to a 6-well-plate for live cell imaging. The cells were incubated 24 hours after seeding in a regular incubator then transferred to Olympus Xcellence Pro inverted fluorescence microscope with a 60X air objective, numerical aperture 1.35. The cells were maintained in microscope incubation chamber for 24 hours at 37 C temperature and 5 % CO₂. Experiments were performed in RPMI medium supplemented with 10% Tetracycline free FBS. A total of 288 frames were recorded at 5 min interval. Multiple stages from each well were imaged during the image acquisition. ANDOR iXon3 Electron Multiplying Charge Coupled Device (EMCCD) was used to record white light illumination and fluorescence. The data was recorded using custom data acquisition software.

2.2.4.8 X-gal staining

Cells grown in 24-well plates were fixed in 0.2% glutaraldehyde (5 min, RT) and rinsed in PBS. The cells were then incubated overnight at 37°C in staining solution (1mg/ml X-gal, 150 mM NaCl, 2 mM MgCl₂, 5 mM K₃Fe(CN)₆, 5 mM K₄Fe(CN)₆, 40 mM NaP (pH 6.0)), washed in PBS and stored in 70% glycerol (4 °C). For quantification, the experiment was done in triplicates. Pictures were taken at total 200X magnification under inverted light microscope, and the cells were assayed as β-galactosidase positive if they have blue precipitate around nucleus. Analysis was done as the mean of triplicates for each condition and for every set, at least 100 cells were assessed.

2.2.4.9 Cell cycle analysis using BD-Accuri-Flow Cytometer

Cells for flow cytometry were trypsinized, washed with PBS and then permeabilized with ice cold 70% ethanol for 30 min at 4°C. The cells were then washed two times with PBS, treated with RNase (100µg/ml, at RT, 15 min) and then stained with Propidium Iodide (50 µg/ml, at RT for 30 min). DNA content was analyzed using BD Accuri flow cytometer.

2.2.4.10 Luciferase Assay

293T cells were seeded in a 24 well plate (50,000 cell/well). Cells were co-transfected with plasmids containing AR^{full-length} or C-terminally truncated, constitutively active isoform ARV7 together with an androgen response element (ARR3tk)-luciferase reporter. A plasmid expressing a GFP-luc fusion protein was used as positive control. 24 hour after transfection of cells were lysed in 100 µl of Luciferase cell lysis buffer (NEB, B3321S) and lysates were transferred into white 96 well-plates (30 µl/well) as triplicates. 100 µL of luciferin buffer (15 mg/ml D-luciferin Potassium Salt (Gold Biotechnology, Cat#LUCK-500) dissolved in 2 mM EDTA, 500 nM Tris pH7.8, 200 nM ATP, 20 mM MgSO₄, 100 mM DTT) was added to the plate using the automatic dispenser, mixed and then read using a Synergy H1 Multi-Mode Reader.

2.2.4.11 qRT-PCR

RNA was isolated using Macherey-Nagel NucleoSpin® RNA Mini kit following manufacturer's instructions. 500-1000 ng RNA was used to synthesize cDNA with M-MLV Reverse Transcriptase (NEB, #M0253). Relative gene expressions were detected by using LightCycler® 480 SYBR Green I Master (Roche). The primers used in these experiments are listed in **Table 7**, the primers for measuring ER stress were taken from [134].

2.2.4.12 Cell viability assay (MTS)

Cells were seeded in a 96-well plate (3000 cell/well). Treatment was done in ½ dilutions starting from first column. Depending on the experiment, cells were grown for 3 or 7 days in 37°C humidified incubator with 5% CO₂. On the day of assay, 15 µl of MTS solution (prepared from MTS Reagent Powder, using manufacturer's protocol, CellTiter 96® Aqueous) was added to each well. After incubation (~2hr) at 37°C with 5% CO₂ the plates were read using a Synergy H1 Multi-Mode Reader.

2.2.5 FRET experiments

2.2.5.1 Ratiometric FRET using live cell imaging

Before transfection, 293T cells were seeded in each well of a 24-well plate (50,000/well). Next day, 250 ng of DNA was transfected into the cells using Fugene transfection reagent in 3:1 ratio (ul of Fugene/ug of DNA). DHT was used as agonist in 1 nM final concentration for the activation of AR and EtOH was used as solvent control.

Following overnight incubation, transfected cells were transferred to Olympus Xcellence Pro inverted fluorescence microscope with a 40X air objective, numerical aperture 0.60. The cells were maintained in microscope incubation chamber during the experiment at 37 °C temperature and 5 % CO₂. Experiments were performed in DMEM medium supplemented with 10% FBS. An ANDOR iXon3 EMCCD camera was used to record white light illumination and fluorescence.

Before the acquisition of each experiment a minimum of 5 different stage positions were recorded for every condition. A total of 72 frames were recorded in 5 min interval unless the otherwise specified. For every field and at each time point the images were acquired in three channels (**Table 13**).

Table 13: Fluorescence channels used in ratiometric FRET experiments.		
Channel	Excitation	Emission
CFP	427±10	475±20
YFP	504±12	542±27
CFP_YFP (FRET)	427±10	542±27

The cell trajectories were estimated by using a custom generated script in MATLAB. Image analysis was done in four steps. In the first step the images were segmented and all images were articulated based on a threshold filter involving calculations to remove the background signal. Pixel noise was removed with a low pass Gaussian kernel filter. From the smoothed images the cell coordinates are estimated for each frame. Using the intensities, the center of a cell is located based on the local maximum which defines the position for each cell in the frame. Within each consecutive image, the displacement of each individual cell was determined from the mean square displacement calculation and position estimation. The position of every cell was recorded for generation of cell-trajectory and statistical analysis.

Based on probability calculations, the position of each cell in each frame was connected to its position in next frame sequentially.

The fluorescence intensity of each cell was measured in three channels (**Table 13**) in its position. The correct measurement of FRET requires the correction factors a and b which are derived from images of cells that express donor or acceptor protein only, the aim of which is prevention of the bleed-through of CFP and YFP fluorescence occurring due to their excitation at the excitation wavelength of CFP [135]. These coefficients are calculated as follows [136]:

$$\alpha = \frac{I_{FRET}}{I_{YFP}} \text{ of acceptor protein, } b = \frac{I_{FRET}}{I_{CFP}} \text{ of donor protein}$$

Instead of calculating the correction coefficients from a single frame, the values a and b are calculated for every frame in the experiment so that both fluorescence intensity increase due to increased protein expression and the decrease in the fluorescence intensity due to exponential decay are taken into consideration within every frame. For the FRET intensity net FRET was calculated using the following formula [137]:

$$\text{net FRET} = I_{FRET} - (I_{YFP} \times a) - (I_{CFP} \times b)$$

$$I_{FRET} = \text{Intensity of FRET}, \quad I_{YFP} = \text{Intensity of YFP}, \quad I_{CFP} = \text{Intensity of CFP}$$

Using the formula above, a non-radiative fluorescence energy transfer from donor to acceptor is interpreted if net FRET value is positive [138]. To prevent the difference in nFRET occurring only because of increased expression of interacting partners, the calculated nFRET value was normalized using correction coefficients of donor and acceptor fluorophores and is represented as normalized FRET (NFRET) [136]:

$$NFRET = \frac{nFRET}{\sqrt{I_{CFP} * I_{YFP}}}$$

2.2.5.2 Acceptor Photobleaching FRET

One day before transfection 200,000 Hep3B cells were seeded on top of a glass slide in each well of six-well plate. Next day, 500 ng of DNA was transfected into the cells using Fugene transfection reagent in 3:1 (ul of Fugene/ug of DNA). R1881 was used as agonist in 100nM final concentration for the AR activated samples.

A Zeiss LSM 520 microscope was used in all experiments. Argon 458/477/488/514 nm lamp and heat platform was turned on at least 30 min before experiment starts to let the light stabilize and to provide 37 °C temperature for the cells, respectively. Plan Neofluar 40x/1.3 Oil objective was used. All the measurements was done with a specific excitation, which was ensured by measuring the transmission % resulting in 5uW 514 nm excitation of YFP and 10uW 458 nm excitation of CFP.

The scan was done in frame mode; generating images with 512x512 pixels size. Scan speed was set to 8 and pixel depth to 8 bit. Zoom factor 1 was used for searching cells and for imaging Acceptor photobleaching FRET it was set to 4.4, which makes pixel size 100 nm.

Both the YFP and CFP signals were scanned twice in the following order:

- First Scan > *Bleaching* > Second Scan

Thus we have the following procedure:

- YFP image > CFP image > YFP bleach > YFP image > CFP image

After scanning YFP and CFP channels, YFP was bleached in a region of interest (previously defined by Martin van Royen, a square of 100x100 pixels in the middle of the image). Specifically, region was picked from nucleus. Scanning of ROI 25 times with YFP excitation wavelength (514 nm) at high laser power (100%) with 25 iterations was used to bleach most of YFP.

The cells were kept on 37°C to maintain the cell viability. To prevent focal plane shifts caused by temperature changes, cells were allowed to reach 37 °C after the cover slide containing cells were put on the microscope stage. Cells focused with white light, then fluorescent light was used to pick cells which were successfully transfected. A flat, healthy cell was picked and aligned to the middle of the image, if required; the image was cropped to have cells in the middle. Zoom factor was adjusted to 4.4. The bleach region was defined. Each cell is measured by Start button on the window of the software. From each condition, ~15 cells were measured.

Chapter 3: Functional Characterization of Androgen Receptor Variant ARV7

3.1 Introduction

Understanding how AR-V7 can cause constitutive transcriptional activity is critical to understanding the mechanism of CRPC. However, it is unclear if the AR-V7 functions *in situ* as a homodimer or heterodimer with numerous conflicting studies supporting each theory. To clarify this role, we aimed to develop an inducible AR-V7 cell line that would allow us to control both the expression of the variant and also inhibit the AR^{full-length} with antiandrogens. With this “tunable” model we could then study the differences in cell cycle progression and AR signaling upon induced expression of ARV7. At the end, this study might shed light on the treatment of CRPC based on the inhibition of transcription regulated by ARV7 instead of directly targeting wild-type AR itself.

Therefore, the specific aims of the work presented in this chapter are:

- To clone ARV7 gene into an inducible vector
- To generate ARV7 expressing stable cell lines by transducing cells with inducible ARV7 expressing lentiviral particles
- To isolate single cell clones of ARV7 expressing cells
- To characterize the effect of ARV7 expression on cell viability, cellular proliferation, and cell cycle

3.2 Results

3.1.1 Generation of inducible ARV7 expressing LNCaP cell lines using TetO-FUW backbone

3.2.1.1 Cloning of ARV7 gene into TetO-FUW plasmid

We initially cloned ARV7 into TetO-FUW-EGFP (**Figure 2-1**). To remove EGFP, TetO-FUW-EGFP was digested with EcoRI, gel purified, and then dephosphorylated with Calf Intestinal Alkaline Phosphatase. The gene encoding ARV7 was PCR amplified from pENTR1A_ARV7 plasmid using the primers in the **Table 5**. The resulting PCR product (1916 bp) was purified, digested by EcoRI restriction enzyme, and ligated with the dephosphorylated TetO-FUW- backbone with T4 ligase.

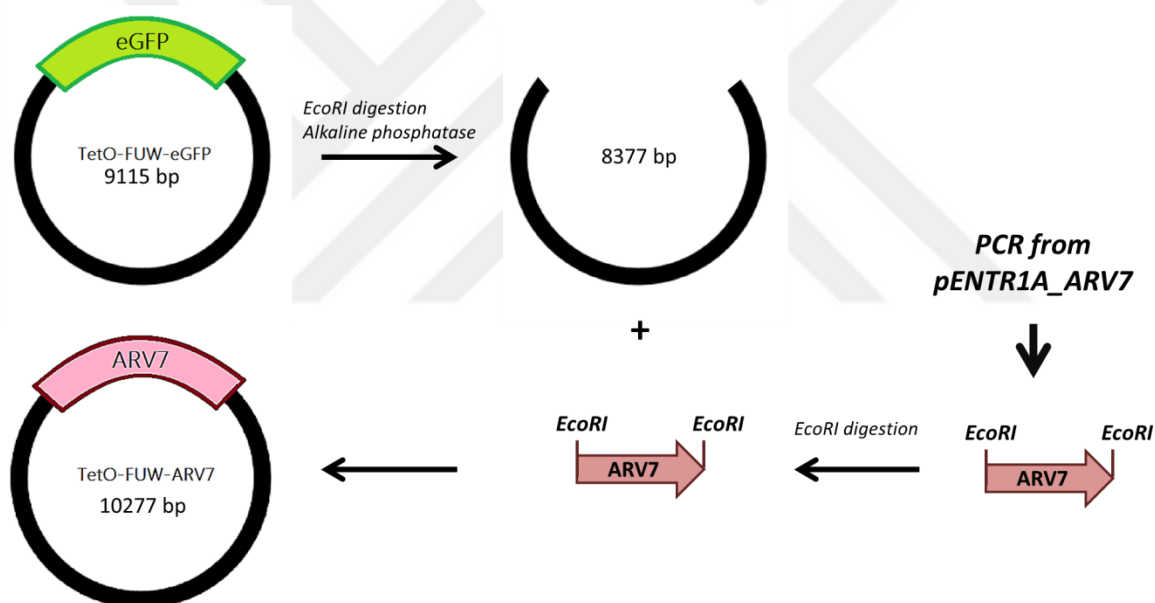


Figure 3-1: Cloning strategy used to generate TetO-FUW-ARV7.

3.2.1.2 Lentiviral Packaging of TetO-FUW-ARV7

Lentiviral particles of TetO-FUW-ARV7, TetO-FUW-EGFP, CMV-EGFP and rTTA were generated using a standard protocol (**Figure 3-2**) described in section **2.2.4.2**.

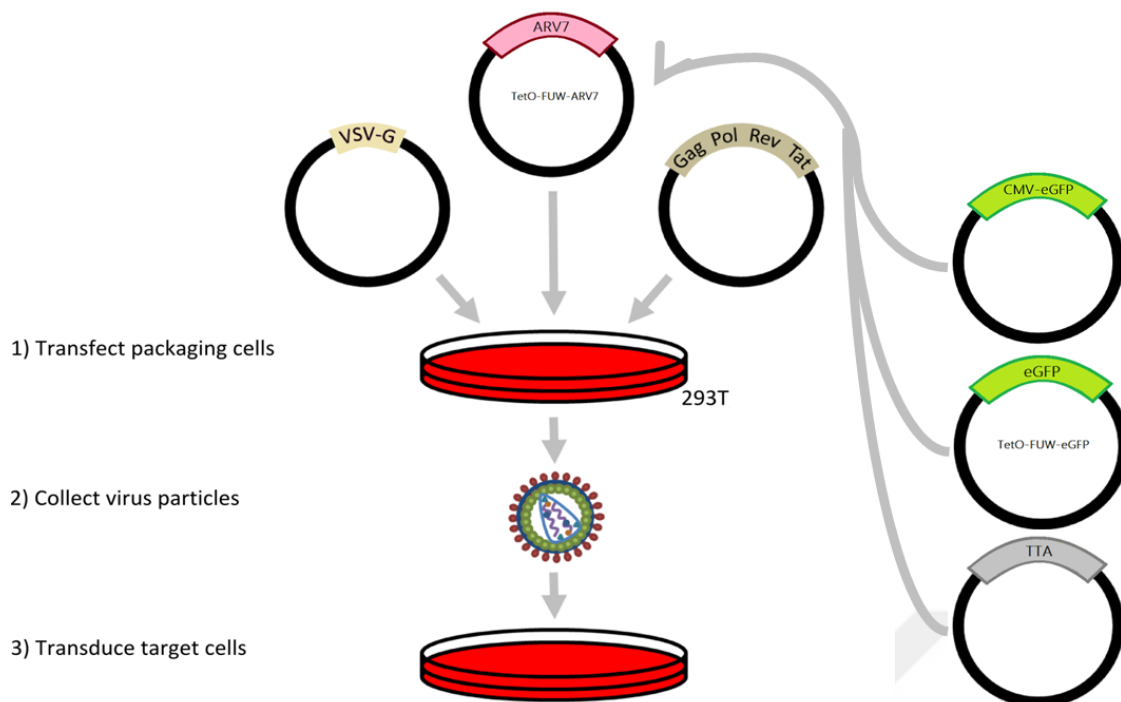


Figure 3-2: Outline for lentiviral packaging.

3.2.1.3 Transduction of LNCaP cells

The cells were transduced and then selected with puromycin. The cells were treated with doxycycline (2 $\mu\text{g/ml}$) for 24 h and the lysates were collected for western blotting as described in section 2.2.3.2. LNCaP cells were seeded into a 6-well plate (200,000/well) and transduced with following viruses:

Virus	rTTA	Doxycycline	Expected expression
CMV-eGFP	-	-	eGFP
No inducible virus	+	-	No expression
TetO-FUW-eGFP	-	-	No expression
TetO-FUW-eGFP	+	-	No expression
TetO-FUW-eGFP	+	+	EGFP
TetO-FUW-ARV7	-	-	No expression
TetO-FUW-ARV7	+	-	No expression
TetO-FUW-ARV7	+	+	ARV7

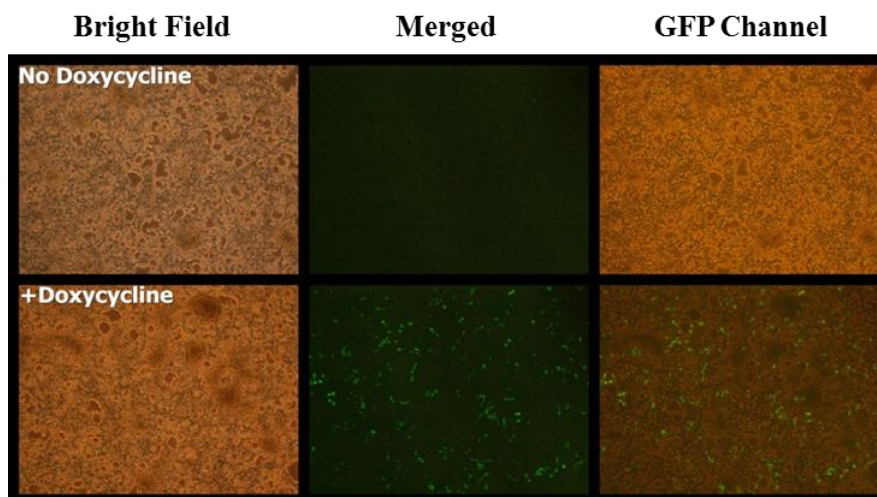


Figure 3-3: LNCaP cells transduced with TetO-FUW-eGFP and rTTA viruses. The cells were selected with Puromycin and then treated with doxycycline for 24 h to check the inducible gene expression. Images were taken at 4X objectives with total 40X magnification under inverted fluorescent microscope.

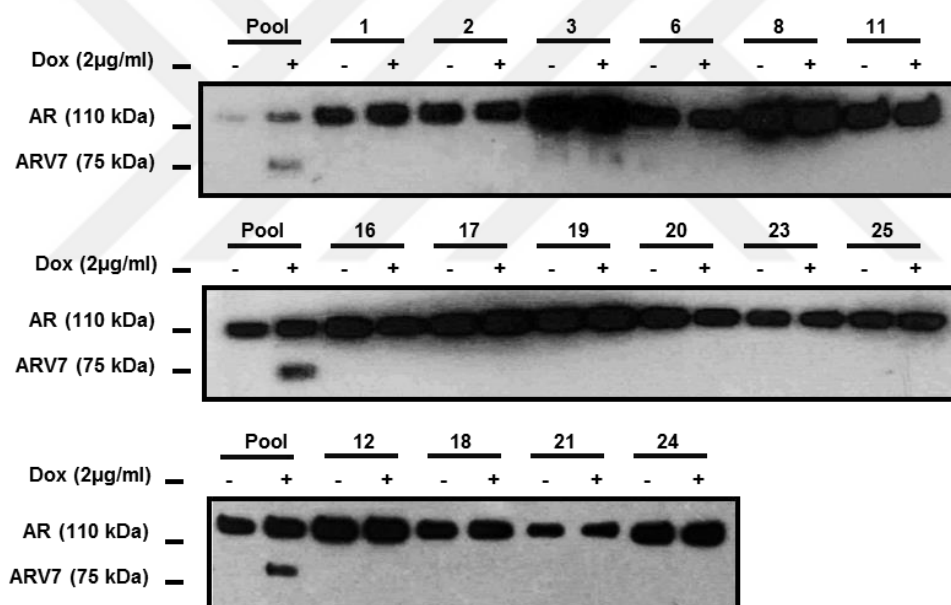


Figure 3-4: Single cell clones of TetO-FUW-ARV7. Sixteen representative single cell clones were tested following TetO-FUW-ARV7 and rTTA transduction. Each colony was grown with/without doxycycline (2 μ g/ml) to check the level of ARV7 expression. At 24 h post treatment cell lysates were prepared and subjected to western blotting. Pool indicates the transduced cell population before single cell clone isolation.

As the pooled sample showed ARV7 expression (**Figure 3-4**), single cell clone screening was done. However, none of 48 single cell clones isolated expressed ARV7 in the presence of doxycycline. As the system requires transduction of both TetO-FUW-ARV7 and rTTA encoding viruses we have decided to try an “all-in-one” doxycycline model.

3.2.2 Generation of inducible ARV7 expressing LNCaP cell lines using pLIX_402 backbone

Given the results using an inducible system that requires two plasmids, we moved into an “all-in-one” system that contains both components. Specifically, we chose to work with a pLIX_402 plasmid that expresses rTTA-VP16-2A-puro from the PGK promoter (**Figure 2-2**). Transduced cells expressing the rTTA-advanced element that have been treated with doxycycline will express the gene that is controlled by the tight TRE promoter (**Figure 3-5**). As the rTTA component of the Tet-On inducible system is also present in the backbone itself, transduction of the cells with the virus generated by this single plasmid can allow inducible gene expression.

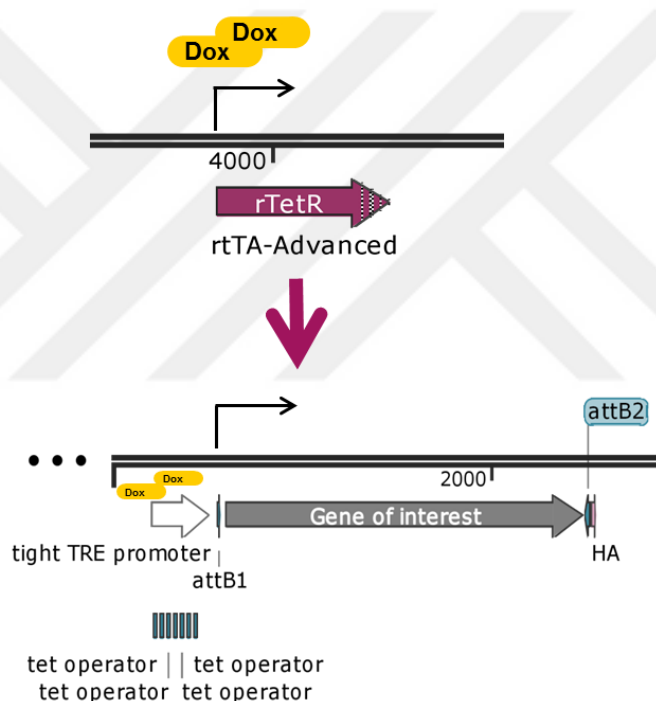


Figure 3-5: Tet-On system summary.

3.2.2.1 Cloning of ARV7 into pLIX_402 backbone

ARV7 was previously cloned into a gateway compatible pENTR1A entry vector by Dr. Nathan Lack. With this construct we moved ARV7 into the destination pLIX_402 vector using an LR recombination reaction (2.2.2.7.4). The construct was validated by restriction enzyme digestion and sequencing (**Figure 2-3**).

3.2.2.2 Transduction of wtLNCaP cells with pLIX_402-ARV7 lentiviruses

To test our inducible system, we transduced wtLNCaP with lentiviruses containing pLIX_402-ARV7 (2.2.4.3) and selected transduced cells with Puromycin (2 µg/ml) for 72 h. With the selected cell we then tested ARV7 expression by inducing expression with doxycycline (2 µg/ml). As determined by western blotting, ARV7 was clearly expressed in transduced and doxycycline-treated wtLNCaP cells (Figure 3-6).

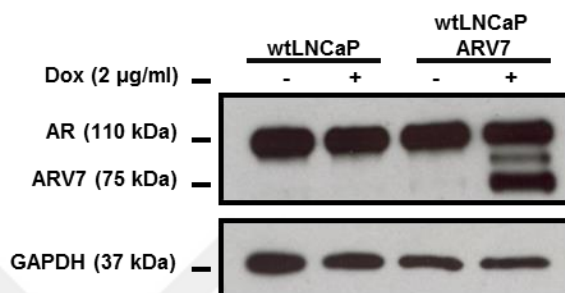


Figure 3-6: ARV7 expression in LNCaP cells transduced with pLIX_402-ARV7. Cells (200,000/well) were transduced 24 h after seeding and were treated with doxycycline for 24 h. Cell lysates were prepared for protein characterization as described in section 2.2.3. GAPDH was used as internal control.

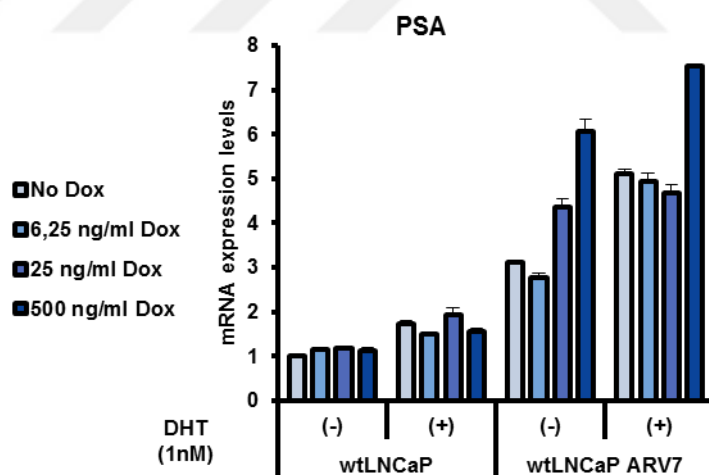


Figure 3-7: PSA levels in wtLNCaP and ARV7 expressing LNCaP cells with change in Dox. mRNA expressions of PSA and GAPDH in cells were detected by qRT-PCR. RNA isolation, cDNA synthesis, and qRT-PCR were done as described (2.2.4.11). GAPDH was used as internal control. Fold change of each mRNA transcript in each cell was relative to that of wtLNCaP cells which were treated with neither doxycycline nor DHT.

3.2.2.3 Single cell clones of ARV7

When working with the transduced population, we observed a flattened morphology in a small percentage of LNCaP cells. To determine if this was due to cellular variability we isolated single cell clones of the LNCaP Tet-V7 by limiting dilution (2.2.4.6). A total of 28 different single cell clones were isolated and expanded for characterization. With these clones we initially tested the V7 expression by western blotting (Figure 3-8). Each single cell clone showed different level of ARV7 expression depending on the copy number of integrated viruses. There were cells which did not express ARV7, those with both AR^{full-length} and ARV7 and those which express high levels of ARV7 (Figure 3-9).

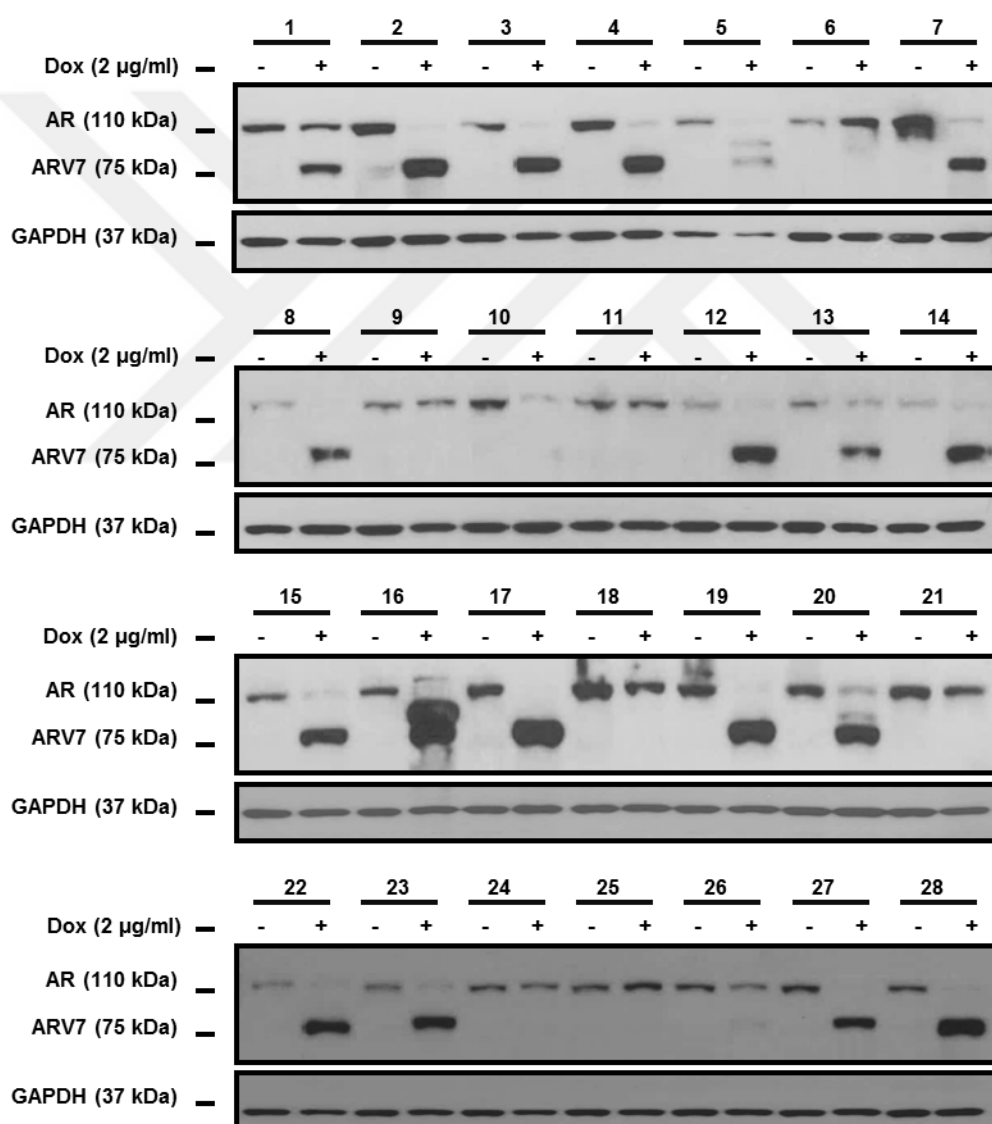


Figure 3-8: ARV7 expressing single cell clones of LNCaP cells. Single cell clones were treated with doxycycline for 24 h and lysates were collected for protein characterization. GAPDH was used as internal control.

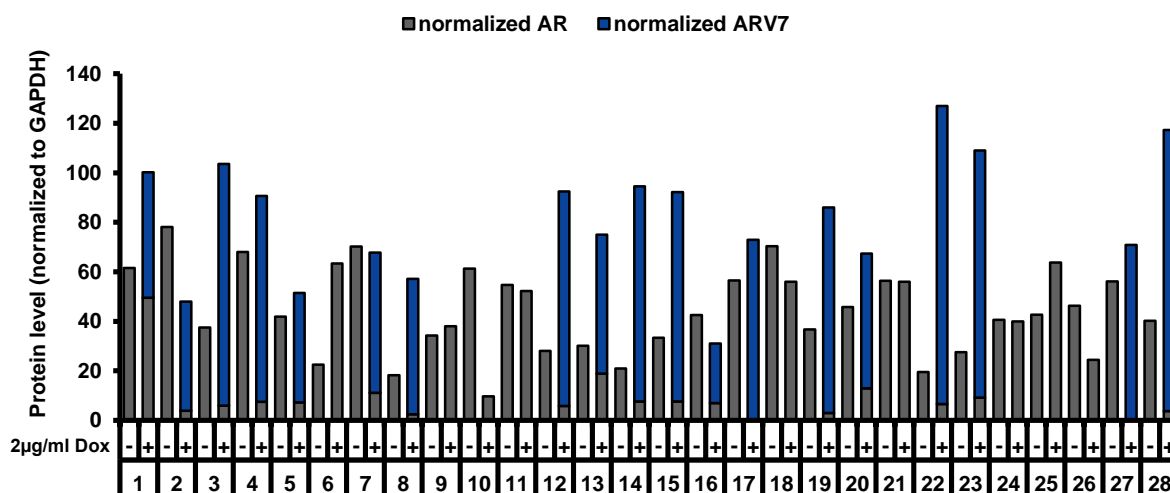


Figure 3-9: Quantification of the levels of AR^{full-length} and ARV7 in single cell clones. The levels of AR^{full-length} and ARV7 expression were quantified using ImageJ software. The level of expression for each protein in a single cell clone was normalized to its GAPDH.

From these results we picked a single cell clone with high levels of ARV7 expression for future studies (Single Cell Clone #7 (SCC7)). We treated SCC7 with various doxycycline concentrations (0-500 ng/ml) and analyzed ARV7 expression by western blotting. The ARV7 expression was concentration dependent and similar to previous work AR^{full-length} expression was down-regulated by ARV7 expression (**Figure 3-10**).

We picked three different doxycycline concentrations for our experiments, representing three distinct levels of ARV7 expression in prostate cancer patients; 6.25 ng/ml for low levels of ARV7 and high levels of AR^{full-length}, 25 ng/ml for similar levels of ARV7 and AR^{full-length}, and 500 ng/ml for high levels of ARV7 and low levels of AR^{full-length}.

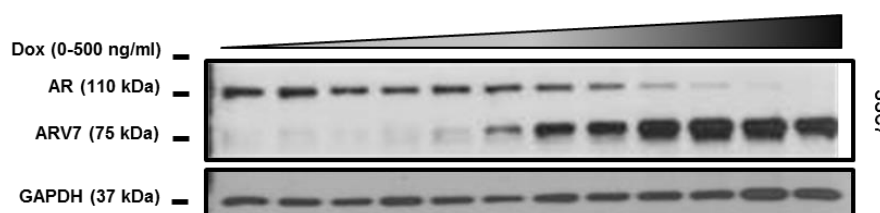


Figure 3-10: ARV7 expression in SCC7. Cells were treated with increasing concentrations of doxycycline (0-500 ng/ml). Cellular lysate was collected 24 h after treatment the cells and then analyzed by western blotting (2.2.3.2). GAPDH was used as internal control.

3.2.2.4 Live cell imaging of the change in morphology of SCC7

Live-cell microscopy is a powerful technique which allows for imaging cells under different conditions to compare their growth *in vitro* [139]. As we observed a morphological change in the ARV7 expressing clone, we did a live cell imaging experiment to better study this observation. Similar to what we observed in the pooled population and SCC7 cells, there was a gross morphological change as the cells became large and flat (**Figure 3-11**). As treating eukaryotic cells with tetracycline and its derivatives can affect the mitochondrial genome translation and induce cellular respiration defects [140], we also treated wtLNCaP cells with doxycycline, and did not observe similar changes in these cells.

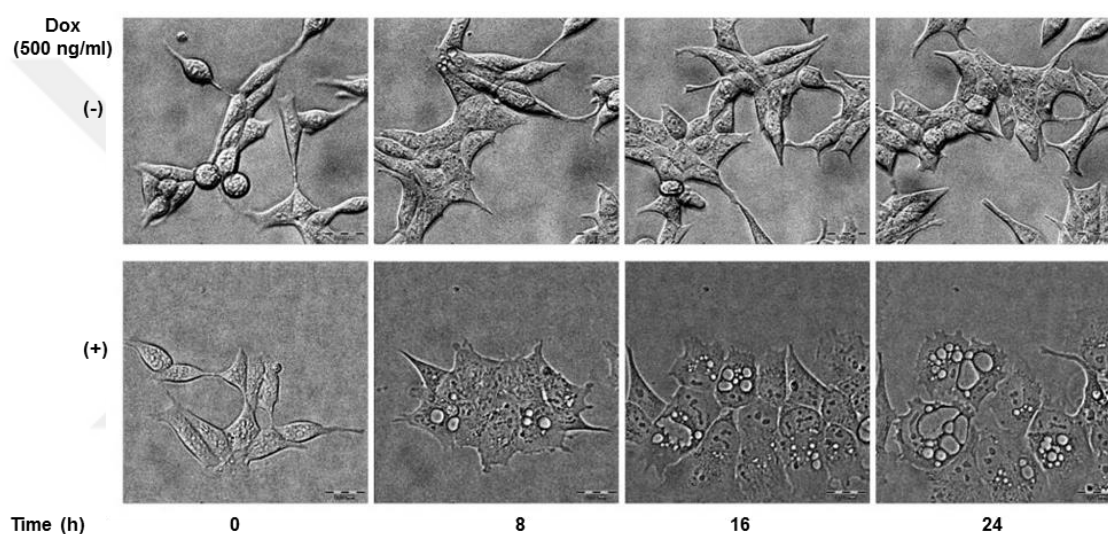


Figure 3-11: Live cell imaging of morphology of SCC7 cells.

After seeding SCC7 cells, the plate were transferred to Olympus Xcellence Pro inverted fluorescence microscope with a 60X air objective, numerical aperture 0.7. We incubated the cells for 24 hours at 37 °C temperature and 5 % CO₂. A total of 288 frames were collected in 5 min intervals following doxycycline treatment.

3.2.2.5 Autophagy marker in SCC7 cells

In addition to flattened and enlarged morphology, we observed vacuolization in ARV7 expressing SCC7, suggestive of either autophagy or senescence.

Microtubule-associated protein 1A/1B-light chain 3 (LC3) is a soluble protein distributed in cells. During autophagy, it is conjugated to phosphatidylethanolamine to form LC3-phosphatidylethanolamine conjugate (LC3-II), which is recruited to autophagosomal membranes similar to other cytoplasmic components including cytosolic proteins and organelles. After LC3-I is engulfed in autophagosomes upon fusion of autophagosomes with lysosomes, it is degraded in autolysosomal lumen. As LC3B degradation is linked to autophagosomal degradation, detection of LC3B-II isoform in western blot is used as marker for autophagy.

To test for autophagy we induced ARV7 expression in wtLNCaP and SCC7 cells and checked the levels of LC3B-II isoform by western blotting (2.2.3.2). Despite the increase in ARV7 expression, there was no change in the level of LC3B-II isoform suggesting that the cells are not undergoing autophagy (Figure 3-12).

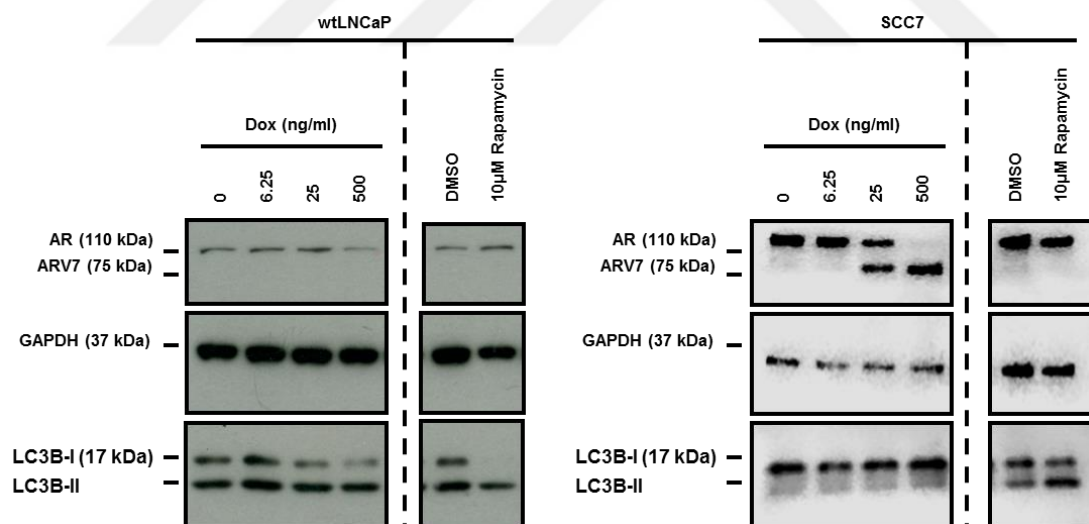


Figure 3-12: Autophagy marker in doxycycline-treated wtLNCaP and SCC7.

Rapamycin was used as positive control for autophagy. Following incubation of cells with doxycycline for 24 h, cellular lysates were collected samples for western blotting. GAPDH was used as loading control and the AR and ARV7 expression is also shown. Summary results shown above from n=2.

3.2.2.6 EMT markers in ARV7 expressing LNCaP cells

As we saw a difference in morphology of ARV7 expressing single cell clone of LNCaP cells, we hypothesized that this morphological change may be due to epithelial-mesenchymal (EMT) transition.

To test this, the expression of various EMT related genes was quantified following induction of ARV7 in wtLNCaP and SCC7 cells. The levels of E-cadherin and N-cadherin did not change significantly while the Snail is expressed less in response to ARV7 expression and Vimentin is expressed higher when the cells are expressing ARV7.

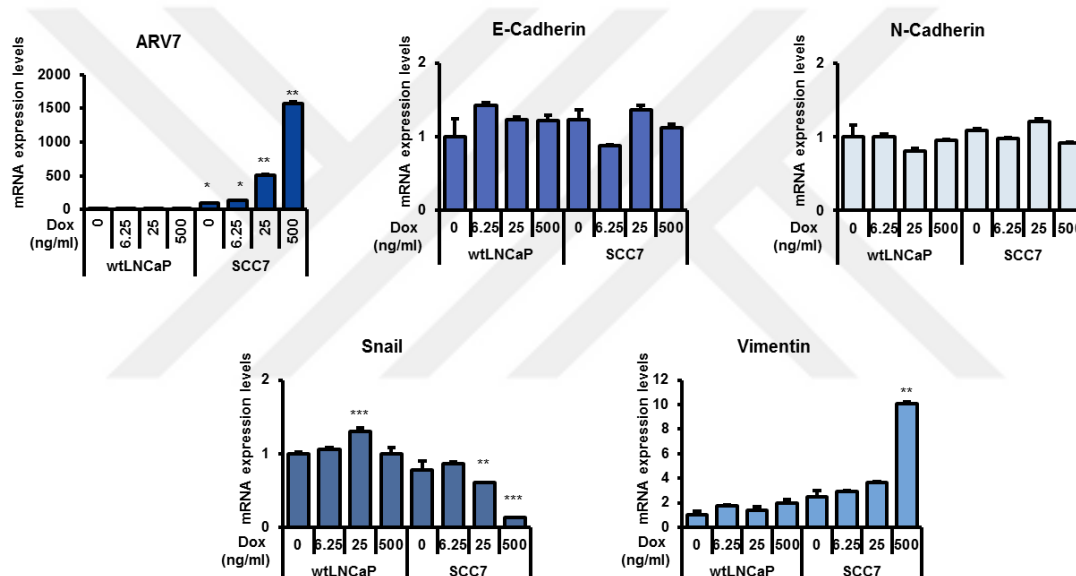


Figure 3-13: Epithelial-mesenchymal transition (EMT) gene expression in doxycycline-treated wtLNCaP and SCC7 cells.

mRNA expressions of E-cadherin, N-cadherin, Snail, Vimentin and GAPDH in cells were detected by qRT-PCR. GAPDH was used as internal control. Fold change of each mRNA transcript in each cell was relative to that of non-treated wtLNCaP cells. (* for $p < 0.05$, ** for $p < 0.01$, *** for $p < 0.001$; $n=2$)

3.2.2.7 Unfolded protein response genes in ARV7 expressing cells

In this work we used an inducible lentiviral expression system to increase protein expression of ARV7. The level of ARV7 expression increases in less than 24 hours to such a high level that we see a decrease in the levels of AR^{full-length} protein. Since we are expressing very high levels of an exogenous protein the proteins might not be folded properly which can cause unfolded protein response (UPR) in endoplasmic reticulum. Thus, we wanted to check whether inducible ARV7 expression resulted in ER stress. In this, wtLNCaP and SCC7 cells were treated with three different concentrations of doxycycline for 24 hours. Further, the cells were treated with 1.5 μ M Thapsigargin, 10 μ M Tunicamycin, and 2 mM DTT for 5 hours as positive control (Tunicamycin inhibits N-linked glycosylation, Thapsigargin blocks the ER calcium ATPase pump, and DTT is a strong reducing agent blocking disulfide-bond formation [134, 141]). The mRNA expression of sXBP1, usXBP1, totalXBP1, ATF4, BiP and GRP94 were quantified by qRT-PCR as a marker of the UPR (2.2.4.11).

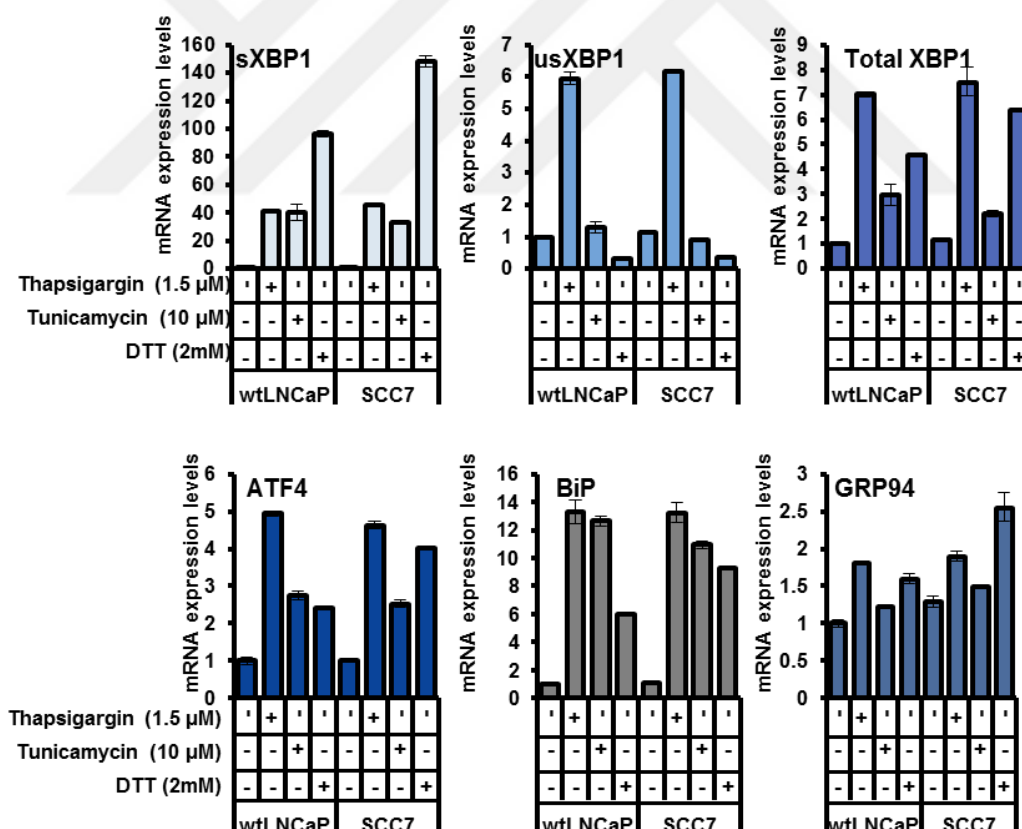


Figure 3-14: ER stress markers with UPR inducing chemicals.

Cells treated with indicated chemicals were collected for qRT-PCR for quantification of ER stress markers (2.2.4.11). GAPDH was used as internal control. Fold change of each mRNA transcript in each cell was relative to that of non-treated wtLNCaP or SCC7 cells.

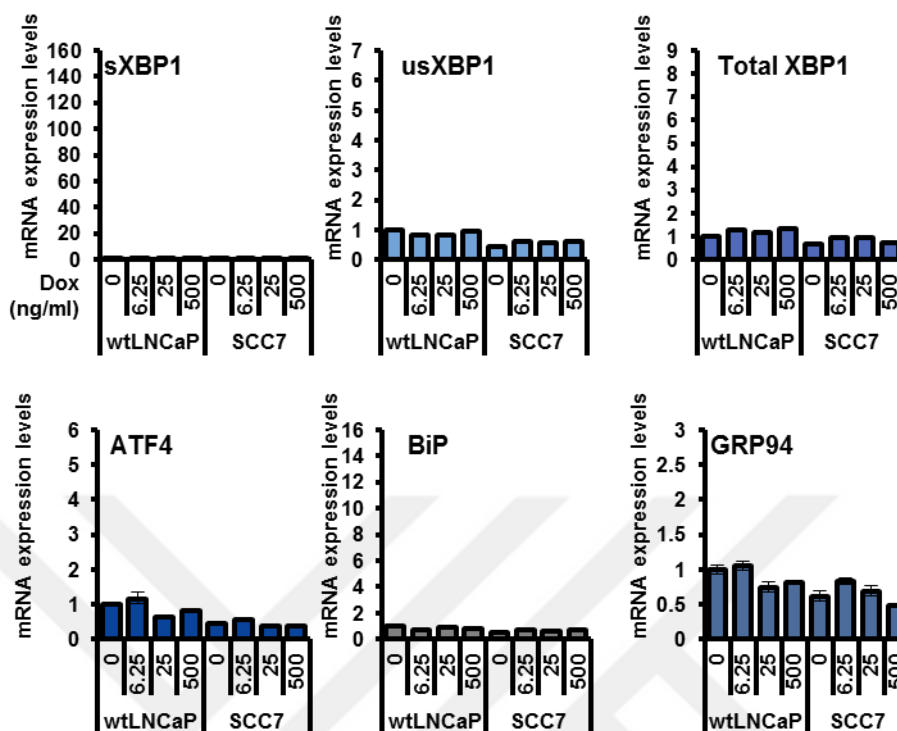


Figure 3-15: ER stress markers in doxycycline treated wtLNCaP and SCC7 cells. mRNA expressions of sXBP1, usXBP1, totalXBP1, ATF4, BiP, GRP94 and GAPDH in cells were detected by qRT-PCR. GAPDH was used as internal control. Fold change of each mRNA transcript in each cell was relative to that of non-treated wtLNCaP cells.

Although Tunicamycin, Thapsigargin and DTT target different components of ER, their effect at the end is unfolded protein response. Demonstrating that the system is working, we observed a marked increase in ER stress markers in cells treated with these chemicals. However, we did not observe a significant increase in the levels of XBP-1, sXBP-1, total XBP-1, ATF4, BiP and GRP94 mRNA levels after 24 h doxycycline treatment, indicating that ARV7 expression does not cause an UPR.

3.2.2.8 ARV7 expression and cellular senescence

Given that the cellular phenotype was not driven by autophagy or EMT transition, we hypothesized that it is due to senescence. To test for this we used the common senescence biomarker, Senescence-Associated β -galactosidase (SA- β -gal). Extensive studies have demonstrated that lysosomal β -D-galactosidase (encoded by GLB1 gene) activity is increased in senescence [91].

In our experiments, ARV7 expression caused a dramatic increase in SA- β -gal activity (**Figure 3-16**) in 24 h time frame. The phenotype was dependent on the level of ARV7 expression and was more significant in single cell clone (**Figure 3-17**).

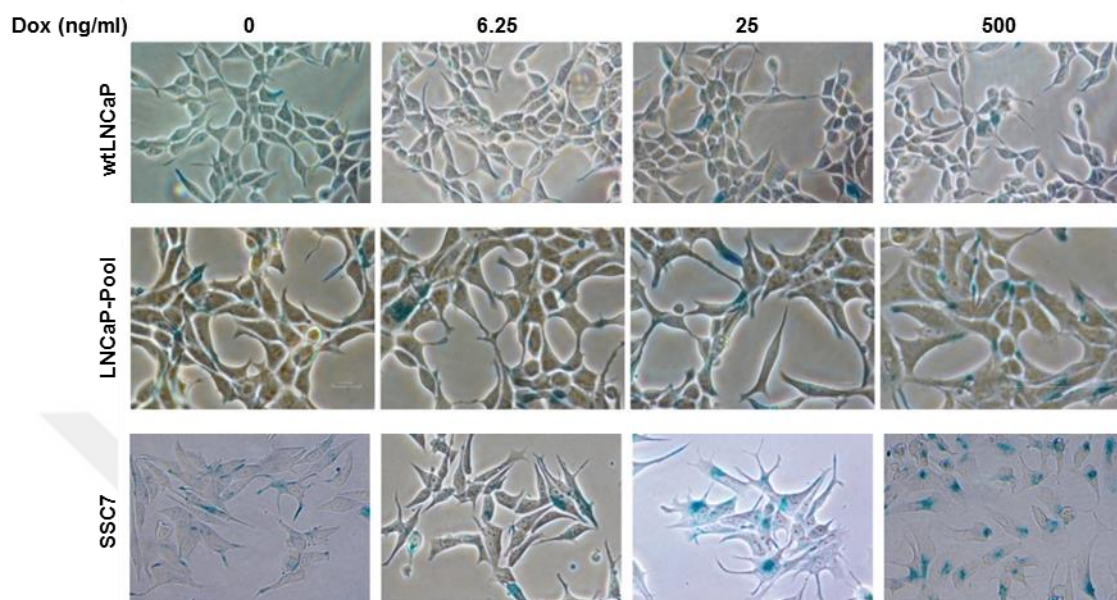


Figure 3-16: Senescence-associated β -galactosidase staining in ARV7 expressing LNCaP cells.

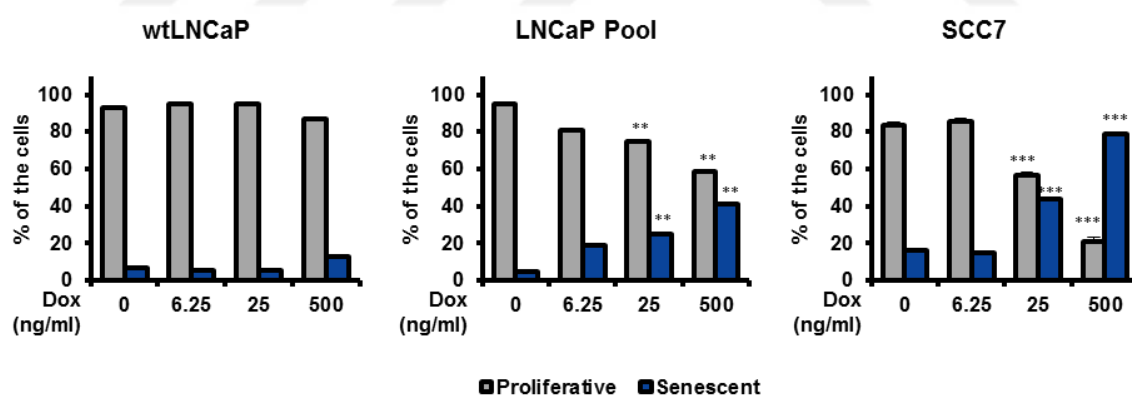


Figure 3-17: Quantification of proliferative and senescent cells.

The cells seeded in 12-well plates in triplicates were treated with indicated concentration of doxycycline for 24 h. Xgal staining was done as described in section 2.2.4.8. The quantification was done by taking pictures for each condition in total 200X magnification and the cells were counted as senescent if the morphology was flattened and blue-precipitate was formed. (* for $p < 0.05$, ** for $p < 0.01$, *** for $p < 0.001$)

Next, we wanted to show that the cells which are positive SA- β -gal are not actively dividing and have arrested at cell cycle. We induced ARV7 and analyzed the cell cycle distribution by quantification of DNA content as described in section 2.2.4.9. The cell cycle distribution of

wtLNCaP cells treated with doxycycline did not change, while ARV7 expression in SCC7 and LNCaP pool dramatically increased the number of cells in G₀/G₁ (Figure 3-18). This is consistent with a senescent phenotype.

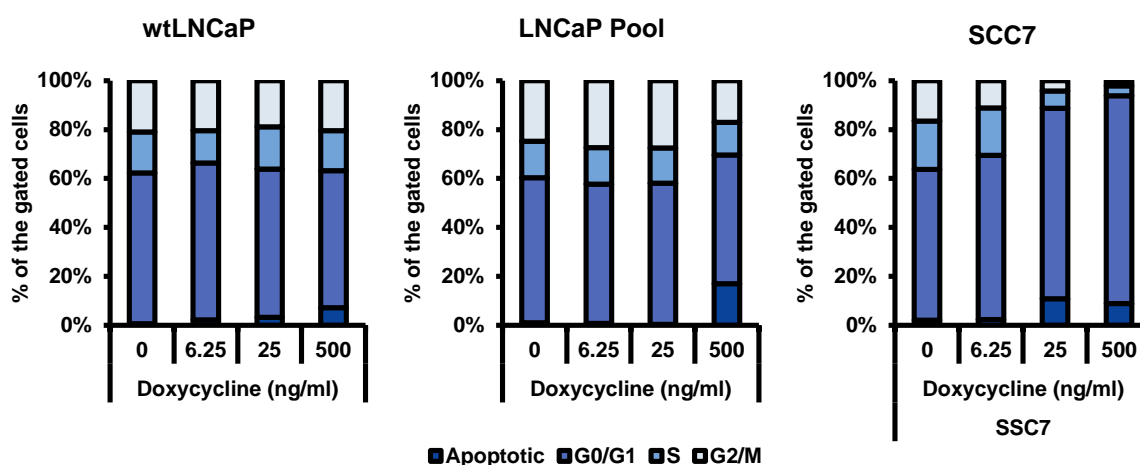


Figure 3-18: Cell cycle distribution of ARV7 expressing LNCaP cells.

We then confirmed the arrest in G₀/G₁ state by quantifying the cells grown in different concentrations of doxycycline for 3 days as described in section 2.2.4.12. In this we observed a dose-dependent decrease in cell viability in upon ARV7 expression in LNCaP cells (Figure 3-19).

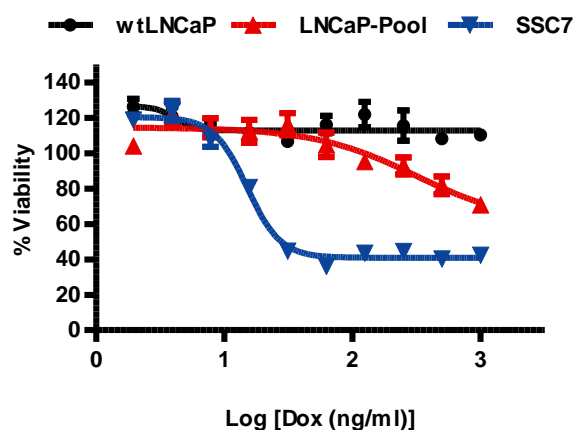


Figure 3-19: Cell viability in ARV7 expressing LNCaP cells.

The cells were treated with the indicated doses of Dox and cell viability, measured by MTS assay, was detected 3 days after treatment.

In a heterogeneous pooled population of ARV7 transduced LNCaP cells show intermediate levels of change in the senescence markers, i.e., increase in SA-β-gal staining (Figure 3-17) G1/S cell cycle arrest (Figure 3-18) and decrease in proliferation (Figure 3-19). However, in SCC7, the change in the markers is more significant.

To demonstrate that the senescence phenotype was not unique to the single cell clone selected, we tested 27 other single cell clones. The expression levels of ARV7 were determined by western blotting (**Figure 3-9**) and senescence was quantified by β -galactosidase staining at 28 different single cell clones treated with doxycycline (minimum 100 cells/condition). We found that the observed senescence is not unique to SCC7 and that the percentage of senescence was strongly correlated to the level of ARV7 expression (**Figure 3-20**).

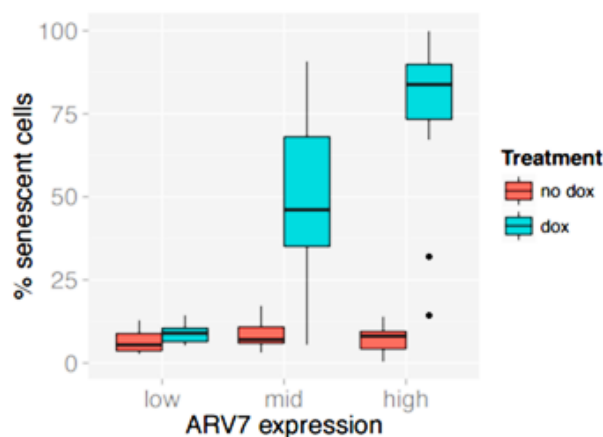


Figure 3-20: ARV7 expression correlates to percentage of senescent cells.

3.2.2.9 G_0/G_1 arrest at cell cycle is permanent

Our studies demonstrated that ARV7 expression causes LNCaP cells to accumulate at G_0/G_1 , stain for SA- β -gal and have a marked decrease in proliferation. We wondered if this was due to senescence or quiescence. Quiescence would allow the recovery of the phenotype after removal of induction; thus, if doxycycline was removed the cells should transition from G_0/G_1 and decrease SA- β -gal staining.

To test this, ARV7 was induced for 24 h and the medium was changed to remove doxycycline. Following 72 h recovery, the level of ARV7 decreased and AR expression was reconstituted (**Figure 3-21**). However, the senescence phenotype was retained in the majority of the population (**Figure 3-21**, **Figure 3-22**, **Figure 3-23**) demonstrating that the proliferation arrest is not quiescence.

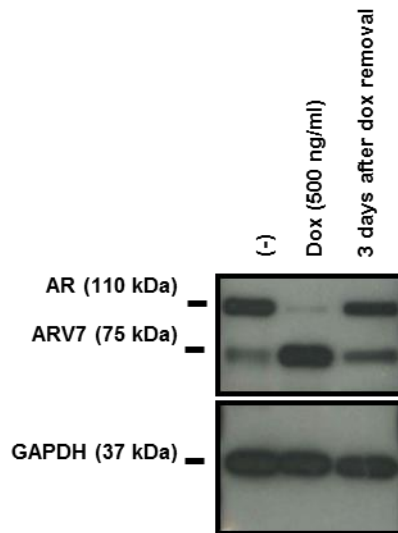


Figure 3-21: Recovery of AR and ARV7 protein levels after Dox removal. Cells were treated with 500 nM doxycycline for 24 h. After Dox treatment, we changed the medium to Tet-free media and incubated the cells for 72 h. Following recovery (96 h after t=0) we assessed the senescence markers in the cells.

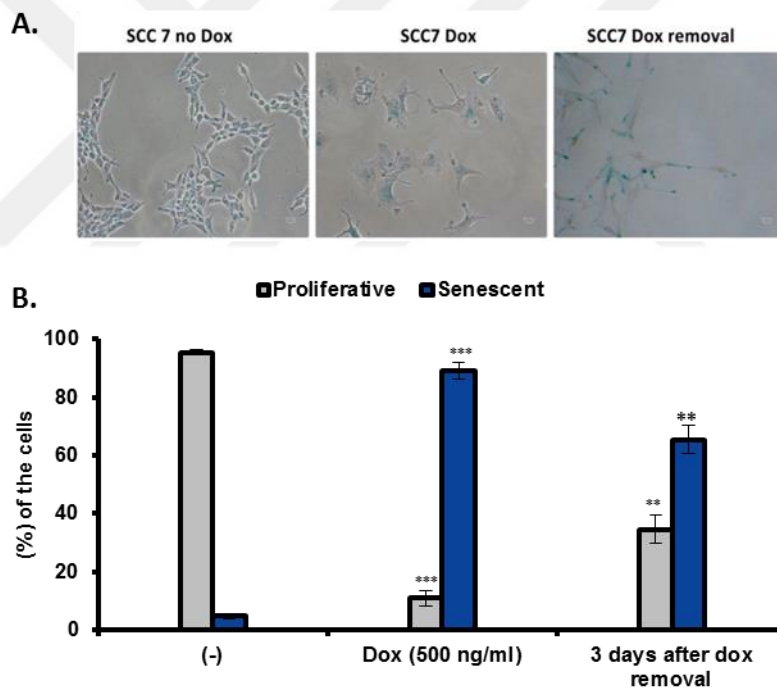


Figure 3-22: SA β -gal staining in SCC7 after Dox removal. **A.** SA β -gal staining in SCC7 after Dox removal. The pictures were taken in 20X objectives. **B.** Quantification of senescent cells. The experiment was done in triplicates and for every condition, at least 100 cells were counted. All the samples were compared to negative control. (* for $p < 0.05$, ** for $p < 0.01$, *** for $p < 0.001$)

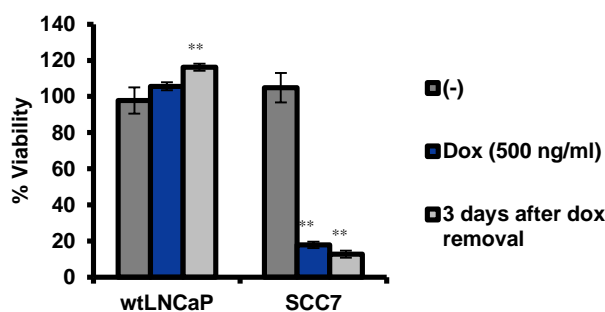


Figure 3-23: Viability of wtLNCaP and SCC7 cells after dox removal. The cell viability measured by MTS assay. The comparisons were made within wtLNCaP or SCC7. (* for $p < 0.05$, ** for $p < 0.01$, *** for $p < 0.001$)

3.2.2.10 Senescence is not due to decrease in expression of $AR^{full-length}$

As previous studies have shown that androgen deprivation can induce cellular senescence we wanted to confirm that the ARV7-induced senescence was not due to the suppression of $AR^{full-length}$. Therefore, we cloned $AR^{full-length}$ into pLIX_402 backbone using the LR recombination reaction (2.2.2.7.4) and transduced Tet-inducible ARV7 LNCaP cells with the pLIX_402- $AR^{full-length}$ lentiviruses. When these cells were treated with doxycycline, there is exogenous expression of both ARV7 and $AR^{full-length}$ (Figure 3-24, Figure 3-25). Demonstrating that the senescence is not due to decreased expression of $AR^{full-length}$, even when AR expression is maintained the cells still demonstrated a senescence cellular morphology and markers of senescence including decrease in proliferation (Figure 3-26), cell cycle arrest at G_0/G_1 (Figure 3-27). Overall, this suggests that increased ARV7 expression in LNCaP cells induce cellular senescence independent of $AR^{full-length}$ expression.

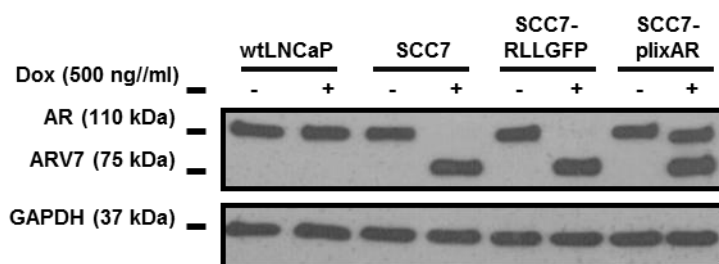


Figure 3-24: Protein levels of $AR^{full-length}$ and ARV7 after co-transduction of Tet-on AR & Tet-on ARV7.

The cells were treated with doxycycline for 24 h and lysates were collected for protein characterization. GAPDH was used as internal control.

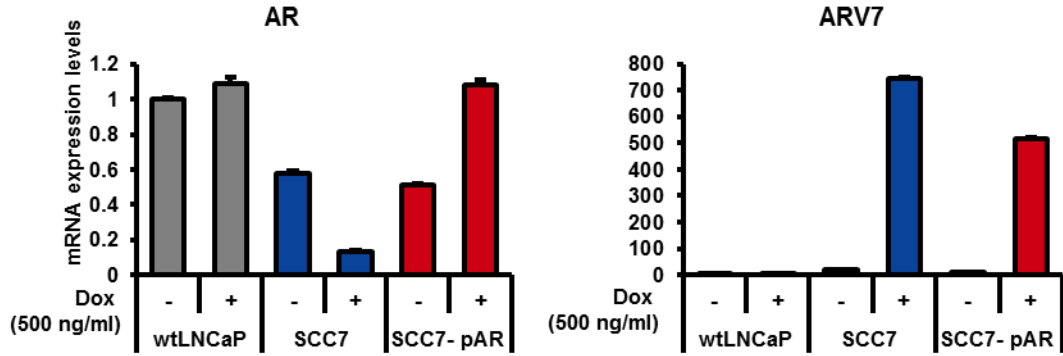


Figure 3-25: mRNA quantification of AR and ARV7 levels with RT-PCR in wtLNCaP, SCC7 and SCC7 cells expressing inducible AR^{full-length}.

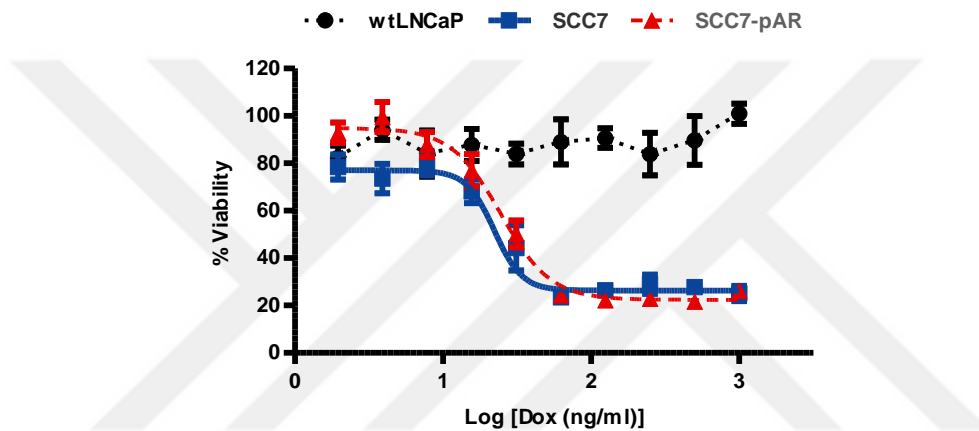


Figure 3-26: Viability of treated cells measured by the MTS assay.

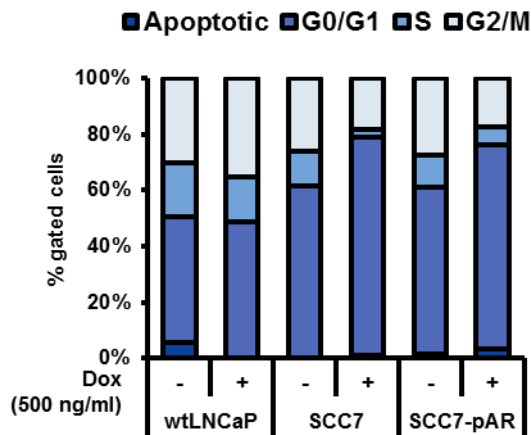


Figure 3-27: Cell cycle distribution of AR recovered cells.

3.2.2.11 Activation of tumor suppressor networks in ARV7 expressing LNCaP cells

The activation of senescence is commonly mediated by the p53 and p16INK4A–RB signal transduction cascades [100, 101]. Increased p53 p16INK4A–RB activity results in increase in the cyclin-dependent kinase (CDK) inhibitors p16, p15, p21, and p27 [100, 101]. Activation of CDK inhibitors result in inhibition of cyclin dependent kinases and eventually leading to hypophosphorylation of Rb [102]. Similarly, following expression of ARV7 in LNCaP cells we observed increased transcription of p14, p16, and p21 (**Figure 3-28**), and decreased levels of Cyclin D1 and E2F (**Figure 3-29**). Matching the previously observed accumulation of cells in G₁/G₀, there was a dramatic decrease in Rb phosphorylation in ARV7 expressing cells (**Figure 3-30**).

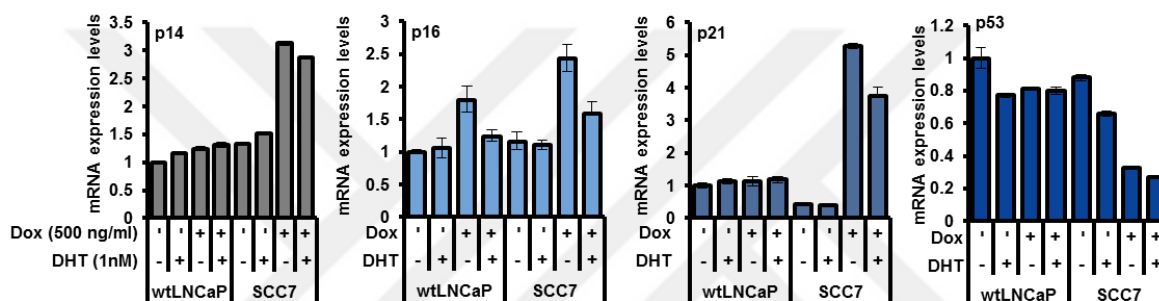


Figure 3-28: mRNA expression levels of tumor suppressors in wtLNCaP and SCC7 cells with Dox and DHT treatment.

mRNA expressions of p14, p16, p21, p53 and GAPDH in cells were detected by qRT-PCR. GAPDH was used as internal control. Fold change of each mRNA transcript in each condition was relative to that of wtLNCaP cells which were treated with neither doxycycline nor DHT.

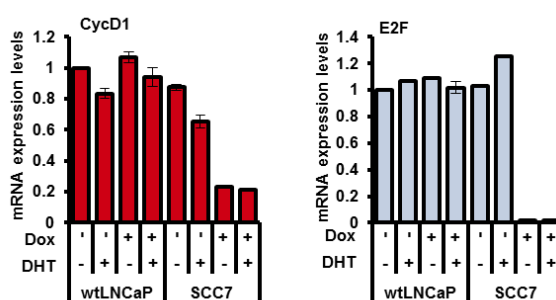


Figure 3-29: mRNA expression levels of genes controlling G₁/S transition.

mRNA expressions of CycD1, E2F and GAPDH in cells were detected by qRT-PCR. GAPDH was used as internal control. Fold change of each mRNA transcript in each condition was relative to that of wtLNCaP cells which were treated with neither doxycycline nor DHT.

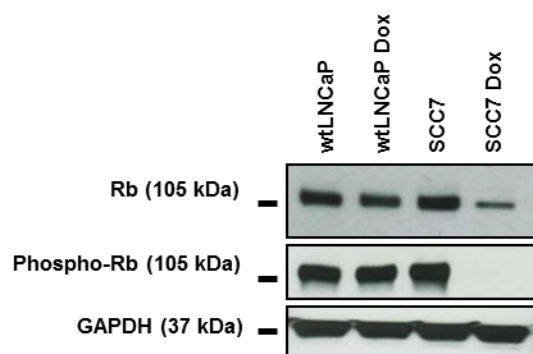


Figure 3-30: The levels of phosphorylated Rb protein upon ARV7 expression. Cells were treated with doxycycline for 24 h and lysates were prepared for protein characterization. GAPDH was used as internal control.

3.2.2.12 Assessment of DNA Double-Strand-Breaks (DSB) in ARV7 expressing cells

H2AX is found in the histone octamer in nucleosomes. Kinases including ataxia telangiectasia mutated (ATM) and ATM-Rad3-related (ATR) of the PI3K pathway phosphorylates H2AX variant at the γ position in order to mark regions for DNA repair [116, 141, 142]. Oncogene-driven hyper-replication or ionizing radiation can induce double-strand breaks in DNA and results in γ H2AX foci formation on DNA, which can be used as indication DSBs. Hence, immunofluorescence against γ -H2AX is commonly used to quantify DSBs in cells [141]. Previously it has been shown that that androgen stimulation promotes co-recruitment of androgen receptor and topoisomerase II beta (TOP2B) to sites of TMPRSS2-ERG genomic breakpoints, and it triggers TOP2B-mediated DSBs that lead to recombination [143]. Similarly, since ARV7 is constitutively active isoform, we have determined if ARV7 expressing LNCaP cells would show DNA damage response.

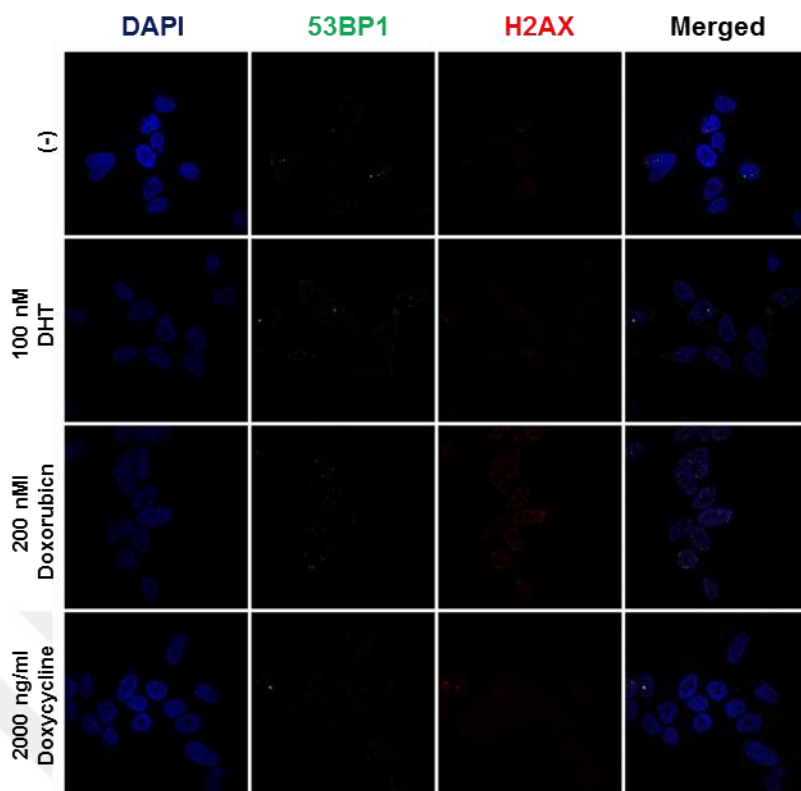


Figure 3-31: DNA double-strand break (DSB) foci detected via H2AX/53BP1 co-staining. (green=53BP1, red=H2AX) for LNCaP cells cultured under the indicated conditions.

We treated these cells as indicated based on previously published work (DHT for 2 h, doxorubicin for 12 h, and doxycycline for 24 h) and did immunofluorescence for γ H2AX and 53BP1 to detect DSBs (**Figure 3-31**). In doxorubicin-treated wtLNCaP cells, the number of γ -H2AX foci per cell increases upon doxorubicin treatment and the foci is colocalized with p53 binding protein 53BP1. Treatment of wtLNCaP cells with 100 nM DHT for 2 h also increases the number of foci per cell, but the increase is not as much as that induced by doxorubicin. As expected, we did not observe an increase in the γ H2AX foci in doxycycline induced wtLNCaP cells.

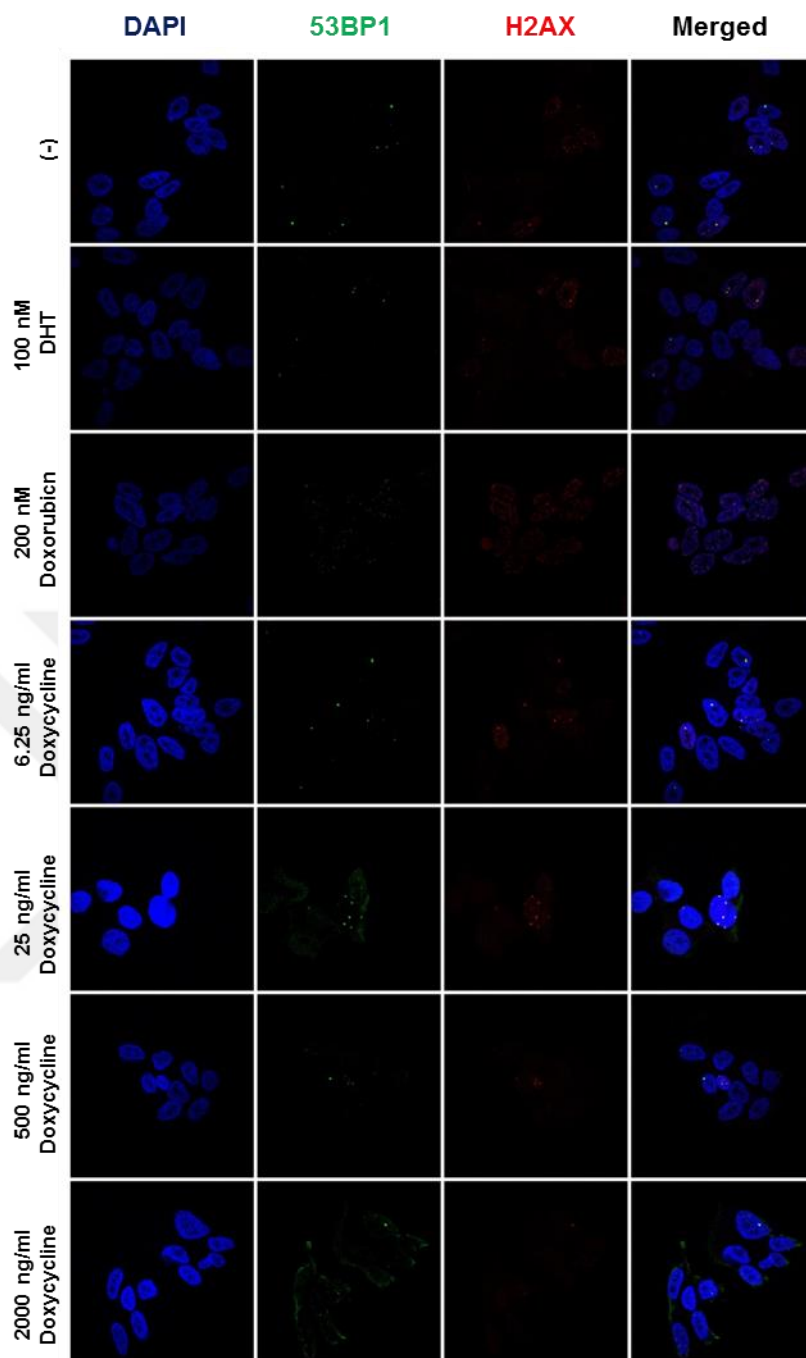


Figure 3-32: DNA double-strand break (DSB) foci detected via H2AX/53BP1 co-staining. (green = 53BP1, red = H2AX) for SCC7 cells cultured under the indicated conditions.

Next, we have detected the effect of ARV7 expression on gamma-H2AX-foci formation in wtLNCaP cells by treating SCC7 cells with different concentrations of doxycycline (**Figure 3-32**). Interestingly we observed no significant change in the number of co-stained foci in ARV7 expressing single cell clones. In addition, no senescence associated heterochromatic foci was formed in response to Dox treatment.

3.2.2.13 Generation of DNA Binding Mutant of pLIX402 ARV7

Our previous data demonstrated that ARV7 expression results in senescence in LNCaP cells. To clarify if this occurs due to protein expression or transcriptional activity of ARV7 we generated a mutation in DNA binding domain of ARV7. If senescence is caused by transcriptional activation, then cells with mutant ARV7 should not enter senescence. Therefore, using a Q5 site-directed mutagenesis kit we mutated two nucleotides of ARV7 (A596T/S597T) in the the pENTR1A ARV7 plasmid (**Table 6**) [24]. Following confirmation by sequencing, the ARV7^{A596T/S597T} was recombined into the pLIX402 plasmid by LR reaction and then packaged into lentiviruses as previously described (**2.2.4.2**).

The site of mutation was validated by sequencing and pENTR1A ARV7^(A596T/S597T) was recombined into pLIX402 plasmid using LR Clonase kit (**2.2.2.7.4**).

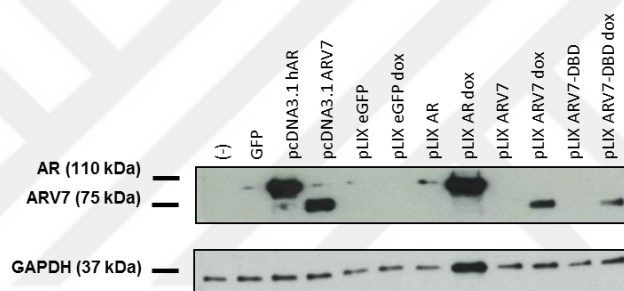


Figure 3-33: AR and ARV7 expression in transduced 293T cells.

pCDNA3.1 AR and pCDNA3.1 ARV7 were transfected into cells with fugene as a positive control. Cells were treated with doxycycline for 24 h and lysates were prepared for protein characterization as described in section **2.2.3**. GAPDH was used as internal control.

To test the expression and transcriptional activity of this mutant ARV7^(A596T/S597T), 293T cells were transduced with lentiviruses encoding pLIXAR, pLIXARV7, pLIX ARV7^(A596T/S597T) and pLIX GFP lentiviruses and then selected with puromycin. Western blotting of the cellular lysates demonstrated that transduced cells expressed AR, ARV7 and ARV7^(A596T/S597T) when induced with doxycycline and that the mutation did not significantly affect expression (**Figure 3-33**). 293T cells transduced with pLIX lentiviruses were transfected with ARR3TK-luciferase reporter plasmid and then assessed for AR transcriptional activity. AR^{full-length} was transcriptionally active in the presence of testosterone, while constitutively active ARV7 was transcriptionally active independent of presence of testosterone (**Figure 3-34**). Importantly our ARV7^(A596T/S597T) mutant was transcriptionally inactivity, indicating that transcriptional activity of ARV7 is dependent on DBD.

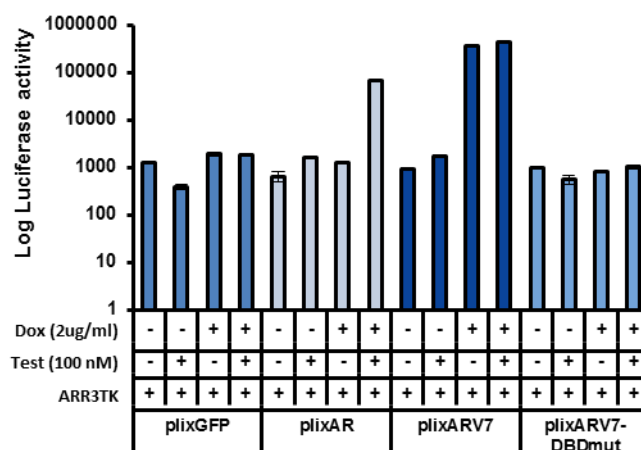


Figure 3-34: Transcriptional activity of pLIX constructs shown by luciferase assay.

3.2.2.14 Generation of ARV7-DBD expressing single cells of LNCaP cells.

LNCaP cells transduced with pLIX-ARV7 and pLIX ARV7^(A596T/S597T) lentiviruses were tested for ARV7 expression (**Figure 3-35**). Both the ARV7 and ARV7^(A596T/S597T) could be expressed in LNCaP cells following induction with doxycycline.

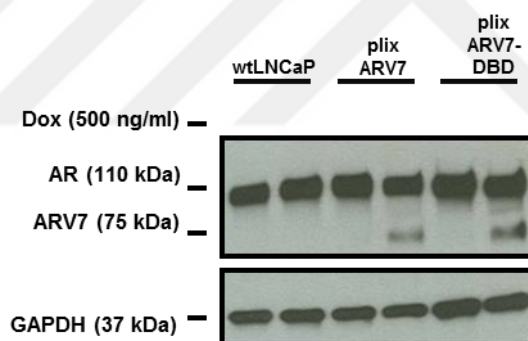


Figure 3-35: ARV7 and ARV7-DBD expression in LNCaP cells.

Western blotting of the lysates collected after transduction, with and without doxycycline (500 nM) treatment for 24 h. (Antibody dilutions used were as follows: AR-N20, 1:1000; GAPDH, 1:4000; 1:4000 anti-rabbit HRP-conjugated secondary antibody).

After validation of expression of ARV7-DBD expression in LNCaP cells, we did serial dilution to isolate single cell clones of LNCaP expressing ARV7-DBD in cells. Four single cell clones expressing DBD-mutant ARV7 were isolated (**Figure 3-36**) and Colony #2 was selected for further characterization.

The ARV7^(A596T/S597T) expressing single cell clones of AR expression was not significantly affected by ARV7 expression (**Figure 3-36, Figure 3-37**) with no significant changes in

morphology, proliferation and SA-β-gal stained cells. These results demonstrate that the senescence phenotype is caused by ARV7 transcriptional activity.

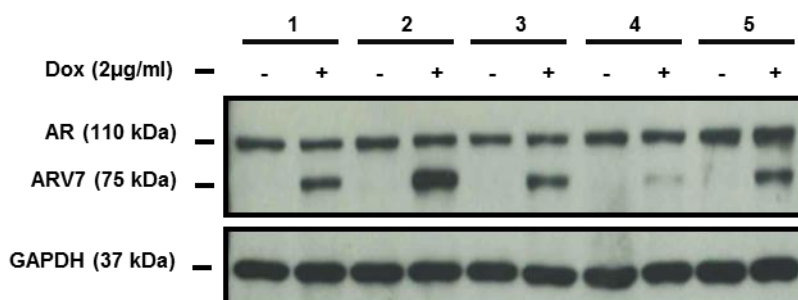


Figure 3-36: Single cell clones of ARV7-DBD expressing LNCaP cells. Single cell clones were treated with doxycycline for 24 h and lysates were prepared for protein characterization as described in section 2.2.3. GAPDH was used as internal control.

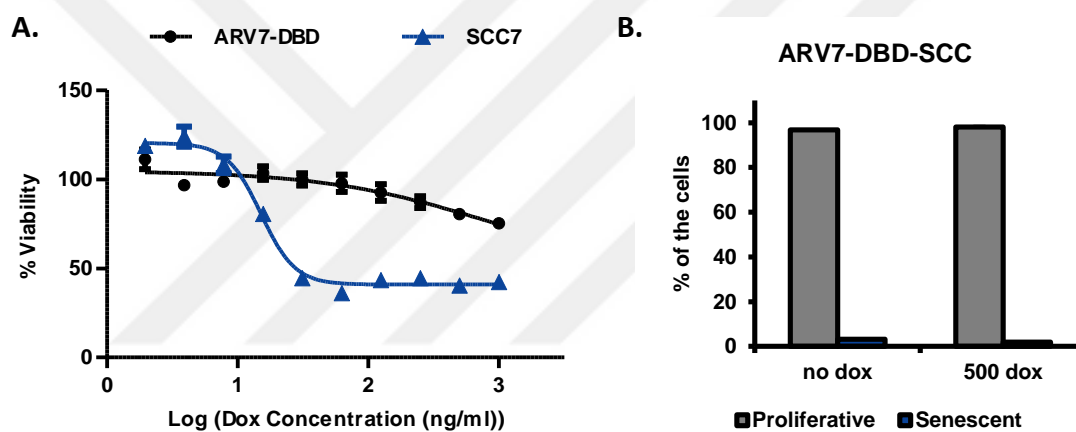


Figure 3-37: Cell viability (A) and SA-β-gal staining (B). Cell viability (A) and SA-β-gal staining (B) in LNCaP ARV7^(A596T/S597T) colony #2 response to doxycycline.

3.2.2.15 Testing ARV7 resistant single cell clones

Our results contrast clinical studies that demonstrate ARV7 correlates to prostate cancer progression and antiandrogen resistance (1.1.6). We proposed that expression of the variants may act as a “barrier” that the cancer cells must overcome in an androgen-independent environment. Therefore, by isolating single cell clones we aimed to find colonies that expressed ARV7 but were resistant to senescence. Among 28 different single cell clones tested (3.2.2.3), two outlier colonies (SSC22 and SSC23) expressed high levels of ARV7 but showed very low SA-β-gal (Figure 3-16).

Functional Characterization of Androgen Receptor Variant ARV7

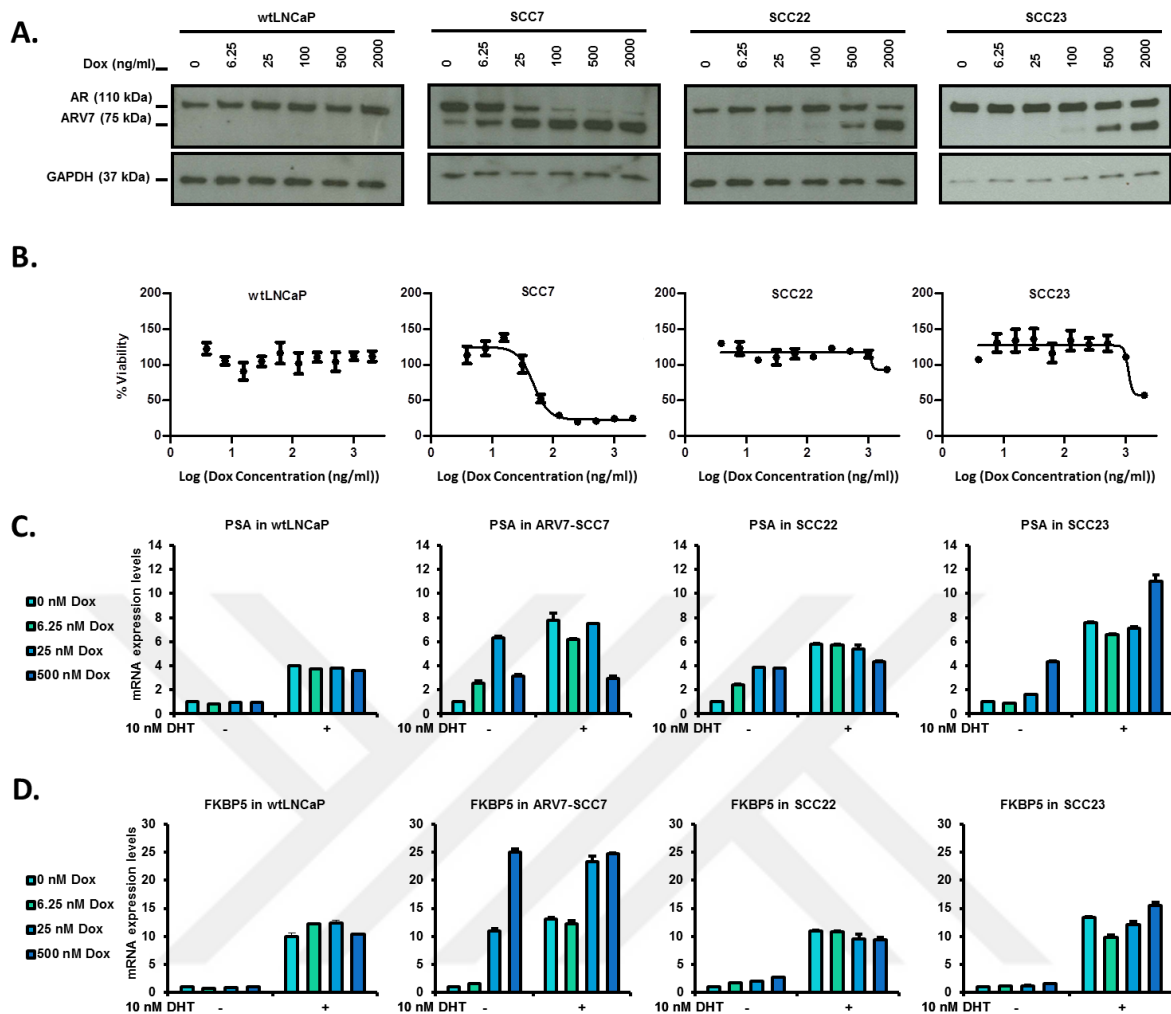


Figure 3-38: Characterization of SCC22 and SCC23.

ARV7 expression in wtLNCaP, SCC7 and SCC23 cells was tested by western blotting (**Figure 3-38-A**). Increasing concentrations of doxycycline resulted in an increase of ARV7 in SCC7, SCC22, and SCC23 cells but the level of ARV7 expression at low doxycycline concentration in SCC22 and SCC23 cells was less than that of SCC7 treated with the same concentration. **Figure 3-38-B** shows proliferation of these cells in response to ARV7 expression. Increased concentrations of doxycycline did not alter the viability of wtLNCaP cells, while there was a dose-dependent decrease in viability of SCC7 cells ($IC_{50} \sim 50nM$). As previously described, when the ARV7 is expressed the AR^{full-length} protein decreases. For SCC22 and SCC23 clones, cellular proliferation only slightly decreased at very high concentration of doxycycline. The transcriptional activity was tested of AR and ARV7 in wtLNCaP, SCC7, SCC22 and SCC23 cells with and without DHT (**Figure 3-38-C and -D**). In wtLNCaP PSA expression increased by 4 fold while FKBP5 expression show 10-fold increase upon 10 nM DHT treatment cells. Importantly, there was no increase in PSA and

FKBP5 with doxycycline with wtLNCaP cells. Treatment of SCC7 cells with increasing concentration of doxycycline resulted in increased PSA and FKBP5 expression even if the cells are not stimulated by DHT. Stimulation of SCC7 cells with 10 nM DHT increases the mRNA fold expression up to 8 fold. The PSA expression increased significantly with increasing concentrations of doxycycline in the absence of DHT while FKBP5 expression shows dose-dependent increase, with and without DHT stimulation. The response of SCC22 cells to doxycycline treatment is similar to SCC7 cells but to a lesser extent. In the absence of DHT, the levels of PSA increase until the doxycycline results in mainly ARV7 expression. In the presence of DHT, the gradual increase in the PSA mRNA fold expression is not seen, being at most 6-fold. ARV7 in SCC22 cells affect FKBP5 expression levels only in the absence of doxycycline, where it results in a slightly gradual increase in FKBP5, in a dose-dependent manner. SCC23 cells respond to doxycycline and DHT stimulation differently. The levels of PSA increase gradually in the presence or absence of DHT stimulation, but the increase is more in the presence of DHT. On the other hand, ARV7 expression results in increased FKBP5 mRNA expression only in the cells treated with DHT.

3.2.3 Characterization of effect of ARV7 on other prostate cancer cell lines

To determine if expression of ARV7 causes cellular senescence in other prostate cancer cell lines we generated inducible ARV7 expression in androgen independent, androgen dependent, normal and ARV7 expressing prostate cell lines (**Table 15**). We tested the effect of ARV7 in PC3, LNAI and LNCaP-Abl cell lines (androgen-independent cells), RWPE1 and BPH1 (normal prostate cells), and 22RV1 (ARV7 expressing prostate cell lines). Cells were transduced with lentiviruses of CMV-eGFP, pLIX-eGFP, pLIXAR, pLIX ARV7 and stable cell lines were generated. All the experiments were done in pooled population and no single cell clones were isolated.

Table 15: Properties of common prostate cancer cell lines used in this study.

Name	Source	AR expression	PSA expression	Androgen sensitivity
LNCaP	Lymph node	Yes	Yes	Yes
PC3 [144]	grade IV bone metastasis in a 62-year-old Caucasian male with prostate cancer.	No	No	No
RWPE1 [145]	human prostatic epithelium (HPE) cell from the peripheral zone	Yes	Yes	Yes
BPH1[146]	benign prostatic hypertrophy or hyperplasia (BPH) tissues obtained through transurethral resection	No	No	Yes
LNAI [147]	xenograft tumors of the androgen-dependent LNCaP cell line	Yes	Yes*	No
22RV1 [148]	xenograft CWR22R isolated from a patient with bone metastasis	Yes	Yes	Yes
LNCaP-Abl[149]	LNCaP-derived cell line	Yes	Yes*	No

* LNAI and LNCaP-Abl cells are androgen independent cells but they still have AR expression. Since they are grown in androgen free media (charcoal stripped serum) they won't have PSA expression as long as the medium is provided with androgens.

3.2.3.1 ARV7 expression in PC3 cells

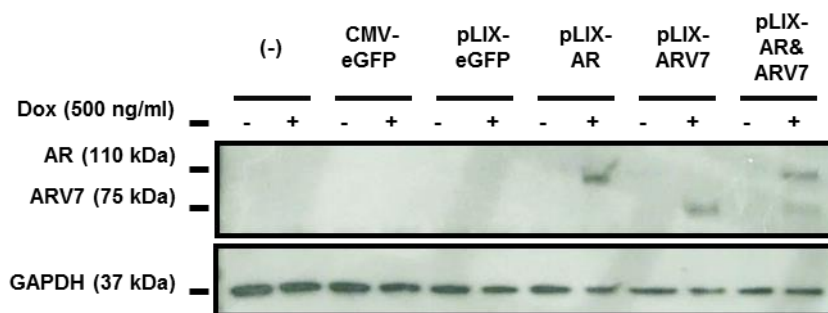


Figure 3-39: Protein levels of AR and ARV7 in transduced PC3 cells. Cells were treated with doxycycline for 24 h and lysates were prepared for protein characterization. GAPDH was used as internal control.

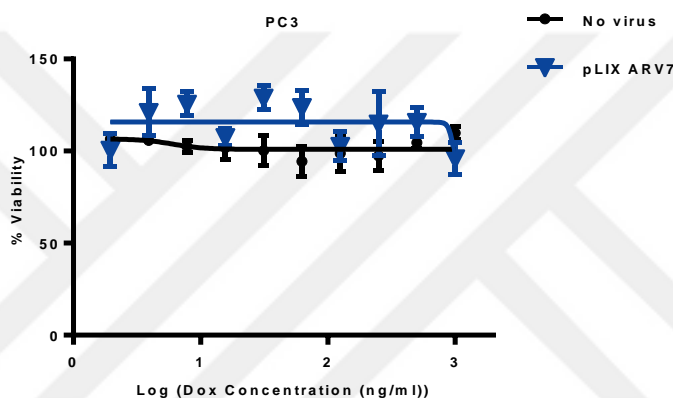


Figure 3-40: Viability of PC3 cells that express ARV7 upon Doxycycline treatment. The cells were treated with the indicated doses of Dox and cell viability, measured by MTS assay, was detected 7 days after treatment.

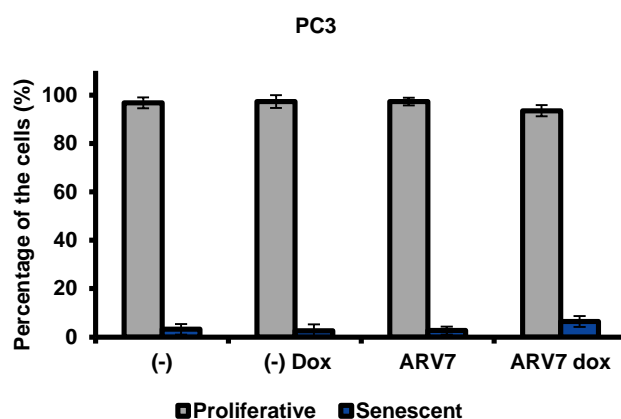


Figure 3-41: The percentage of senescent cells in PC3 cells. In X-gal staining, each condition was seeded in triplicates. Following to 24 h doxycycline treatment for the indicated conditions, the cells were stained overnight for β -galactosidase activity. Quantification was done as described (2.2.4.8). (* for $p < 0.05$, ** for $p < 0.01$, *** for $p < 0.001$).

3.2.3.2 ARV7 expression in RWPE1 cells

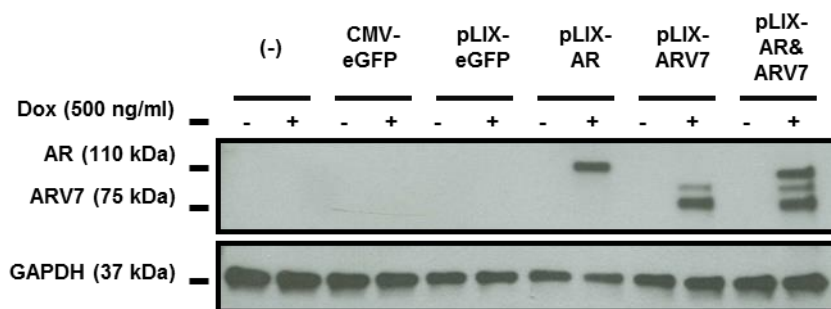


Figure 3-42: Protein levels of AR and ARV7 in transduced RWPE1 cells. Cells were treated with doxycycline for 24 h and lysates were prepared for protein characterization. GAPDH was used as internal control.

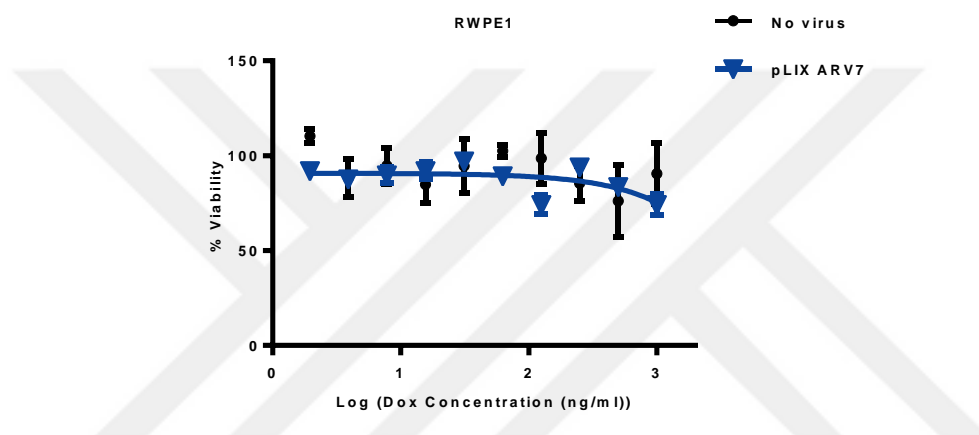


Figure 3-43: Viability of RWPE cells that express ARV7 upon Doxycycline treatment. The cells were treated with the indicated doses of Dox and cell viability, measured by MTS assay, was detected 7 days after treatment.

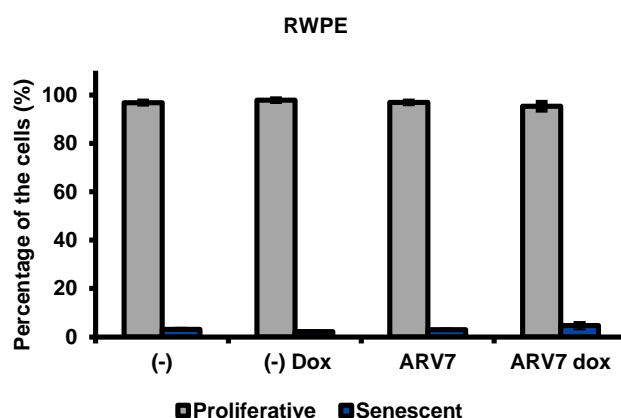


Figure 3-44: The percentage of senescent cells in RWPE1 cells. In X-gal staining, each condition was seeded in triplicates. Following to 24 h doxycycline treatment for the indicated conditions, the cells were stained overnight for β -galactosidase activity. Quantification was done as described (2.2.4.8). (* for $p < 0.05$, ** for $p < 0.01$, *** for $p < 0.001$).

3.2.3.3 ARV7 expression in BPH1 cells

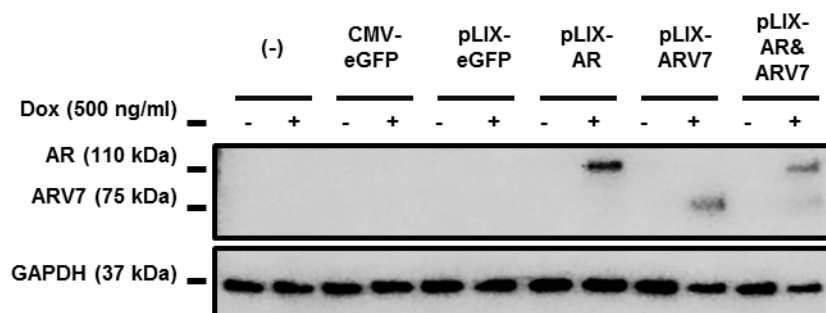


Figure 3-45: Protein levels of AR and ARV7 in transduced BPH1 cells. Cells were treated with doxycycline for 24 h and lysates were prepared for protein characterization. GAPDH was used as internal control.

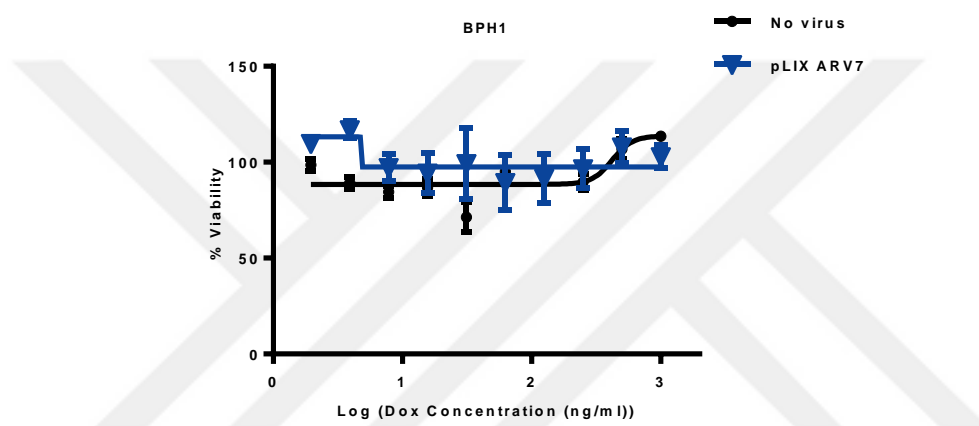


Figure 3-46: Viability of BPH1 cells that express ARV7 upon Doxycycline treatment. The cells were treated with the indicated doses of Dox and cell viability, measured by MTS assay, was detected 7 days after treatment.

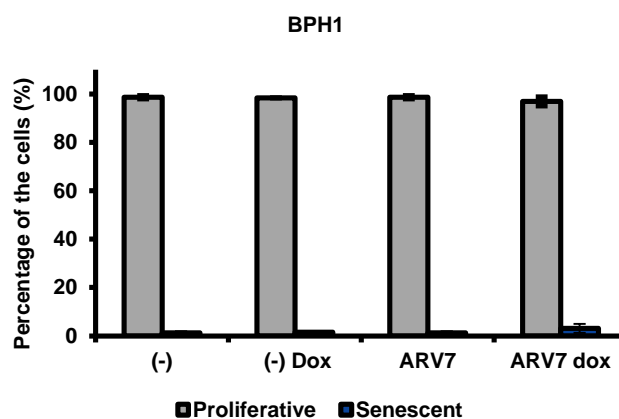


Figure 3-47: The percentage of senescent cells in BPH1 cells. In X-gal staining, each condition was seeded in triplicates. Following to 24 h doxycycline treatment for the indicated conditions, the cells were stained overnight for β -galactosidase activity. Quantification was done as described (2.2.4.8). (* for $p < 0.05$, ** for $p < 0.01$, *** for $p < 0.001$).

3.2.3.4 ARV7 expression in LNAI cells

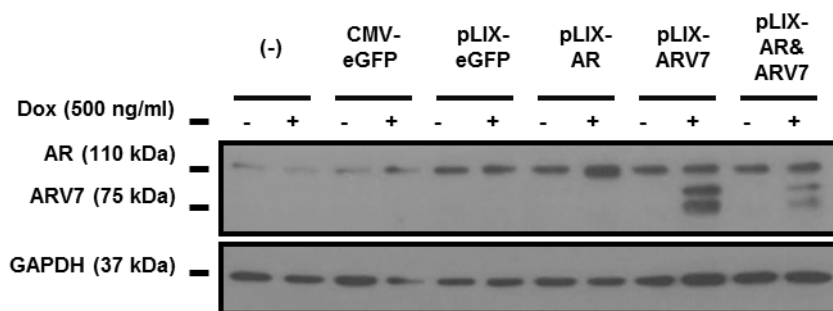


Figure 3-48: Protein levels of AR and ARV7 in transduced LNAI cells. Cells were treated with doxycycline for 24 h and lysates were prepared for protein characterization. GAPDH was used as internal control.

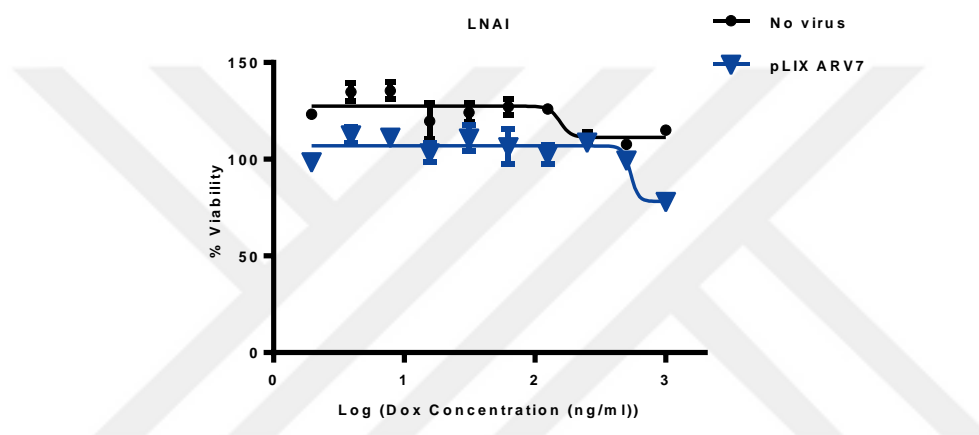


Figure 3-49: Viability of LNAI cells that express ARV7 upon Doxycycline treatment. The cells were treated with the indicated doses of Dox and cell viability, measured by MTS assay, was detected 7 days after treatment.

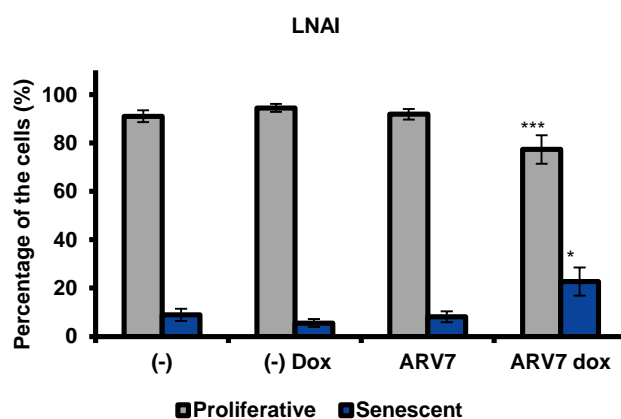


Figure 3-50: The percentage of senescent cells in LNAI cells. In X-gal staining, each condition was seeded in triplicates. Following to 24 h doxycycline treatment for the indicated conditions, the cells were stained overnight for β -galactosidase activity. Quantification was done as described (2.2.4.8). (* for $p < 0.05$, ** for $p < 0.01$, *** for $p < 0.001$).

3.2.3.5 ARV7 expression in 22RV1 cells

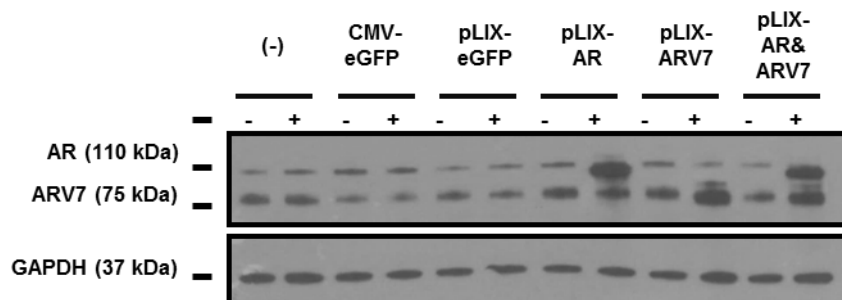


Figure 3-51: Protein levels of AR and ARV7 in transduced 22RV1 cells. Cells were treated with doxycycline for 24 h and lysates were prepared for protein characterization. GAPDH was used as internal control.

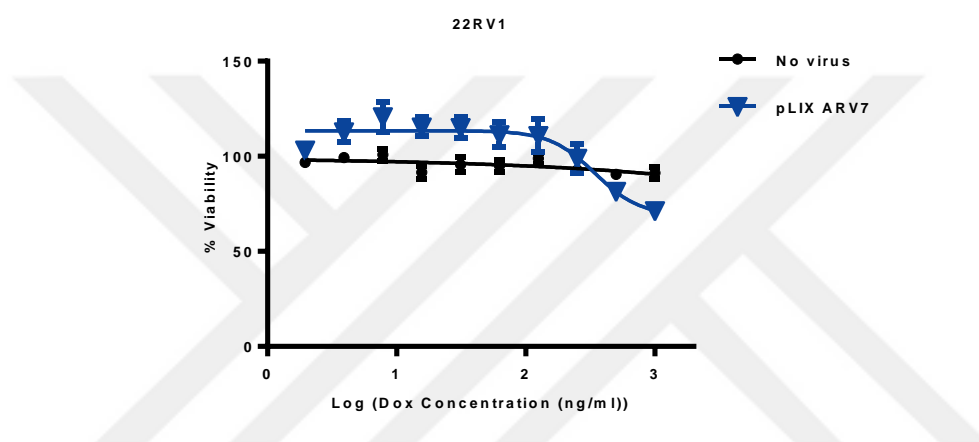


Figure 3-52: Viability of 22RV1 cells that express ARV7 upon Doxycycline treatment. The cells were treated with the indicated doses of Dox and cell viability, measured by MTS assay, was detected 7 days after treatment.

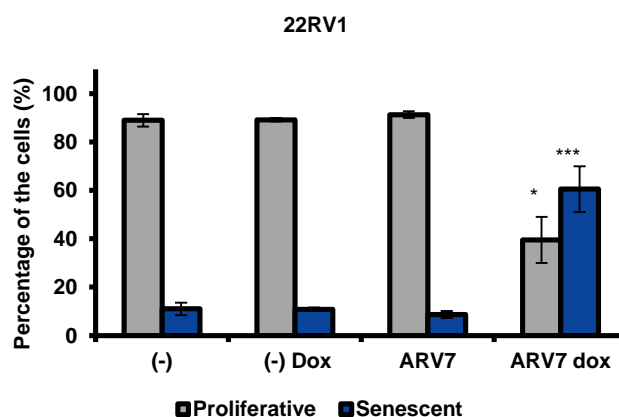


Figure 3-53: The percentage of senescent cells in 22RV1 cells. In X-gal staining, each condition was seeded in triplicates. Following to 24 h doxycycline treatment for the indicated conditions, the cells were stained overnight for β -galactosidase activity. Quantification was done as described (2.2.4.8). (* for $p < 0.05$, ** for $p < 0.01$, *** for $p < 0.001$).

3.2.3.6 ARV7 expression in LNCaP-Abl cells

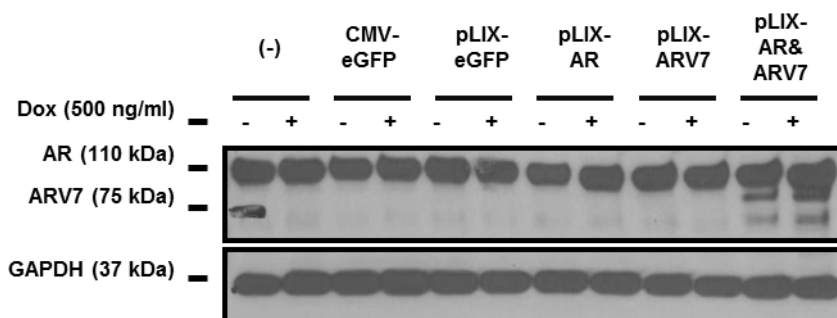


Figure 3-54: Protein levels of AR and ARV7 in transduced LNCaP-Abl cells. Cells were treated with doxycycline for 24 h and lysates were prepared for protein characterization. GAPDH was used as internal control.

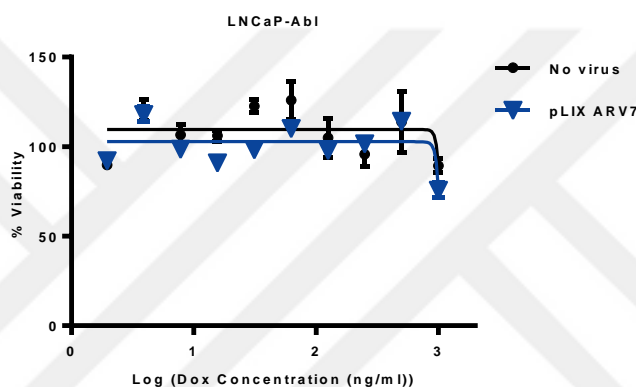


Figure 3-55: Viability of LNCaP-Abl cells that express ARV7 upon Doxycycline treatment. The cells were treated with the indicated doses of Dox and cell viability, measured by MTS assay, was detected 7 days after treatment.

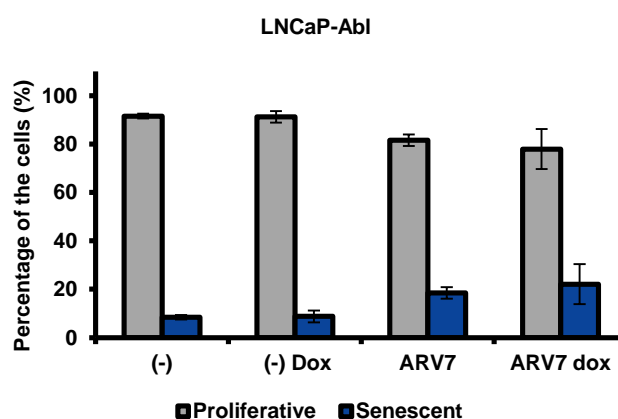


Figure 3-56: The percentage of senescent cells in LNCaP-Abl cells. In X-gal staining, each condition was seeded in triplicates. Following to 24 h doxycycline treatment for the indicated conditions, the cells were stained overnight for β -galactosidase activity. Quantification was done as described (2.2.4.8). (* for $p < 0.05$, ** for $p < 0.01$, *** for $p < 0.001$).

With each cell line, the expression of ARV7 proteins was quantified by western blotting (**Figure 3-39**, **Figure 3-42**, **Figure 3-45**, **Figure 3-48**, **Figure 3-51**, and **Figure 3-54**). Next the effect of ARV7 expression on these cells were tested by MTS assay on cellular proliferation and X-gal staining to see if the cells are undergoing cellular senescence upon ARV7 expression.

Interestingly, we did not observe a significant change in proliferation and senescence in PC3, RWPE1, BPH1 cells upon ARV7 expression. In contrast, 22RV1 and LNAI cells show a dramatic decrease in proliferation and a corresponding increase in senescence following ARV7 expression. There was a slight decrease in proliferation and an increase in percentage of senescent cells in ARV7 expressing LNCAP-Abl cells.



3.3 Discussion

Androgen deprivation therapy is the standard of care following surgery and radiation in patients with prostate cancer. Although ADT slows disease progression, the cancer often develops resistance to ADT. Interestingly, there is extensive evidence that the androgen receptor is still active despite castrate levels of androgens [36]. Several possible explanations have been proposed for this castrate resistance progression, including AR amplifications, AR point mutations which prevent binding of antiandrogens, epigenetic modifications, and presence of androgen receptor splice variants.

ARVs are C-terminally truncated splice variants the AR which show constitutive activity independent of presence of androgens [150]. ARV7 is the most commonly studied isoforms among these. ARV7 expression has been shown to correlate to resistance against AR antagonists Enzalutamide and Abiraterone [151].

To better understand the role of ARV's in prostate cancer progression we developed a tunable model of variant expression. Our studies demonstrated that ARV7 could be expressed and was enzymatically active. Surprisingly, in single cell clones we demonstrated that ARV7 induced p53 activity dependent premature senescence that permanently arrests the cells at a G₀/G₁ stage of cell cycle. This result was surprising as previous studies have linked ARV7 expression to prostate cancer proliferation in a castrate environment. Our system is partially in agreement with these results as at low levels of ARV7 expression, there was an increase in PSA levels and low levels of senescence. Moreover, while studies that have used a similar inducible model have not seen this phenotype they have only worked with pooled populations. Our data strongly suggests that it is helpful when when studying AR variants to work with a homogenous population.

Previous studies have linked ARV7 expression to castration resistance, due to its constitutive activity and ARV7 expression has been linked to Enzalutamide and Abiraterone resistance. Our system validates this information at low levels of ARV7 expression, i.e., PSA levels increase in ARV7 expressing cells. On the other hand, we have observed cellular senescence in high ARV7 expression condition or prolonged exposure to ARV7 expression. In heterogeneous population, there will be both cells that express low ARV7 and are antiandrogen resistance and those cells that express high ARV7 and are senescent. Since senescence is anti-proliferative, those cells that enter senescence will not be seen in the population compared to those by the cells which gain proliferation advantage upon ARV7

expression. This might explain why ARV7 is observed at extremely low levels in early stage prostate cancer, and only becomes prominent in environment whereby it is an evolutionary advantage (e.g. when patients are treated with antiandrogens). Those cells which do not enter into senescence will dominate the others. Similarly, we also identified two other single cell clones which express ARV7 in high levels but show low senescence. Although high ARV7 expressing in cells generally showed high levels of senescence, the presence these resistant cells might explain patients with high ARV7 expression. This behavior has also been observed in senescence driven by oncogene expression. While *myc* is required for the proliferation of many cancers, if expressed in fibroblasts the cells enter senescence.

We found that binding of ARV7 on DNA does not cause double stranded breaks on DNA. Previous study has shown that binding of AR upon DHT stimulation cause DNA double stranded breaks mediated by topoisomerase II beta (TOP2B) activity just after recruitment on DNA [143]. However, our results indicate that binding of ARV7 on DNA does not cause DNA damage, but the changes in the transcriptome upon ARV7 expression results in cellular stress leading to senescence.

Studies linking ARV7 expression to anti-androgen treatment have focused on the ARV7 expression in circulating tumor cells. It has been shown that patients with higher ARV7 expression had lower PSA in patients treated with Enzalutamide and Abiraterone [151]. Given that ARV7 expression is not observed in normal prostate condition, and requires activation of mechanisms that are not active in benign cells like alternative splicing, it is highly probable that the cells which have higher genomic instability due to increased tumorigenesis will express this non-naturally occurring splice isoform. Thus, the correlation between ARV7 expression and resistance might not be a fair comparison and resistance might be linked to another process which give rise to ARV7 expression instead.

Further, the studies suggesting that ARV7 expression can mediate EMT [152] are not supported by our work. Previous studies have linked EMT to taxane resistance but ARV7 expression did not cause resistance to taxanes, in a recently published study [153]. We found the increased expression of Vimentin and decreased expression of Snail but we did not propose an EMT due to this, as the levels of N-cadherin and E-cadherin were not changed significantly. In addition, Snail has been indicated to play role in cell survival and motility, and its role in inhibiting cellular senescence in metastatic cell lines has been shown [154] and Vimentin has been shown to be increased in senescent cells and it sequesters the increased

levels of p53 in cytoplasm [155]. Thus, the genes which were up and downregulated in EMT were modulated of cellular senescence.

Overall, our results suggest that the role of ARV7 in CRPC is not as straightforward as has been proposed. Although increased ARV7 expression levels may correlate to resistance to antiandrogens in patients, ARV7 can itself stop the growth of the cancer if expression is too high or if the cells are not tolerant of the level of activity.



Chapter 4: Structural Interaction of Androgen Receptor and Androgen Receptor Variant ARV7

4.1 Introduction

Nuclear receptors (NRs) are transcription factors regulated by ligand binding. They are critical in both human physiology and diseases. The transcriptional activation of some of the NRs, Androgen Receptor (AR), for example, are regulated by the binding of the ligand to the ligand binding domain (LBD) located at the carboxy-terminal domain (LBD). It was previously shown that, upon ligand binding, the AR rapidly undergoes an allosteric modification that allows the NTD and LBD to form an N-C intramolecular interaction [156]. Following nuclear localization the AR dimerizes via DNA binding domain, where it binds to major groove of DNA.

Given the truncation of the LBD in splice variant forms of AR, it is unclear if the variants can undergo a similar homodimerization or in fact they heterodimerize with the AR^{full-length}. Here we aim to show the putative inter or intramolecular interaction between ARV7 or AR^{full-length} and ARV7, through the measurement of FRET between fluorophores attached to the N terminal and C terminal of the two proteins.

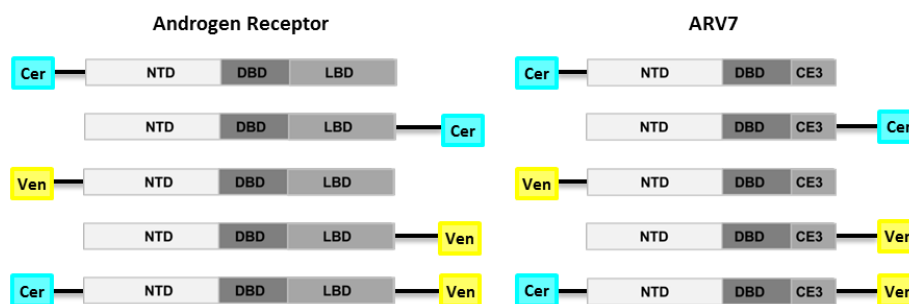


Figure 4-1: Cerulean and Venus fusion proteins used in this project.

Therefore, the specific aims of the project presented in this chapter are as follows:

- Generation of fusion AR^{full-length} and ARV7 with Cerulean and Venus fluorescent proteins FRET pairs (**Figure 4-1**)
- Expression of the constructs in 293T cells and validating the expression and transcriptional activity
- Studying the intramolecular ARV7, intermolecular ARV7 homodimerization and intermolecular ARV7 and AR^{full-length} interactions.

4.2 Results

4.2.1 Cloning of AR^{full-length} and ARV7 fusion constructs with Cerulean and Venus FRET pair

4.2.1.1 Cloning of Cerulean-AR-Venus and Cerulean-ARV7-Venus

To study the intramolecular interaction within AR, Cerulean and Venus proteins were cloned to the N and C-terminal of the AR^{full-length} and ARV7, respectively. In this the AR^{full-length} was cloned into pCR2.1®-TOPO® TA vector for subcloning (2.2.2.7.6). For generation of the fusion construct, pC17V vector (**Figure 2-4**) and AR containing pCR2.1®-TOPO® TA vector were digested with XhoI and SalI restriction endonucleases (2.2.2.6) and the backbone was ligated with the AR^{full-length}. Cerulean- ARV7-Venus construct was also generated following the same protocol. Following validation, the constructs were sequenced to confirm the correct identity.

4.2.2 Cloning of constructs for studying intermolecular interactions among AR and ARV7

To study the homodimer and heterodimer interactions between the proteins, Cerulean and Venus proteins are cloned to the N or C-terminal of the AR^{full-length} and ARV7. AR/ARV7-Venus fusion proteins was generated by amplifying AR and ARV7 (**Table 4**) and then cloning them into mVenusN1 plasmid. Cerulean-AR/ARV7 fusion proteins was generated by amplifying AR and ARV7 (**Table 4**) and then cloning into mCeruleanC1 plasmid. C-terminus Cerulean fusion proteins were generated by removal of AR and ARV7 from AR-Venus and ARV7-Venus and insertion into mCeruleanN1 plasmid. N-terminus Venus fusion proteins of AR and ARV7 were generated by removal of AR and ARV7 from Cerulean-AR and Cerulean-ARV7 and insertion into mVenusC1 plasmid.

4.2.3 Expression of FRET constructs in 293T cells

To test for expression, each FRET construct was transfected into 293T cells (2.2.4.5). Following transfection the lysates were collected for western blot (Figure 4-2).

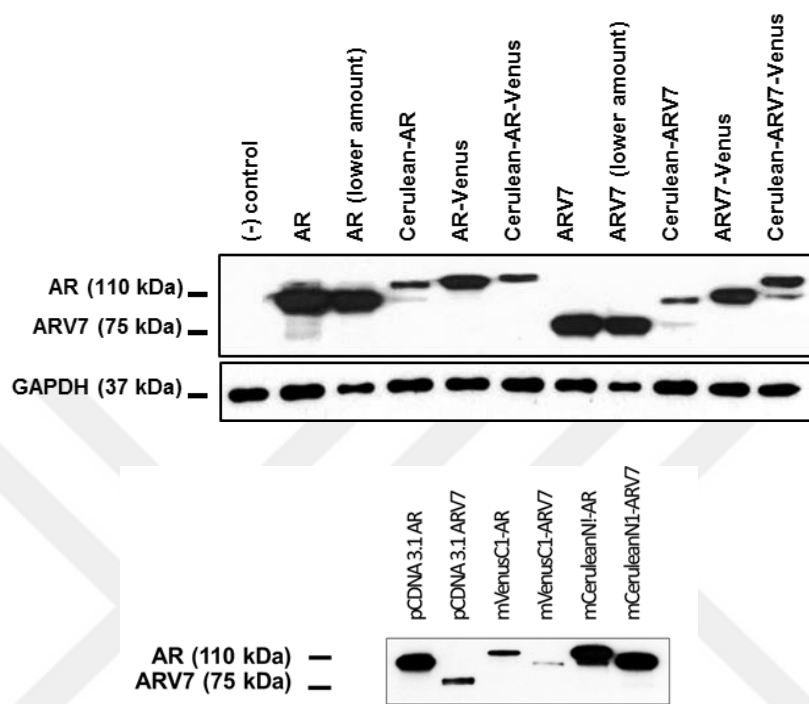


Figure 4-2: Expression of FRET constructs in 293T cells.

The fusion constructs were transfected into 293T cells in equal amount (2.2.4.5). The level of protein expression was detected by western blotting (2.2.3.2) Antibody dilutions used are listed in Table 8. pCDNA3.1 AR and pCDNA3.1 ARV7 plasmids were used as positive control for AR^{full-length} and ARV7 expression.

As the bands from transfection of positive controls were intense, the samples of them were also loaded in half amount to prevent improper comparison due to saturated bands. The constructs generated were folded properly and expressed in 293T cells. Overall, the constructs carrying fluorescent proteins at the C termini of AR or ARV7 were expressed more than those carrying fluorescent proteins at N-termini of AR or ARV7.

To check the transcriptional activity of AR and ARV7 constructs, we have transfected AR-null PC3 cells with each of the FRET fusion constructs and ARR3TK-luciferase reporter plasmid (Figure 4-3, Figure 4-4).

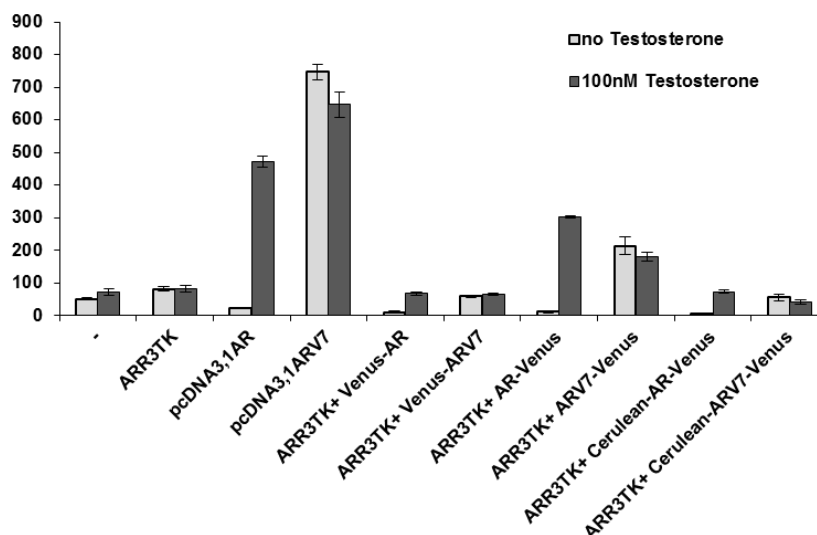


Figure 4-3: Transcriptional activity of Venus fusion constructs.

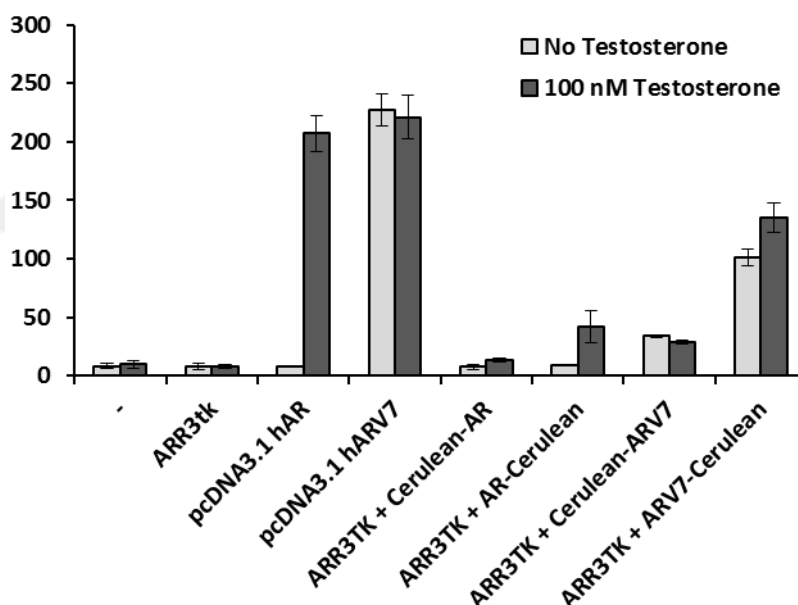


Figure 4-4: Transcriptional activity of Cerulean constructs.

Since ARV7 is a constitutively active isoform of AR, there is luciferase activity even in the absence of testosterone. The results are in agreement with western blot in that, the constructs carrying fluorescent proteins at the C termini of AR or ARV7 have higher transcriptional activity than those carrying fluorescent proteins at N-termini of AR or ARV7.

4.2.4 Measuring FRET intensity using live cell- imaging microscopy

In this work we wanted to study the interactions of AR and ARV7 using live cell FRET microscopy. First, we determined if we can measure actual FRET from recorded images, we used pC17V plasmid encoding Cerulean-Venus separated from each other by 17 amino-acid length as positive control. The **Figure 4-5** indicate the fluorescent intensity of pC17V transfected cells in YFP and CFP channel, and FRET signal after derivation of correction coefficients generated from Cerulean and Venus only transfected condition. FRET signal is indicated as heatmap blue indicate lowest measured FRET while yellow indicate the highest FRET.

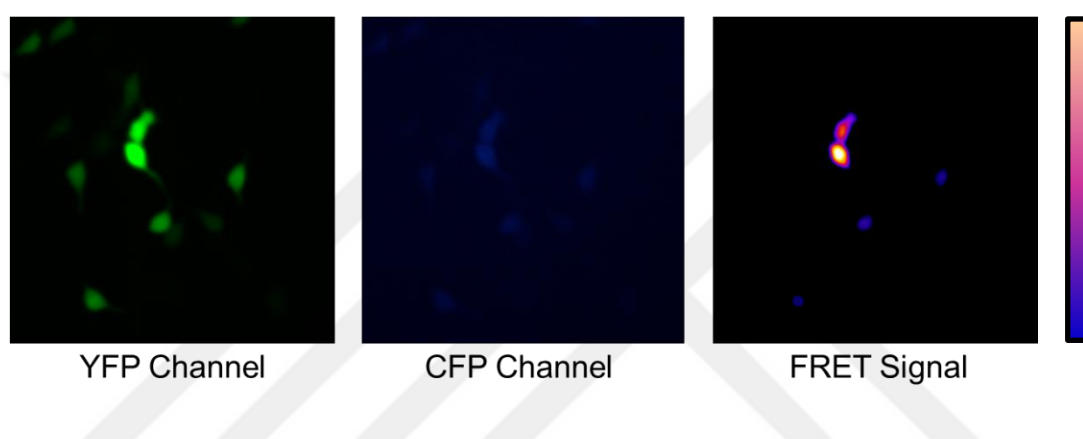


Figure 4-5: 293T cells transfected with pC17V plasmid. The images were recorded in 40X objectives in YFP, CFP, and FRET channel. FRET signal is colored as heat-map.

In order to quantify the FRET in our live cell imaging experiments, we developed a custom analysis pipeline in collaboration with Dr. Halil Bayraktar (2.2.5.1). This approach allows us to determine the FRET signal from each individual cell even as they grow and divide during the experiment.

4.2.5 Measurement of intramolecular and intermolecular AR^{full-length}

Before proceeding to study the interactions of ARV7 we next wanted to demonstrate that our system could quantify intramolecular interactions with AR^{full-length}. In this we transfected 293T cells with Cerulean-AR-Venus construct and performed live cell imaging experiment in Olympus Xcellence-RT microscope for 7 hours. Images were recorded in 5 min intervals. Two hours after the start of experiment, cells were treated with 1nM DHT to activate the AR. Following the experiment, image analysis was done in four steps: the image was segmented based on a threshold filter, jointed with a low pass Gaussian kernel filter to remove the pixel

noise (**Figure 4-6-A**), the cell coordinates were determined from the smoothed images (**Figure 4-6-B**), and finally the center position of each cell was located based on the local maxima in every frame. The tracking of individual cells were obtained by linking the displacement (mean square displacement) of each local maxima giving fluorescence intensity measured in three channels for each consecutive displacement (**Figure 4-6-C**). The intensity of each cell was determined from its local maxima and FRET intensity was measured by subtracting the multiplication of intensity measured in YFP channel and its correction coefficient and the multiplication of intensity measured in CFP channel (**Figure 4-6-D**).

A non-radiative fluorescence energy transfer from donor to acceptor was indicated if net FRET value is positive [138]. To prevent the difference in nFRET occurring only because of increased expression of interacting partners, the calculated nFRET value was normalized using correction coefficients of donor and acceptor fluorophores and is represented as normalized FRET (NFRET) [136]:

$$NFRET = \frac{nFRET}{\sqrt{I_{CFP} * I_{YFP}}}$$

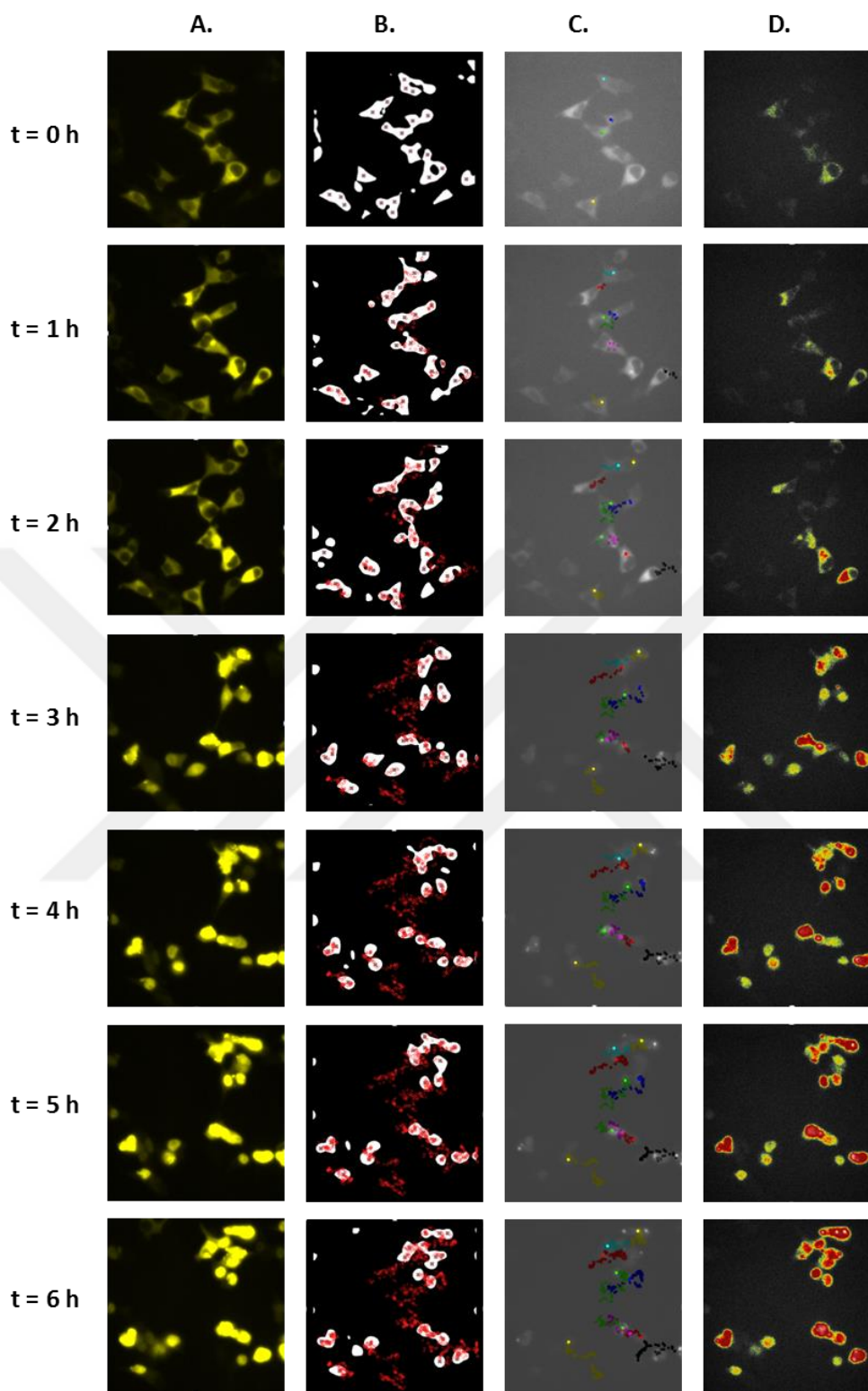


Figure 4-6: Single cell tracking steps of Cer-AR-Ven interaction.

A. Cer-AR-Ven in YFP channel. **B.** A mask generated from YFP images is used for area calculations and determination of migrational boundaries. **C.** Tracking of individual cells. **D.** Calculated FRET values are overlaid with bright-field images. Images were taken with 40X objectives.

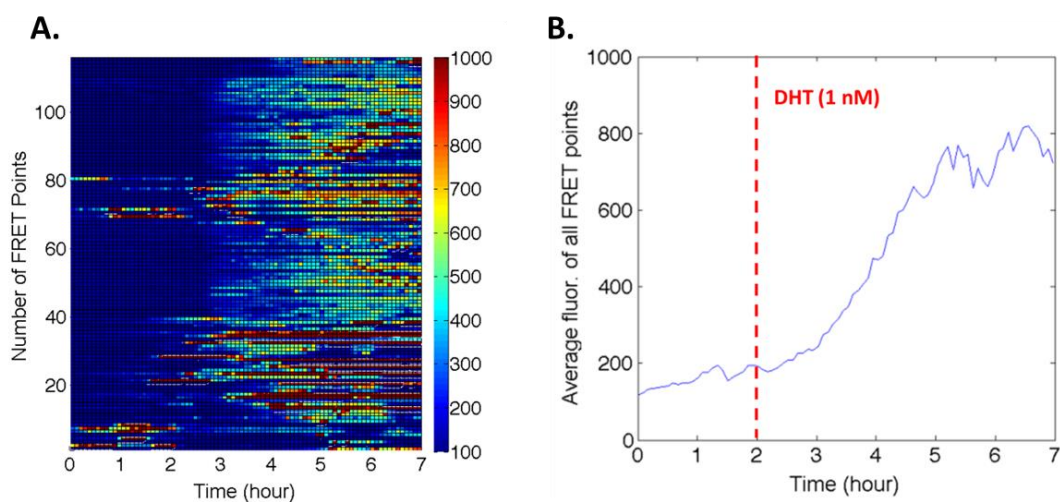


Figure 4-7: AR dimerization and NTD-to-LBD intramolecular interactions by FRET microscopy.

FRET intensity was calculated for every point, and the change in the intensity of different points are indicated in **A**. For all the cells the, average fluorescence intensity was calculated and plotted in **B**.

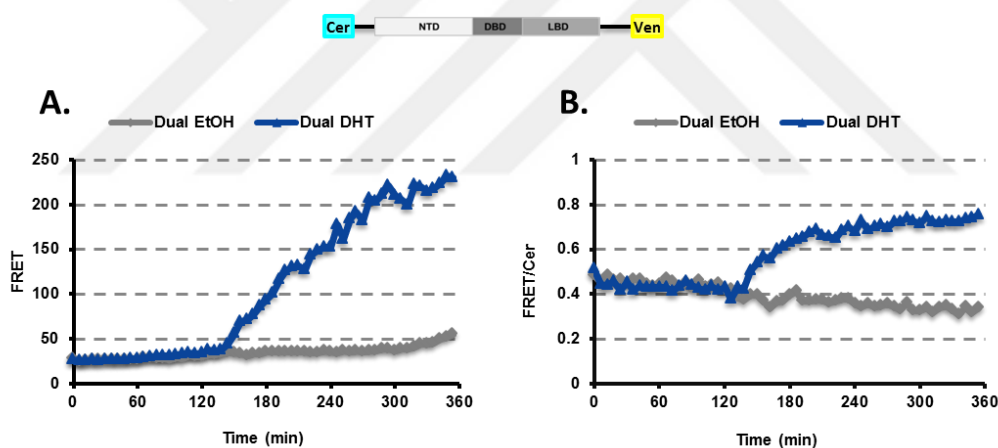


Figure 4-8: FRET analysis of Cerulean-AR-Venus constructs in 6 h.

A is drawn by FRET intensity for each time point (5 min interval). As the FRET increases by time due to increased protein expression, for correction of false negative increase the FRET intensity coming from increased protein expression, FRET intensity of each point was divided by donor intensity for that point, and the plot in **Figure 4-8-B** shows the average FRET/CFP for each time point. EtOH was used as solvent control.

We observed an increase in FRET signal upon addition of DHT in cells expressing dual-labeled form of AR. The FRET intensity of EtOH treated sample was similar to that of DHT condition, before AR activation. Results indicate that the custom generated script on MATLAB can be used to detect ratiometric FRET intensity in live cell imaging microscopy.

4.2.6 Intermolecular Interactions of Androgen Receptor

The interactions of Androgen Receptor at its N and C terminus were studied using Cerulean-AR-Venus construct. To investigate the intermolecular dimerization between two AR, single labeled constructs were used. Similar to previous experiments 293T cells transfected with single labeled FRET pair constructs and then imaged for 6 h. AR was activated after 2 hr with 1 nM DHT and EtOH was used as negative control.

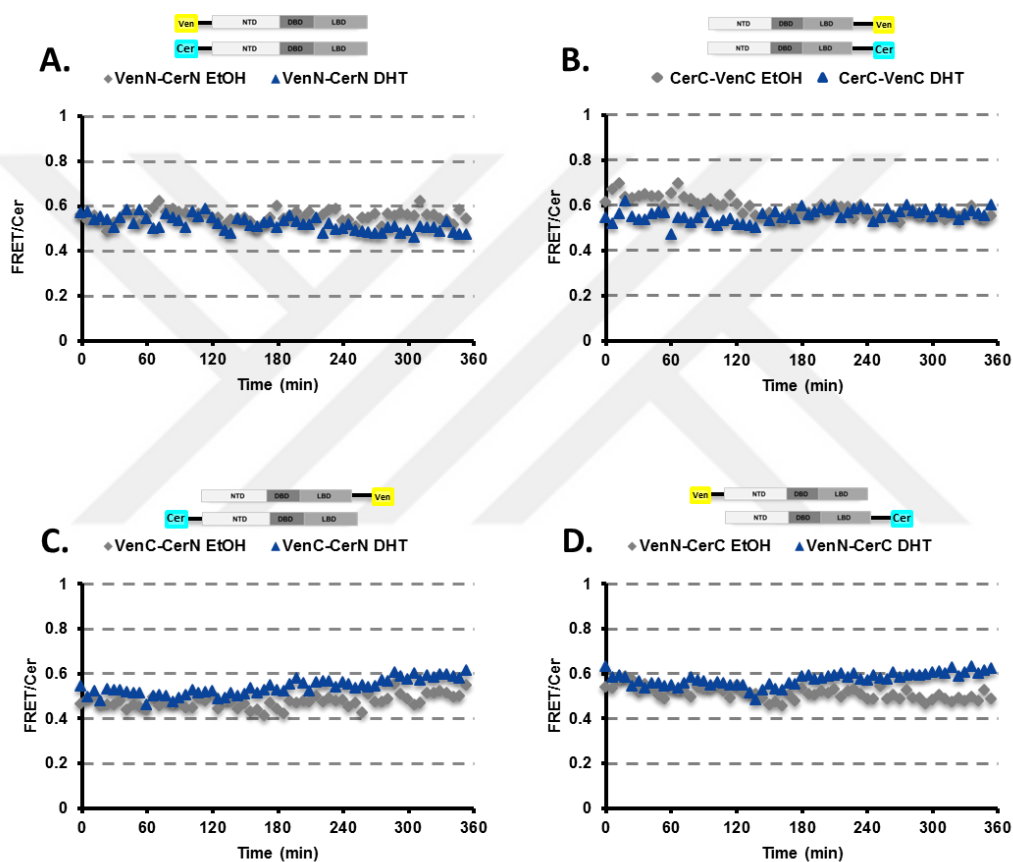


Figure 4-9: Intermolecular interactions of AR.

A and **B** indicate the interaction N-N and C-C interactions of androgen receptor while **C** and **D** indicate the N-C interactions of AR using different constructs.

Upon DHT stimulation, N-N and C-C interactions were not significantly different from EtOH-treated samples, while there is small increase in FRET intensity in N-C interactions of AR (**Figure 4-9**). We see an N-C interaction in AR upon activation with DHT, but the FRET signal measured in these conditions of transfections was 20% less than that of dual labeled AR. The FRET signal coming from dual labeled AR occurs due to both inter and intramolecular interaction of AR while that of single labeled constructs indicate only the

intermolecular interaction of AR which happens due to dimerization. This can be observed in the graphs; FRET signal increases right after DHT stimulation in dual labeled AR as AR folds on itself bringing N-C domains close to each other to give a FRET signal (**Figure 4-8**) while the increase in FRET is delayed in condition where the cells are transfected with single labeled fusion proteins of AR and N-C intermolecular interaction occurs after nuclear localization upon DHT treatment (**Figure 4-9**).

The signal measured in intermolecular interaction of AR was increased only slightly after DHT treatment. We hypothesized that the low FRET signal was due to unequal expression of individual donor and acceptor in these experiments (**Figure 4-2**). The equal expression of donor and acceptor pairs is necessary for correct measurement in ratiometric FRET experiments. As previous studies demonstrated intermolecular interactions of AR, we thought that future work with ARV7 would be limited by the unequal expression of single labeled FRET pairs in our study. Therefore, we aimed to equalizing the expression of the constructs.

4.2.6.1 Transfection of the constructs in different ratios

In Cerulean-Venus fusion constructs, as the protein is translated from a single transcript the donor and acceptor protein expression have an equal expression ratio that is required for ratiometric FRET studies. By changing the ratio of donor and acceptor ratio in transfection, we aimed to get the desired correlation between the expressions of single labeled constructs using the Cerulean-AR-Venus construct as a control (equal concentration of each fluorophore). The donor and acceptor intensities of more than 40 cells were measured by finding the local maxima in CFP channel and measuring the donor and acceptor intensities at same point in each cell using ImageJ software. **Figure 4-10** represent 5/10 representative conditions for transfection in different ratios. In an equal expression of donor and acceptor condition, YFP has median intensity around 1500 while the median intensity of Cerulean is around 550. None of the numerous conditions tested could we give correct correlation between donor and acceptor intensity measured in Cerulean-AR-Venus construct.

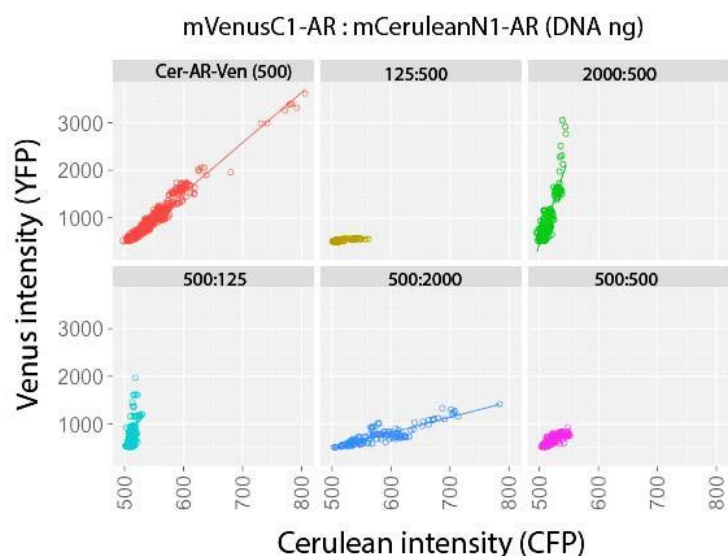


Figure 4-10: The correlation between donor and acceptor intensities in different transfection ratios.

4.2.6.2 Changing linker size in FRET constructs

As we could not get the desired ratio for donor and acceptor by changing the transfection ratio we aimed to equalize the expression by changing the constructs themselves. We observed that constructs that have fluorescent tag at the N-terminus are expressed less than that of the constructs that have fluorescent tag at the C-terminus. Given that the linker size of the one was 18 bp while the other was 42 bp, we decided to test the effect of linker size on the protein expression and thus we have extended the linker size from 18 nt to 42 nt in the constructs that have fluorescent tag at the N-terminus.

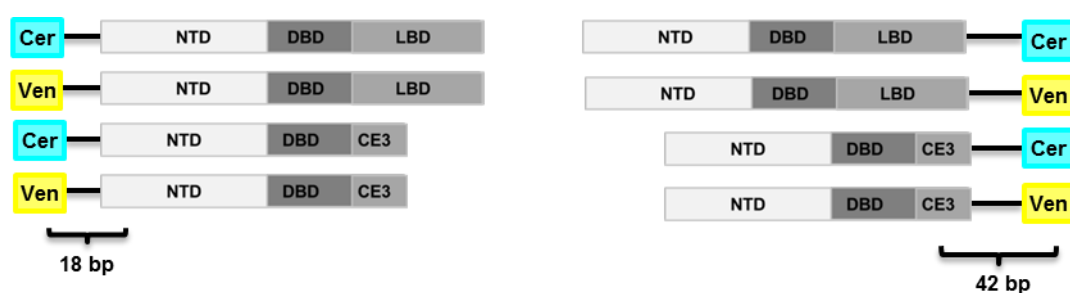


Figure 4-11: Linker size between fluorescence protein in Cerulean and Venus fusion proteins. To increase the linker size in mVenusC1 and mCeruleanC1 constructs, we cloned synthesized oligonucleotides (2.2.2.7.3) into linker region. Extending the linker size from 18 nt to 42 nt length did not help to equalize the expression levels in N- or C- fusion constructs of AR (Figure 4-12).

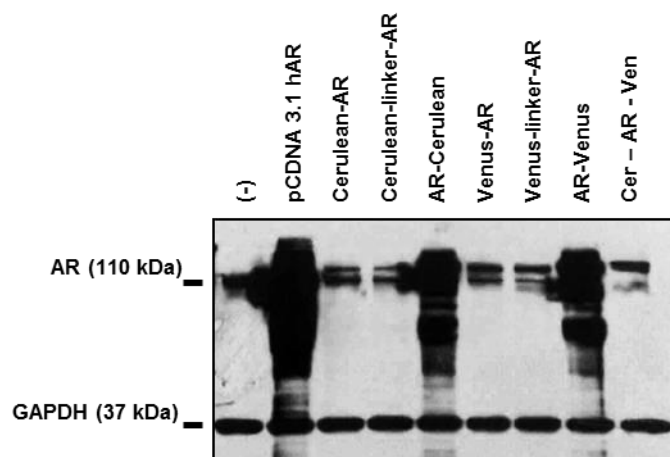


Figure 4-12: Expression of all AR constructs.

The fusion constructs were transfected into 293T cells in equal amount (2.2.4.5). The level of protein expression was detected by western blotting (2.2.3.2). Antibody dilutions used are listed in Table 8. pCDNA3.1 AR was used as positive control for AR^{full-length} expression.

We shortened the linker of mVenusC1 and mCeruleanC1 plasmids by site-directed mutagenesis (2.2.2.7.5) to 18, 25 and 30 nt length. The level of protein expression in AR-Cerulean construct with shortened linker is shown by western blotting (Figure 4-13). Unfortunately, shortening the linker size did not cause a change in the Cerulean-AR construct.

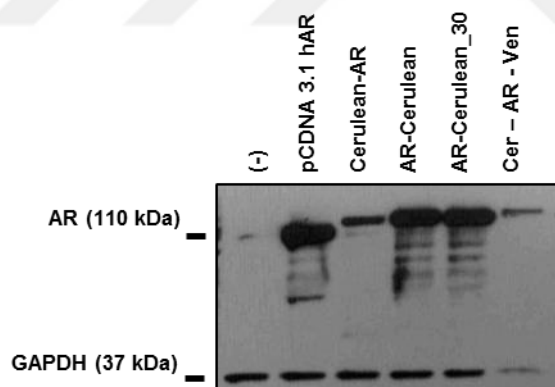


Figure 4-13: Expression level in the construct with shortened linker.

The fusion constructs were transfected into 293T cells in equal amount (2.2.4.5). The level of protein expression was detected by western blotting (2.2.3.2). pCDNA3.1 hAR plasmid was used as positive control for androgen receptor expression.

4.2.6.3 Changing the linker composition in the fusion proteins

Next, we aimed to change the linker in our constructs from what was present in the plasmid to a 6(GA) repeat used in previously published work [24]. To generate these fusion protein, we inserted PCR amplified Cerulean into AR-CFP plasmid following the removal of CFP. In contrast we have generated Venus-6(GA)-AR construct by inserting 6-(GA)-AR from YFP-6-(GA)-AR into a mVenusC1 plasmid. Fortunately, replacing the linker in AR constructs resulted in similar expression of fusion proteins in both N- and C- terminus constructs.



Figure 4-14: The linker composition in the constructs used in acceptor photobleaching FRET.

In all the constructs fluorescent protein is separated from androgen receptor by 6 (GA) repeat and the expression of the constructs is the same.

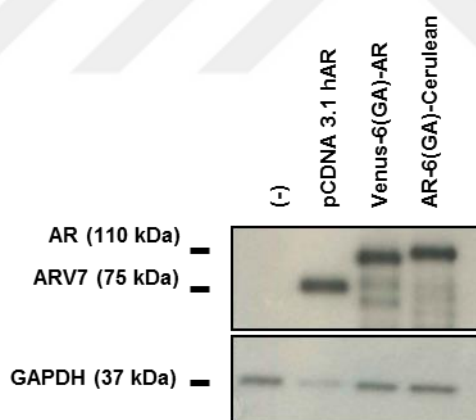


Figure 4-15: Expression of AR constructs with 6(GA) repeats.

The fusion constructs were transfected into 293T cells in equal amount (2.2.4.5). The level of protein expression was detected by western blotting (2.2.3.2) Antibody dilutions used are listed in Table 8. pCDNA3.1 AR was used as positive control for AR^{full-length} expression.

With these results we then generated ARV7-6(GA)-Cerulean and Venus-6(GA)-ARV7 fusion proteins by site-directed mutagenesis to remove their linker and then introducing a 6GA-linker by oligonucleotide cloning. Similar to the full length protein, exchange the linker resulted in similar expression of ARV7 fusion proteins in both N- and C- terminus constructs.

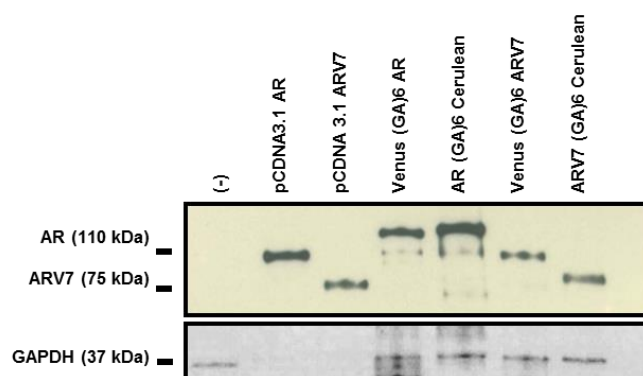


Figure 4-16: AR and ARV7 constructs with 6(GA) linker.

The fusion constructs were transfected into 293T cells in equal amount (2.2.4.5). The level of protein expression was detected by western blotting (2.2.3.2). pCDNA3.1 hAR plasmid was used as positive control for androgen receptor expression.

4.2.7 Androgen Receptor intermolecular and intramolecular interactions using Acceptor Photobleaching

In several previous studies acceptor photobleaching FRET was used to study stepwise androgen receptor dimerization. Since we had problems with obtaining correct ratio of donor and acceptor expression, we wanted to study the interactions of AR and ARV7 using acceptor photobleaching FRET.

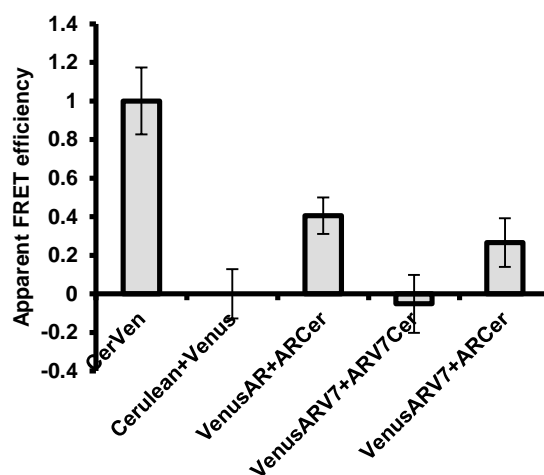


Figure 4-17: AR and ARV7 interactions using acceptor photobleaching.

In collaboration with Dr. Martin Van Royen, HEP3B cells were transfected with the indicated plasmid combinations and then treated with R1881 for activation of the AR. We were able to clearly see the FRET in positive control, and FRET in combination of Venus-AR and AR-Cerulean constructs, which was expected to be less than one-third of positive control. However, due to a problem in our negative controls, we could not get consistent results from

two independent experiments. While a FRET signal could be obtained for the dual labeled AR, our Cerulean tagged constructs were not suitable for this experimental protocol as the photobleaching was reversible thereby preventing the interpretation of the results (**Figure 4-18**).

In our Cerulean only control, we observed an increase in the signal due to reversible bleaching. When we select the cell for the FRET measurement we were zooming in and placing the cell of interest in the center of image, and then we measured the FRET before after Venus bleaching. In our Cerulean control, the intensity in the initial image was less than that of second image after Venus bleaching which was because of reversible bleaching of Cerulean itself (**Figure 4-18**).

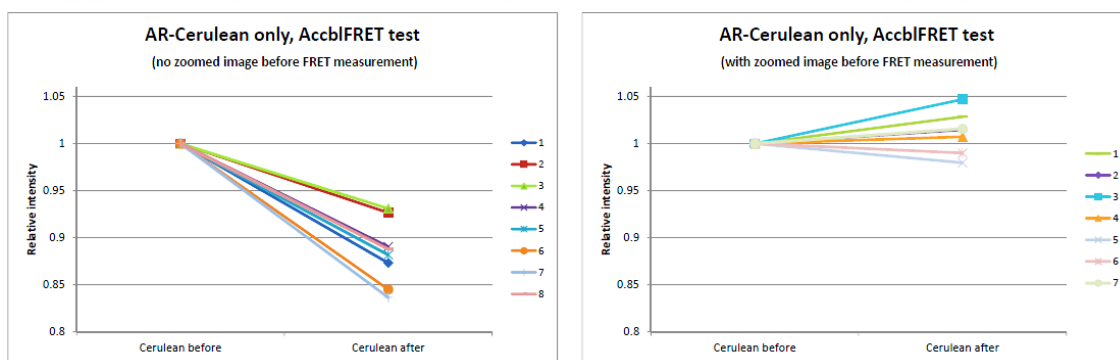


Figure 4-18: Temporary bleaching of Cerulean in acceptor photobleaching. FRET measurements were compared with (right graphs) and without (left graphs) this initial image before the FRET measurement. Each line represents an individual cell.

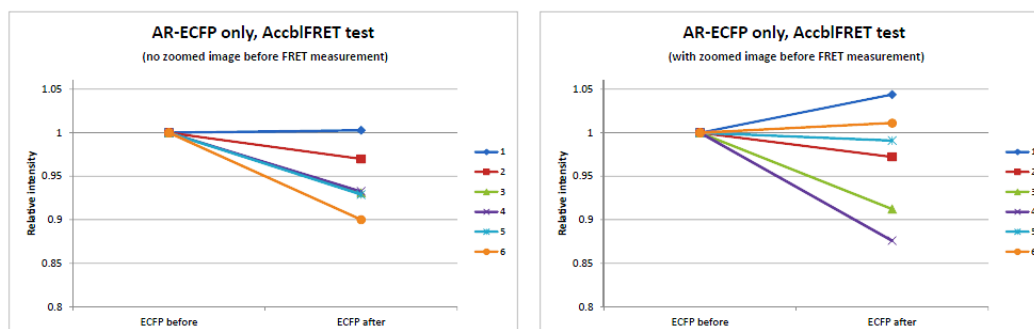


Figure 4-19: The effect of zooming on relative intensity of CFP. FRET measurements were compared with (right graphs) and without (left graphs) this initial image before the FRET measurement. Each line represents an individual cell.

4.2.8 Studying interactions of AR and ARV7 using CFP-YFP as FRET pair

Given the problems we experienced with Cerulean and Venus fusion pairs doing photobleaching FRET, we moved on to study the interactions of AR and ARV7 by using CFP-YFP fusion proteins. AR-CFP and YFP fusion proteins were kindly provided by Martin van Royen. We cloned ARV7-CFP by taking ARV7-6(GA) from ARV7-6(GA)-Cerulean plasmid and introducing it into CFP-AR plasmid (from Martin) following the removal of AR. We then cloned a YFP-ARV7 construct by taking 6-(GA)-ARV7 from Venus-6(GA)-ARV7 plasmid and putting that into CFP-AR plasmid (from Martin) after removal of AR. All constructs were validated by restriction endonuclease digest and Sanger sequencings. Similar to studies with the Venus and Cerulean tagged proteins with the 6(GA) linker, the expression of the two constructs was similar (**Figure 4-20**).

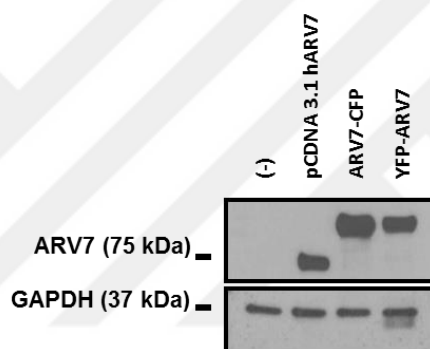


Figure 4-20: Expression of ARV7-CFP and YFP-ARV7 constructs.

The fusion constructs were transfected into 293T cells in equal amount (**2.2.4.5**). The level of protein expression was detected by western blotting (**2.2.3.2**). pCDNA3.1 hARV7 plasmid was used as positive control for ARV7 expression.

4.2.9 Transcriptional activity of FRET constructs

In addition to Cerulean and Venus fusion proteins, we have generated several other fusion proteins of both AR and ARV7 to have equal expression of single constructs which can be used in ratiometric FRET analysis.

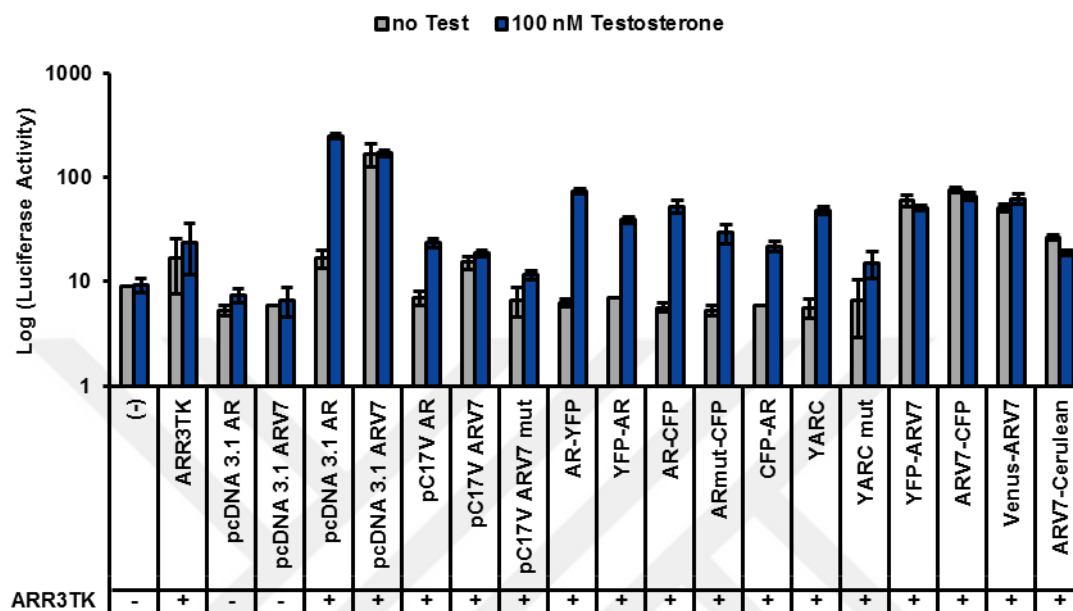


Figure 4-21: Transcriptional activity of constructs with equal expression.

293T cells were transfected with indicated constructs together with ARR3TK-luc constructs to show transcriptional activity by luciferase activity. The cells were treated with/without 100 nM Testosterone for the activation of AR. 24 h after transfection the cells were lysed for measuring the luciferase activity. pCDNA3.1 AR and pCDNA3.1 ARV7 used as positive control for the assay. Bars represent Log (luciferase activity) and error bars indicate \pm standard deviation.

All AR constructs show increased transcriptional activity with Testosterone treatment. AR-YFP, YFP-AR, AR-CFP, CFP-AR and YFP-AR-CFP (from Martin) show similar transcriptional activity with Testosterone treatment. ARmut-CFP and YFP-AR-CFP-mut constructs which have mutation in DNA binding domain (A596T/S597T) show decreased transcriptional activity as compared to their wild type counterparts. YFP-ARV7 and ARV7-CFP (**Figure 4-20**) show similar transcriptional activation independent of presence of Testosterone treatment. The transcriptional activity of Venus-ARV7 and ARV7-Cerulean (**Figure 4-15**) differ slightly, but this difference is comparable to that seen in plasmids generated by Dr. Van Royen. Results indicate that a 6(GA) separation between fluorescent protein and AR or ARV7 results in equal expression of the fusion proteins.

4.2.9.1 Intermolecular interactions of AR^{full-length} using YFP-AR-CFP fusion protein

With the CFP and YFP fluorophores we then tested the intramolecular FRET signal with the YFP-AR-CFP. A similar experimental protocol was followed to earlier experiments. The net FRET intensity was normalized to the square-root of multiplication of intensity measured CFP and YFP in order to eliminate the effect of increased protein expression in the cells with time on measured FRET intensity.

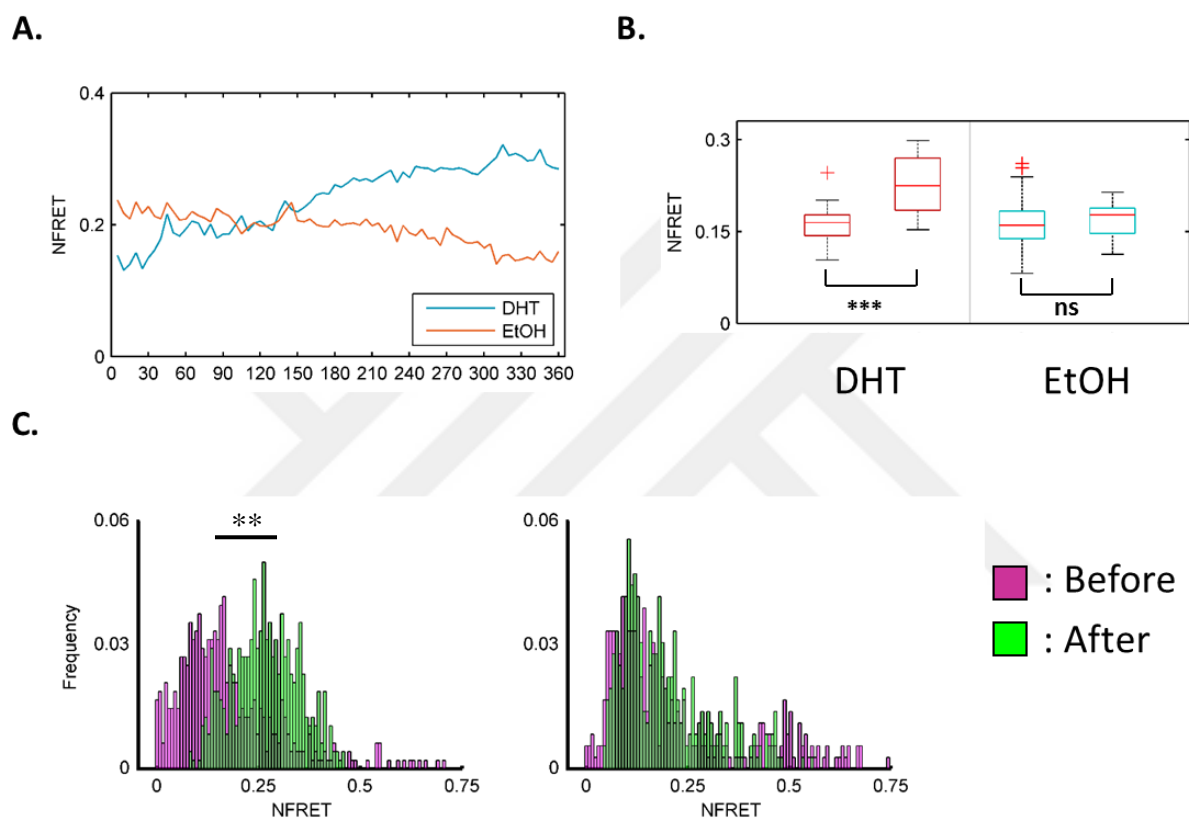


Figure 4-22: Interactions of Androgen Receptor shown by FRET.

The images were recorded for 6 hours in 5 min intervals. 2 h after start of the experiment Androgen Receptor was activated with 1 nM DHT or EtOH as negative control. **Figure 4-22-A** shows the calculated NFRET value for YFP-AR-CFP in EtOH and DHT treated conditions for 360 min. NFRET value increases upon addition of DHT. **Figure 4-22-B** Box plot of NFRET distributions of DHT and EtOH treated conditions. (* for $p < 0.05$, ** for $p < 0.01$, *** for $p < 0.001$). **Figure 4-22-C** NFRET distributions of DHT and EtOH treated conditions. The data represents all the NFRET values from five different 512x512 image, for an image series of 72 frame. Before indicate the NFRET values for a total 24 frames before treatment and after indicate a total 24 frames after treatment.

The NFRET increases after treatment only in DHT treated condition demonstrating intramolecular interactions (**Figure 4-22-A** and **Figure 4-22-B**). When comparing the distribution of all NFRET values in EtOH and DHT treated samples before and after

treatment, there is a clear shift in the distribution of the NFRET values of the cells indicating interaction upon DHT treatment (**Figure 4-22-C**). For the determination of the distribution of the NFRET intensities of every cell in all frames one-sample Kolmogorov-Smirnov test was used. The test is used to check whether a sample comes from a population with a normal distribution [157]. According to this test, the calculated NFRET values in this set of experiment does not show a normal distribution, thus, the statistical significance of the difference between two sets can be calculated using a non-parametric test.

4.2.9.2 The interactions of DNA-binding domain mutated AR

While AR^{full-length} folds into itself through N-C, dimerization of AR^{full-length} is mediated by DNA-binding domain in the second zinc-finger. Three amino acid residues in the D-box interact with their counterpart in the corresponding AR^{full-length} DNA binding domain in an AR^{full-length} homodimer (A596 with T602, S597 with S597 and T602 with A596) [158]. A596T and S597T in YFP-AR-CFP was used to validate the role of the D-box in AR^{full-length} dimerization.

DBD-mutant AR fused to YFP and CFP was a gift from Martin van Royen. Cell preparation and live cell imaging was done as previously described in 2.2.5.1.

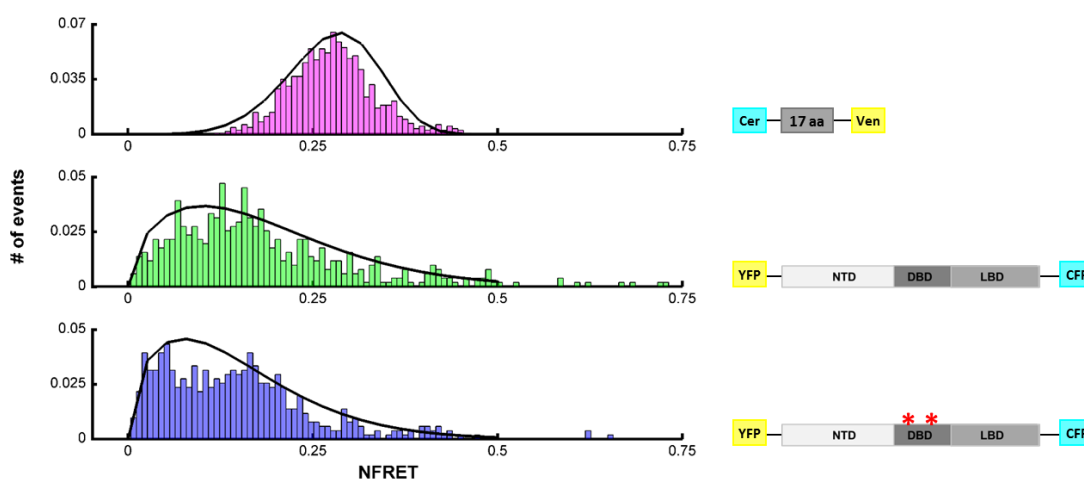


Figure 4-23: The NFRET histograms of C17V, YFP-AR-CFP, YFP-AR(DBD-mutant)-CFP. C17V (magenta), YFP-AR-CFP (green), YFP-AR(DBD-mutant)-CFP (blue). pC17V has Gaussian distribution with a single peak indicating only one possible way of interaction between Cerulean and Venus FRET pair. NFRET histogram of YFP-AR-CFP (green) has three overlapped Gaussian distribution, and high NFRET generating cells toward the right-hand-side of the graphs; indicating three possible interactions bringing CFP and YFP in close proximity. NFRET histogram of YFP-AR-CFP (DBD-mutant) (blue) has three

overlapped Gaussian distribution similar to that of YFP-AR-CFP but with different maximum value of the peaks; the high NFRET generating cells toward the right-hand-side of the graph is lost indicating that the FRET happening due to dimerization of AR (which involves intra and intermolecular interactions of AR) is lost when DNA-binding domain of AR is mutated.

4.2.9.3 The interactions of AR^{full-length} and ARV7

As this system can characterize intramolecular interactions, we chose to exam intermolecular interactions between the full length AR and ARV7. For this reason single labeled constructs of YFP and CFP fusion proteins of AR^{full-length} and ARV7 was used to characterize N-C intermolecular interaction. The plasmids were a gift from Martin van Royen. Cell preparation and live cell imaging was done as previously described in **2.2.5.1**. YFP and CFP fusion proteins of ARV7 constructs were generated with a 6(GA) repeat between fluorescent protein and ARV7 for equal expression. Cell preparation and live cell imaging was done as previously described in **2.2.5.1**.

Unfortunately, AR^{full-length} was found to have a high NFRET in a certain percentage of cells treated with EtOH alone (**Figure 4-24**). This makes it challenging to interpret the intermolecular interactions. The NFRET histograms (**Figure 4-25**) indicated that ARV7 does not form dimers by bringing N-C domains into close enough proximity to give a FRET signal (magenta). As the V7 is the constitutively active isoform of AR, its interaction is not affected by the presence of DHT and NFRET values are within similar regions. In contrast, the C-terminus of AR^{full-length} and C-terminus of ARV7 (green) seem to be interacting in the presence of DHT. The histograms show that, the presence of DHT increased the number of events in the high NFRET region, which is absent in EtOH treated condition. ARV7 is constitutively found in nucleus while AR is found in cytoplasm in the absence of DHT. Thus, stimulation with DHT results in AR nuclear localization and possibly bringing it in close proximity with ARV7. DHT stimulation seems to shift the distribution of NFRET values towards higher values in combination of N terminus of AR and C-terminus of ARV7 (red). The data is consistent with previously published work where they show that ARV7 heterodimerizes by bringing N-C domains together. The N terminus of ARV7 does not seem to be interacting with neither N (blue), nor C terminus of AR (yellow) as the distribution of NFRET values are within same region in both EtOH and DHT treated conditions, spanning values between 0 and 0.25. Additional studies are currently ongoing to better characterize this interaction.

After careful observation of each step from transfection to image analysis, we realized that our custom generated script tracks the already activated cells in EtOH treated condition, which can be present nearly in 5 % of the cells. However, the problem of image analysis might have led to incorrect interpretation of generated data; thus, the custom generated script should be modified to ensure the tracking of all the cells in a frame and throughout duration of the experiment. The script has been modified and is now being used to reprocess the data.

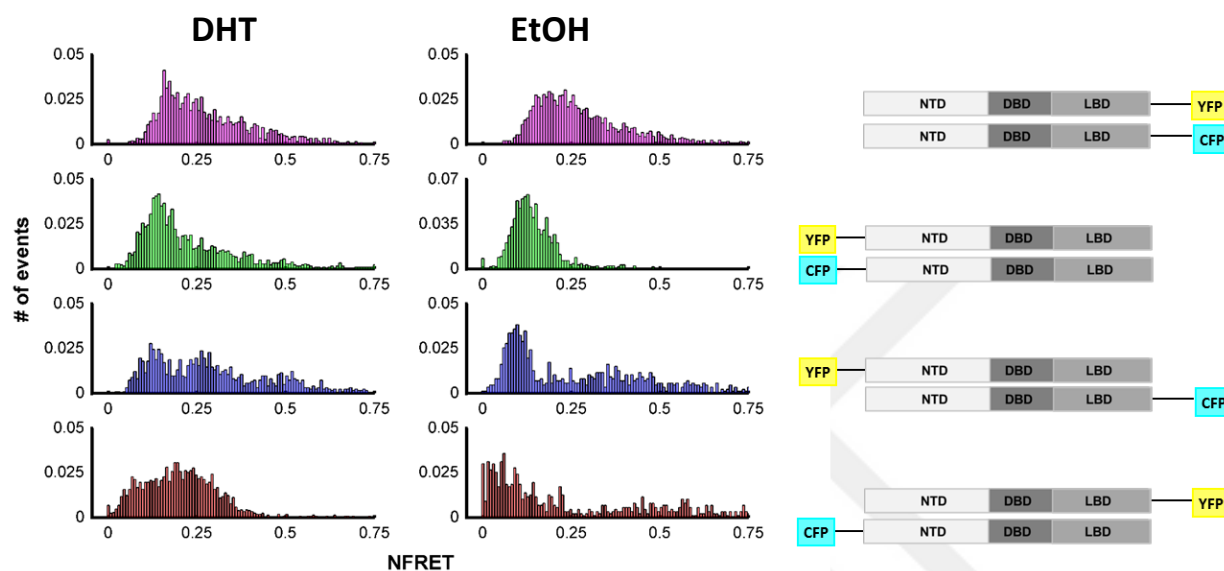


Figure 4-24: The NFRET histograms of intermolecular AR^{full-length} interactions. The histograms indicate intermolecular AR^{full-length} interactions. C-C interaction of AR^{full-length} (Magenta), N-N interaction of AR^{full-length} (green), N-C interaction of AR^{full-length} (blue), N-C interaction of AR^{full-length} (red). The graphs on the left represent DHT treated samples and those on the right are EtOH treated samples. The NFRET distribution of DHT and EtOH treated samples throughout 6 h. x-axis indicates NFRET values, and y-axis indicates the number of events. The interacting partners are indicated in the right-hand-side of the diagram.

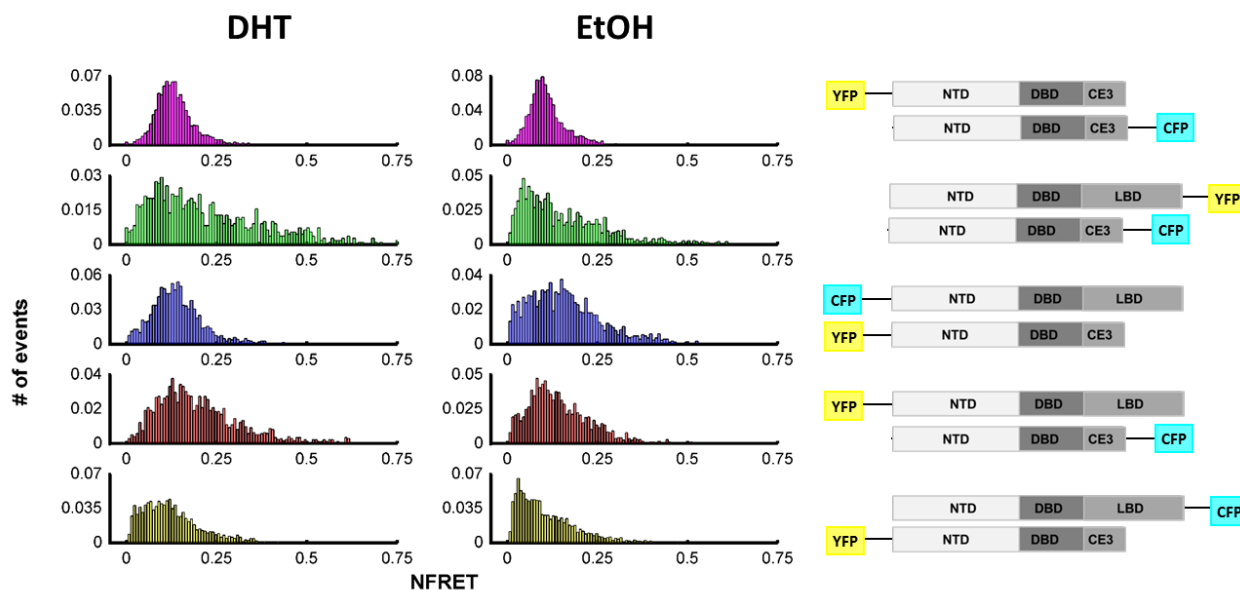


Figure 4-25: The NFRET histograms of interactions of AR^{full-length} and ARV7.

The histograms indicate AR and ARV7 interactions. N-C interaction of ARV7 (Magenta), AR-C and ARV7-C interaction (green), N-AR and N-ARV7 (blue), N-AR and ARV7-C (red), and AR-C and N-ARV7 (yellow). The graphs on the left represent DHT treated samples and those on the right are EtOH treated samples. The NFRET distribution of DHT and EtOH treated samples throughout 6 h. x-axis indicates NFRET values, and y-axis indicates the number of events. The interacting partners are indicated in the right-hand-side of the diagram.

4.2.10 Testing AR and ARV7 interactions using mammalian two hybrid system

To validate our results from the FRET experiments we utilized a mammalian two-hybrid system. The assay is based on the reconstitution of the modular domains of a transcriptional activator. The system involves the expression of the proteins of interest in two plasmids pBIND and pACT to generate fusion proteins with the DNA-binding domain of GAL4 and the activation domain of VP16, respectively. The system also contains one of the pG5luc Vector which contains five GAL4 binding sites upstream of a minimal TATA box, upstream of the firefly luciferase gene (*luc+*). The vectors containing the proteins to-be-tested are cotransfected with pG5luc Vector. In case of interaction, GAL4 and VP16 will come together and bind to GAL4 binding site in the pG5luc vector and result in the expression of firefly luciferase gene. Lysis of the cells and measurement of luciferase activity (2.2.4.10), will reveal the interaction between the proteins.

pBIND and pACT-AR and ARV7 fusion constructs were kindly provided by Dr. Nada Lallous (University of British Columbia, Canada). To study the interactions between AR and ARV7, the plasmids were transfected into 293T cells and luciferase activity was measured as described in 2.2.4.10 (Figure 4-26).

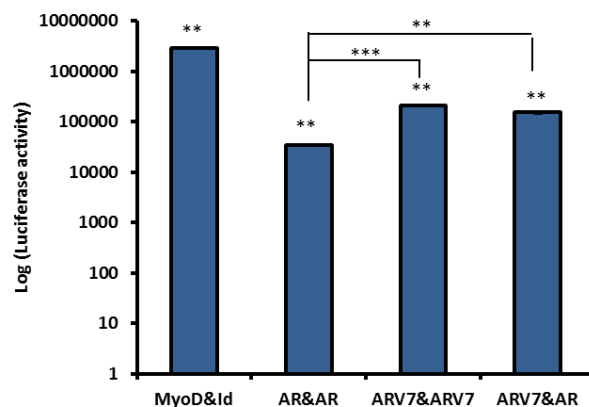


Figure 4-26: Interactions of AR and ARV7 studied by mammalian two hybrid system. Cells transfected with the indicated combinations together with pG5-luc vector. 48 h after transfection the cells were lysed for measuring the luciferase activity. MyoD&Id was used as positive control for the interactions. Bars represent Log (luciferase activity) and error bars indicate \pm standard deviation. (* for $p < 0.05$, ** for $p < 0.01$, *** for $p < 0.001$; $n=2$).

The signal were compared to only pG5-luc transfection. These results suggest that the AR dimerizes with both itself and ARV7 and ARV7 can dimerize with itself (**Figure 4-26**). Interestingly, our preliminary data suggests that the interaction between AR homodimers is significantly lower than that of ARV7 homodimer and AR-ARV7 heterodimer. Further studies are needed to determine if this is due to the level of AR activation.

4.3 Discussion

FRET is non-radiative energy transfer between two fluorophores, defined as a donor and acceptor fluorophore, through dipole-dipole coupling [159–161]. Energy transfer requires an overlap between the excitation of the acceptor and emission of the donor fluorescent proteins and a distance smaller than 10 nm. When two fluorophores suitable for FRET come in close proximity, the emission from the donor excites the acceptor. In ratiometric FRET, the intensity is measured by the emission of the acceptor fluorophore after excitation with the excitation of donor [162].

In this study we wanted to study the interactions between AR and ARV7 by using FRET with Cerulean and Venus as donor and acceptor, respectively. Although we were able to show intramolecular interaction of AR (**Figure 4-7**) the intensity for FRET measuring intermolecular (N-C) interactions were lower than expected in our system (**Figure 4-9**) which was likely due to the unequal expression of interacting pairs. As the technique is less sensitive to varying protein expression, we attempted to study the AR and ARV7 interactions using acceptor photobleaching FRET. Unlike ratiometric FRET, acceptor photobleaching FRET does not require the equal expression of donor and acceptor. However, in our experiments, we observed that our studies involving interactions of AR and ARV7 were limited by the fact that Cerulean was reversibly photobleached during imaging (**Figure 4-18**) giving rise to a false-positive FRET signal. Therefore, to be able to continue our ratiometric FRET experiments we implemented a variety of cloning strategies to equalize the expression of donor and acceptor by changing the exact size and composition of linker between fluorophore and protein of interest. We have successfully generated ARV7 CFP and YFP fusion proteins that express at a similar level by changing the linker as 6(GA) repeats (**Figure 4-16**).

Our ratiometric FRET measurements were analyzed by tracking every cell and recording the intensities during process. The results indicated that we can measure the kinetics of FRET intensity as long as the cells are tracked properly. First, we have studied the intramolecular interactions of AR by using YFP-AR-CFP construct. We observed a significant increase in the NFRET only after DHT treatment (**Figure 4-22**). Upon addition of DHT, the N and C terminus of androgen receptor come in close proximity to give a FRET signal in the presence of FRET pairs. Following this intramolecular interaction, the AR translocalizes to the nucleus and dimerizes with another androgen receptor in head-to-tail orientation, disrupting the intramolecular interaction. When comparing the NFRET distribution of DHT treated pC17V,

YFP-AR-CFP, and YFP-AR-CFP (DBD-mutant) (**Figure 4-23**) we saw that the only possible orientation which gives FRET signal was represented by a single Gaussian fit in pC17V and this interaction occurs due to separation by 17 amino acid distance. NFRET histogram of YFP-AR-CFP (green) indicates all three possible AR interactions. AR in its inactive state is represented at the left-hand-side of the histogram with NFRET value between 0 and 0.1. The interaction of N-terminal domain and ligand binding domain right after DHT addition is represented with a distribution spanning NFRET values around 0.1 and 0.2. Following that region, another distribution peaking at 0.25 indicate the head to tail orientation of androgen receptor in its DNA-bound conformation. The right-most part of the histogram spanning from 0.4 up to 0.75 represents the structure of AR right after translocation to nucleus, where two androgen receptors are in a dimer but each of them has the N-C looping onto itself. The NFRET distribution of YFP-AR-CFP (DBD-mutant) is similar but different from that of YFP-AR-CFP histogram. The second peak in the histogram spans similar region with a similar peak, indicating that DNA binding mutation does not affect the N-C interaction which occurs right after ligand binding. On the other hand, as compared to YFP-AR-CFP histogram, the number of events toward the right hand-side of the graph decreases. This region mainly represents the interactions mediated by DNA-binding domain.

In the studies regarding ARV7 interactions (**Figure 4-25**) the NFRET histograms indicated that ARV7 does not form intramolecular interactions that bring N-C domains close enough to give a FRET signal. As the V7 is the constitutively active isoform of AR, its interaction is not affected by the presence of DHT.

In contrast the intermolecular interactions have not been fully characterized. Our preliminary data suggest that the C-terminus of AR^{full-length} and C-terminus of ARV7 may interact in the presence of DHT. The number of events in the high NFRET region increased in the presence of DHT, which was absent in EtOH treated condition. ARV7 is constitutively found in nucleus while AR is found in cytoplasm in the absence of DHT. Thus, stimulation with DHT would results in AR nuclear localization and possibly bringing it in close proximity with ARV7.

In addition, DHT stimulation shifted the distribution of NFRET values towards higher values in combination of N terminus of AR and C-terminus of ARV7. The data is consistent with previously published work where they show that ARV7 heterodimerizes by bringing N-C domains together. Our studies suggested that the N terminus of ARV7 was interacting with

neither N, nor C terminus of AR. However, additional data analysis is required to clarify how the variant interaction occurs.

We also studied the AR and ARV7 interaction by mammalian two hybrid system. The results supported out FRET findings that, AR and ARV7 were interacting both as homodimer and heterodimer. Our results indicated that AR and ARV7 can both homodimerize and heterodimerize, but the dimerization preference of AR is heterodimerization with ARV7 over homodimerization.

While, AR interactions have been extensively characterizes this work represents one of the first studies to investigate variant dimerization in a spatio-temporal manner. Our experimental setup allowed for localization of the interactions within the cells, the dynamic of the interactions which we can track from single cells. Studies are currently ongoing to clarify the mechanism of AR7 dimerization.

Acknowledgements

I would like to thank Lack Lab members Fatma Özgün, Hilal Saraç, Ceren Şeref, Tunç Morova, Bengül Çetin, Doğançan Özturan; and Can Aztekin, Haroon Qureshi, for their comments and discussions on these experiments; Selen Manioğlu and Asst. Prof Halil Bayraktar for doing image analysis of FRET experiments; Dr. Martin van Royen for the advices and comments in FRET experiments and for giving me chance to perform acceptor photobleaching experiments in Erasmus Optical Imaging Centre (Erasmus MC, Rotterdam); Prof. Halil Kavaklı for mammalian two hybrid system plasmids, Dr. Nada Lallous (University of British Columbia, Canada) for ARV7 and AR constructs used in mammalian two hybrid system; once more Fatma Özgün and Hilal Saraç for their contributions in the experiments and cell counting; Ceren Şeref for her contributions to cloning experiments; Abdullah Salih Budan and Elif Demirtaş for β -galactosidase staining experiments and Deniz Uğurlu for the plix-GFP construct.

Chapter 5: Conclusions and Future Work

5.1 Final Conclusions

The aims stated in Section 3.1 that have been met are summarized below:

- **Generation of inducible ARV7 expressing prostate cancer cell lines**

We have generated inducible ARV7 expressing LNCaP, PC3, RWPE1, BPH1, LNAI, 22RV1 and LNCaP-Abl cell lines with an all-in-one Tet-on pLIX_402 plasmid. Upon doxycycline treatment ARV7 was expressed and transcriptionally active in these cell lines. We have also generated single cell clones of ARV7 expressing LNCaP cell lines, which expressed ARV7 to different extents. In this system, AR^{full-length} expression decreased with ARV7 expression and thus, by using different doxycycline concentrations the cells had different AR^{full-length}/ARV7 expression ratio, which represented different CRPC conditions in patient samples.

- **To characterize the effect of ARV7 on cell-characteristics**

We have found that ARV7 expression resulted in flattened morphology, enlarged nucleus and increased vesicles in the cells. We have ensured that the protein is folded properly and did not cause unfolded protein response in endoplasmic reticulum. There was no epithelial to mesenchymal transition upon ARV7 expression and the vesicles formed were not due to autophagy. In addition, ARV7 expression did not cause double strand breaks in DNA. We also ensured that doxycycline treatment in non-transduced cells does not cause any differences in the characteristics described.

- **To characterize the effect of ARV7 expression on cell viability, cellular proliferation, and cell cycle**

We have found that ARV7 expression results in cellular senescence mediated by activation of the p53 pathway in androgen-dependent LNCaP cell line. The extent of senescence was dependent on ARV7 expression but not to the level of AR^{full-length} expression. The G₀/G₁ arrest was permanent; the cells could not recover from senescence when ARV7 expression was decreased. In addition, we observed that the G₀/G₁ arrest resulted in decreased cellular proliferation. We have isolated two other inducible ARV7 expressing single cell clones of LNCaP; which did not enter senescence upon expression.

- **To characterize the effect of ARV7 expression on several prostate cell lines**

We observed ARV7 expression mediated cellular senescence in several androgen responsive prostate cancer cell lines. Our results indicated that constitutive activity of ARV7 was dependent on the presence of androgen receptor and a shift from androgen receptor mediated growth to ARV7 mediated growth is not tolerated in AR dependent cells.

The aims stated in Section 4.1 that have been met are summarized below:

- **To generate AR^{full-length} and ARV7 fused to FRET pair fluorescent proteins**

We have generated AR^{full-length} and ARV7 fusion proteins with either Cerulean and Venus FRET pair or AR^{full-length} and ARV7 fusion proteins with either CFP and YFP FRET pair. We have checked the expression and transcriptional activity of these constructs for the use in FRET experiments.

- **To establish live cell imaging microscopy for FRET studies**

We have optimized microscopy conditions to measure FRET for the protein-protein interaction studies. We have optimized the preparation of cells for microscopy and imaging conditions for correct measurements.

- **To calculate FRET intensity from single cells in spatio-temporal manner**

In collaboration with Asst Prof. Halil Bayraktar (Koç University), we have generated a custom generated script in MATLAB for image analysis to measure the FRET intensity from single cells. The analysis method enabled us tracking the cells in spatial manner and intensity of FRET was measured in temporal manner in these cells.

- **To study the interactions of AR^{full-length} and ARV7 using FRET microscopy**

We have validated the previously published AR interactions by FRET using live cell imaging. We were able to show intermolecular and intramolecular interactions of AR in a spatio-temporal manner. In addition to revealing the interactions of AR, our studies provided us with kinetics of these interactions. We were able to show the interactions of ARV7 and AR. We have found that AR and ARV7 were interacting through their C-C domains and also through N-terminal domain of AR and C-terminal domain of ARV7.

5.2 Future work

- **ARV7 expression and cellular senescence**

We have found that the induction of ARV7 expression for only 24 h causes in cellular senescence mediated by activation of the p53 pathway in androgen-dependent LNCaP cell line. Future studies are needed to validate this hypothesis with RNAi targeting p53. Further, the mechanism through which ARV7 mediated cellular senescence requires further characterization of cells to better understand the mechanism.

Interestingly, we were able to generate resistant single cell clones (SCC22 and SCC23). These suggest that the cell can develop “tolerance” to the ARV7. If this mechanism can be identified this offers the possibly to develop a potential anti-proliferative drug that could induce senescence in ARV7 expressing cells. CRPC patients could be targeted with treatment of this novel drug to induce cellular senescence.

Further, all experimental work done in this project was done *in vitro*. It is unclear if this phenotype can occur *in vivo*. Therefore, it would be valuable to test the effects of ARV7 by injecting inducible ARV7 expressing LNCaP in mice and testing the effect of ARV7 on tumor growth. This can be done by injecting inducible ARV7 expressing cells and feeding the animal with different concentrations of doxycycline to further link the level of ARV7 expression on tumorigenesis. In addition, ARV7 expressing cells can be injected in mice together with cells which does not express ARV7, to mimic the prostate cancer tumors which involves both androgen dependent, androgen independent and ARV7 expressing cells in heterogeneity.

- **The interactions of AR and ARV7**

Preliminary studies suggested that the AR and ARV7 may interact, but additional studies are needed to better understand the dimerization preference for AR or ARV7. The custom generated script should be modified to track all the cells for correct comparison. In future studies, inducible unlabeled AR and ARV7 can be used as a “sink” for decreasing the interaction between FRET fusion proteins to establish the preference of AR or ARV7 for dimerization. If AR preferentially dimerizes with ARV7 instead of AR, then there will be more decreased intermolecular interaction of AR in the presence of non-fluorescent ARV7 expressing cells as compared to the cells expressing non-fluorescent AR.

Our established FRET microscopy to study AR/ARV7 interactions can be extended to identify new antagonists for the treatment of prostate cancer. Since AR activity requires dimerization, different chemicals can be used in FRET experiments to identify new inhibitors that block AR dimerization. In addition, antagonists targeting N-terminal domain of AR (meanwhile ARV7) or DNA-binding domain can be identified similarly.



Chapter 6: Bibliography

1. Gelmann, E.P.: Molecular Biology of the Androgen Receptor. *J. Clin. Oncol.* 20, 3001–3015 (2002).
2. Lonergan, P.E., Tindall, D.J.: Androgen receptor signaling in prostate cancer development and progression. *J. Carcinog.* 10, 20 (2011).
3. Lu, J., Van der Steen, T., Tindall, D.J.: Are androgen receptor variants a substitute for the full-length receptor? *Nat. Rev. Urol.* 12, 137–44 (2015).
4. Claessens, F., Denayer, S., Van Tilborgh, N., Kerkhofs, S., Helsen, C., Haelens, A.: Diverse roles of androgen receptor (AR) domains in AR-mediated signaling. *Nucl. Recept. Signal.* 6, e008 (2008).
5. Ferro, P., Catalano, M.G., Dell’Eva, R., Fortunati, N., Pfeffer, U.: The androgen receptor CAG repeat: a modifier of carcinogenesis? *Mol. Cell. Endocrinol.* 193, 109–120 (2002).
6. Ding, D., Xu, L., Menon, M., Reddy, G.P.V., Barrack, E.R.: Effect of a short CAG (glutamine) repeat on human androgen receptor function. *Prostate.* 58, 23–32 (2004).
7. Whitacre, D.C.: Delineation of Two Distinct Type 1 Activation Functions in the Androgen Receptor Amino-terminal Domain. *J. Biol. Chem.* 271, 26772–26778 (1996).
8. van der Korput, H.A.G.M.: Identification of Two Transcription Activation Units in the N-terminal Domain of the Human Androgen Receptor. *J. Biol. Chem.* 270, 7341–7346 (1995).
9. Shaffer, P.L., Jivan, A., Dollins, D.E., Claessens, F., Gewirth, D.T.: Structural basis of androgen receptor binding to selective androgen response elements. *Proc. Natl. Acad. Sci. U. S. A.* 101, 4758–63 (2004).
10. Shaffer, P.L., Jivan, A., Dollins, D.E., Claessens, F., Gewirth, D.T.: Structural basis of androgen receptor binding to selective androgen response elements. *Proc. Natl. Acad. Sci.* 101, 4758–4763 (2004).
11. Shaffer, P.L., Jivan, A., Dollins, D.E., Claessens, F., Gewirth, D.T.: Structural basis of

- androgen receptor binding to selective androgen response elements. *Proc. Natl. Acad. Sci. U. S. A.* 101, 4758–63 (2004).
12. Matias, P.M., Donner, P., Coelho, R., Thomaz, M., Peixoto, C., Macedo, S., Otto, N., Joschko, S., Scholz, P., Wegg, A., Bäsler, S., Schäfer, M., Egner, U., Carrondo, M.A.: Structural Evidence for Ligand Specificity in the Binding Domain of the Human Androgen Receptor. IMPLICATIONS FOR PATHOGENIC GENE MUTATIONS. *J. Biol. Chem.* 275, 26164–26171 (2000).
 13. Co, P., Blanchet, J., Labrie, F., Breton, R.: Comparison of crystal structures of human androgen receptor ligand-binding domain complexed with various agonists reveals molecular determinants responsible for binding affinity. 987–999 (2006).
 14. Grossmann, M.E., Huang, H., Tindall, D.J.: Androgen Receptor Signaling in Androgen-Refractory. 93, 1687–1697 (2001).
 15. Hiipakka, R.A., Liao, S.: Molecular mechanism of androgen action. *Trends Endocrinol. Metab.* 9, 317–24 (1998).
 16. Taplin, M.E., Ho, S.-M.: The Endocrinology of Prostate Cancer. *J. Clin. Endocrinol. Metab.* 86, 3467–3477 (2001).
 17. Wein, A., Kavoussi, L., Novick, A., Partin, A., Peters, C.: *Campbell-Walsh Urology*. Elsevier Inc., Philadelphia, PA (2011).
 18. Dehm, S.M., Tindall, D.J.: Molecular regulation of androgen action in prostate cancer. *J. Cell. Biochem.* 99, 333–344 (2006).
 19. Smith, D.F., Toft, D.O.: Minireview: The Intersection of Steroid Receptors with Molecular Chaperones: Observations and Questions. *Mol. Endocrinol.* 22, 2229–2240 (2008).
 20. Pratt, W.B., Toft, D.O.: Steroid Receptor Interactions with Heat Shock Protein and Immunophilin Chaperones¹. *Endocr. Rev.* 18, 306–360 (1997).
 21. van de Wijngaart, D.J., Dubbink, H.J., van Royen, M.E., Trapman, J., Jenster, G.: Androgen receptor coregulators: Recruitment via the coactivator binding groove. *Mol. Cell. Endocrinol.* 352, 57–69 (2012).

22. He, B., Kemppainen, J.A., Wilson, E.M.: FXXLF and WXXLF sequences mediate the NH₂-terminal interaction with the ligand binding domain of the androgen receptor. *J. Biol. Chem.* 275, 22986–94 (2000).
23. Zhou, Z.X., Sar, M., Simental, J.A., Lane, M. V, Wilson, E.M.: A ligand-dependent bipartite nuclear targeting signal in the human androgen receptor. Requirement for the DNA-binding domain and modulation by NH₂-terminal and carboxyl-terminal sequences. *J. Biol. Chem.* 269, 13115–23 (1994).
24. van Royen, M.E., van Cappellen, W. a, de Vos, C., Houtsmuller, A.B., Trapman, J.: Stepwise androgen receptor dimerization. *J. Cell Sci.* 125, 1970–9 (2012).
25. Khorasanizadeh, S., Rastinejad, F.: Nuclear-receptor interactions on DNA-response elements. *Trends Biochem. Sci.* 26, 384–90 (2001).
26. Luisi, B.F., Xu, W.X., Otwinowski, Z., Freedman, L.P., Yamamoto, K.R., Sigler, P.B.: Crystallographic analysis of the interaction of the glucocorticoid receptor with DNA. *Nature.* 352, 497–505 (1991).
27. Dehm, S.M., Tindall, D.J.: Alternatively spliced androgen receptor variants. 183–196 (2011).
28. Tan, M.H.E., Li, J., Xu, H.E., Melcher, K., Yong, E.: Androgen receptor: structure, role in prostate cancer and drug discovery. *Acta Pharmacol. Sin.* 36, 3–23 (2015).
29. Eder, I.E., Haag, P., Bartsch, G., Klocker, H.: Targeting the androgen receptor in hormone-refractory prostate cancer--new concepts. *Future Oncol.* 1, 93–101 (2005).
30. Xu, Y., Chen, S.-Y., Ross, K.N., Balk, S.P.: Androgens induce prostate cancer cell proliferation through mammalian target of rapamycin activation and post-transcriptional increases in cyclin D proteins. *Cancer Res.* 66, 7783–92 (2006).
31. Lorenzo, P.I., Saatcioglu, F.: Inhibition of apoptosis in prostate cancer cells by androgens is mediated through downregulation of c-Jun N-terminal kinase activation. *Neoplasia.* 10, 418–28 (2008).
32. Rubenstein, M., Hollowell, C.M.P., Guinan, P.: In LNCaP cells enhanced expression of the androgen receptor compensates for Bcl-2 suppression by antisense oligonucleotides. *Ther. Adv. Urol.* 3, 51–7 (2011).

33. Huggins, C., Hodges, C. V: Studies on Prostatic Cancer . I . The Effect of Castration , of Estrogen and of Androgen Injection on Serum Phosphatases in Metastatic Carcinoma of the Prostate Studies on Prostatic Cancer I . The Effect of Castration , of Estrogen and of Androgen Carcino. 293–297 (1941).
34. Attard, G., Cooper, C.S., de Bono, J.S.: Steroid hormone receptors in prostate cancer: a hard habit to break? *Cancer Cell*. 16, 458–62 (2009).
35. Gillis, J.L., Selth, L.A., Centenera, M.M., Townley, S.L., Sun, S., Plymate, S.R., Tilley, W.D., Butler, L.M.: Constitutively-active androgen receptor variants function independently of the HSP90 chaperone but do not confer resistance to HSP90 inhibitors ABSTRACT : 4, 691–704 (2013).
36. Sharifi, N., Dahut, W.L., Steinberg, S.M., Figg, W.D., Tarassoff, C., Arlen, P., Gulley, J.L.: A retrospective study of the time to clinical endpoints for advanced prostate cancer. *BJU Int*. 96, 985–9 (2005).
37. Saad, F.: Evidence for the efficacy of enzalutamide in postchemotherapy metastatic castrate-resistant prostate cancer. *Ther. Adv. Urol*. 5, 201–10 (2013).
38. Watson, P.A., Arora, V.K., Sawyers, C.L.: Emerging mechanisms of resistance to androgen receptor inhibitors in prostate cancer. *Nat. Rev. Cancer*. 15, (2015).
39. Cai, C., Balk, S.P.: Intratumoral androgen biosynthesis in prostate cancer pathogenesis and response to therapy. *Endocr. Relat. Cancer*. 18, R175–82 (2011).
40. Harris, W.P., Mostaghel, E.A., Nelson, P.S., Montgomery, B.: Androgen deprivation therapy: progress in understanding mechanisms of resistance and optimizing androgen depletion. *Nat. Clin. Pract. Urol*. 6, 76–85 (2009).
41. Attar, R.M., Takimoto, C.H., Gottardis, M.M.: Castration-Resistant Prostate Cancer: Locking Up the Molecular Escape Routes. *Clin. Cancer Res*. 15, 3251–3255 (2009).
42. Locke, J.A., Guns, E.S., Lubik, A.A., Adomat, H.H., Hendy, S.C., Wood, C.A., Ettinger, S.L., Gleave, M.E., Nelson, C.C.: Androgen Levels Increase by Intratumoral De novo Steroidogenesis during Progression of Castration-Resistant Prostate Cancer. *Cancer Res*. 68, 6407–6415 (2008).
43. Chen, C.D., Welsbie, D.S., Tran, C., Baek, S.H., Chen, R., Vessella, R., Rosenfeld,

- M.G., Sawyers, C.L.: Molecular determinants of resistance to antiandrogen therapy. *Nat. Med.* 10, 33–39 (2004).
44. Buchanan, G., Irvine, R.A., Coetzee, G.A., Tilley, W.D.: Contribution of the androgen receptor to prostate cancer predisposition and progression. *Cancer Metastasis Rev.* 20, 207–23 (2001).
 45. Gottlieb, B., Beitel, L.K., Nadarajah, A., Paliouras, M., Trifiro, M.: The androgen receptor gene mutations database: 2012 update. *Hum. Mutat.* 33, 887–94 (2012).
 46. Veldscholte, J., Ris-Stalpers, C., Kuiper, G.G.J.M., Jenster, G., Berrevoets, C., Claassen, E., van Rooij, H.C.J., Trapman, J., Brinkmann, A.O., Mulder, E.: A mutation in the ligand binding domain of the androgen receptor of human INCaP cells affects steroid binding characteristics and response to anti-androgens. *Biochem. Biophys. Res. Commun.* 173, 534–540 (1990).
 47. Culig, Z., Stober, J., Gast, A., Peterziel, H., Hobisch, A., Radmayr, C., Hittmair, A., Bartsch, G., Cato, A.C., Klocker, H.: Activation of two mutant androgen receptors from human prostatic carcinoma by adrenal androgens and metabolic derivatives of testosterone. *Cancer Detect. Prev.* 20, 68–75 (1996).
 48. Taplin, M.-E., Rajeshkumar, B., Halabi, S., Werner, C.P., Woda, B.A., Picus, J., Stadler, W., Hayes, D.F., Kantoff, P.W., Vogelzang, N.J., Small, E.J.: Androgen Receptor Mutations in Androgen-Independent Prostate Cancer: Cancer and Leukemia Group B Study 9663. *J. Clin. Oncol.* 21, 2673–2678 (2003).
 49. Hara, T., Miyazaki, J., Araki, H., Yamaoka, M., Kanzaki, N., Kusaka, M., Miyamoto, M.: Novel mutations of androgen receptor: a possible mechanism of bicalutamide withdrawal syndrome. *Cancer Res.* 63, 149–53 (2003).
 50. Balbas, M.D., Evans, M.J., Hosfield, D.J., Wongvipat, J., Arora, V.K., Watson, P.A., Chen, Y., Greene, G.L., Shen, Y., Sawyers, C.L.: Overcoming mutation-based resistance to antiandrogens with rational drug design. *Elife.* 2, e00499 (2013).
 51. Korpai, M., Korn, J.M., Gao, X., Rakiec, D.P., Ruddy, D.A., Doshi, S., Yuan, J., Kovats, S.G., Kim, S., Cooke, V.G., Monahan, J.E., Stegmeier, F., Roberts, T.M., Sellers, W.R., Zhou, W., Zhu, P.: An F876L Mutation in Androgen Receptor Confers Genetic and Phenotypic Resistance to MDV3100 (Enzalutamide). *Cancer Discov.* 3,

- 1030–1043 (2013).
52. Terakawa, T., Miyake, H., Kumano, M., Sakai, I., Fujisawa, M.: The antiandrogen bicalutamide activates the androgen receptor (AR) with a mutation in codon 741 through the mitogen activated protein kinase (MARK) pathway in human prostate cancer PC3 cells. *Oncol. Rep.* 24, 1395–9 (2010).
 53. Wu, J.D., Haugk, K., Woodke, L., Nelson, P., Coleman, I., Plymate, S.R.: Interaction of IGF signaling and the androgen receptor in prostate cancer progression. *J. Cell. Biochem.* 99, 392–401 (2006).
 54. Aaronson, D.S., Muller, M., Neves, S.R., Chung, W.-C., Jayaram, G., Iyengar, R., Ram, P.T.: An androgen-IL-6-Stat3 autocrine loop re-routes EGF signal in prostate cancer cells. *Mol. Cell. Endocrinol.* 270, 50–56 (2007).
 55. Bartlett, J.M., Brawley, D., Grigor, K., Munro, A.F., Dunne, B., Edwards, J.: Type I receptor tyrosine kinases are associated with hormone escape in prostate cancer. *J. Pathol.* 205, 522–529 (2005).
 56. Hernes, E., Fosså, S.D., Berner, A., Otnes, B., Nesland, J.M.: Expression of the epidermal growth factor receptor family in prostate carcinoma before and during androgen-independence. *Br. J. Cancer.* 90, 449–454 (2004).
 57. Krueckl, S.L., Sikes, R.A., Edlund, N.M., Bell, R.H., Hurtado-Coll, A., Fazli, L., Gleave, M.E., Cox, M.E.: Increased Insulin-Like Growth Factor I Receptor Expression and Signaling Are Components of Androgen-Independent Progression in a Lineage-Derived Prostate Cancer Progression Model. *Cancer Res.* 64, 8620–8629 (2004).
 58. McGuire, V. a, Gray, A., Monk, C.E., Santos, S.G., Lee, K., Aubareda, A., Crowe, J., Ronkina, N., Schwermann, J., Batty, I.H., Leslie, N.R., Dean, J.L.E., O’Keefe, S.J., Boothby, M., Gaestel, M., Arthur, J.S.C.: Cross talk between the Akt and p38 α pathways in macrophages downstream of Toll-like receptor signaling. *Mol. Cell. Biol.* 33, 4152–65 (2013).
 59. Schweizer, L., Rizzo, C.A., Spires, T.E., Platero, J.S., Wu, Q., Lin, T.-A., Gottardis, M.M., Attar, R.M., Koivisto, P., Linja, M., Chen, C., Grossmann, M., Huang, H., Tindall, D., Buchanan, G., Scher, H., Han, G., Suzuki, H., Taplin, M.-E., Culig, Z., Craft, N., Wen, Y., Chesire, D., Isaacs, W., Logan, C., Nusse, R., Reya, T., Clevers, H.,

- Yardy, G., Brewster, S., Truica, C., Byers, S., Gelmann, E., Yang, F., Chesire, D., Isaacs, W., Pawlowski, J., Chesire, D., Isaacs, W., Song, L., Terry, S., Schweizer, L., Varmus, H., Cong, F., Tepper, C., Veldscholte, J., Wilding, G., Chen, M., Gelmann, E., Fenton, M., Tan, J., Hara, T., Esquenet, M., Taille, A. de la, Chen, G., Tetsu, O., McCormick, F., He, T., Amir, A., Wang, Q., Carroll, J., Brown, M., Ford, O., Scher, H., Sawyers, C., Zhu, H., Verras, M., Jarow, J., Kaku, H., Cronauer, M., Chang, C., McDonnell, D., Yang, X., Reya, T., Austin, T., Korinek, V., Pinto, A., Poleskaya, A., Seale, P., Rudnicki, M., Liu, B., Cunha, G., Bastacky, S., Shah, R., Shang, Y., Myers, M., Brown, M.: The androgen receptor can signal through Wnt/ β -Catenin in prostate cancer cells as an adaptation mechanism to castration levels of androgens. *BMC Cell Biol.* 9, 4 (2008).
60. Gregory, C.W., He, B., Johnson, R.T., Ford, O.H., Mohler, J.L., French, F.S., Wilson, E.M.: A mechanism for androgen receptor-mediated prostate cancer recurrence after androgen deprivation therapy. *Cancer Res.* 61, 4315–9 (2001).
61. Halkidou, K., Gnanapragasam, V.J., Mehta, P.B., Logan, I.R., Brady, M.E., Cook, S., Leung, H.Y., Neal, D.E., Robson, C.N.: Expression of Tip60, an androgen receptor coactivator, and its role in prostate cancer development. *Oncogene.* 22, 2466–2477 (2003).
62. Heemers, H. V., Tindall, D.J.: Androgen Receptor (AR) Coregulators: A Diversity of Functions Converging on and Regulating the AR Transcriptional Complex. *Endocr. Rev.* 28, 778–808 (2007).
63. Xu, K., Wu, Z.J., Groner, A.C., He, H.H., Cai, C., Lis, R.T., Wu, X., Stack, E.C., Loda, M., Liu, T., Xu, H., Cato, L., Thornton, J.E., Gregory, R.I., Morrissey, C., Vessella, R.L., Montironi, R., Magi-Galluzzi, C., Kantoff, P.W., Balk, S.P., Liu, X.S., Brown, M.: EZH2 oncogenic activity in castration-resistant prostate cancer cells is Polycomb-independent. *Science.* 338, 1465–9 (2012).
64. Hu, R., Dunn, T.A., Wei, S., Isharwal, S., Veltri, R.W., Humphreys, E., Han, M., Partin, A.W., Vessella, R.L., Isaacs, W.B., Bova, G.S., Luo, J.: Ligand-independent androgen receptor variants derived from splicing of cryptic exons signify hormone-refractory prostate cancer. *Cancer Res.* 69, 16–22 (2009).
65. Wilson, C.M., McPhaul, M.J.: A and B forms of the androgen receptor are present in

- human genital skin fibroblasts. *Proc. Natl. Acad. Sci. U. S. A.* 91, 1234–8 (1994).
66. Tepper, C.G., Boucher, D.L., Ryan, P.E., Ma, A.-H., Xia, L., Lee, L.-F., Pretlow, T.G., Kung, H.-J.: Characterization of a novel androgen receptor mutation in a relapsed CWR22 prostate cancer xenograft and cell line. *Cancer Res.* 62, 6606–14 (2002).
 67. Libertini, S.J., Tepper, C.G., Rodriguez, V., Asmuth, D.M., Kung, H.-J., Mudryj, M.: Evidence for Calpain-Mediated Androgen Receptor Cleavage as a Mechanism for Androgen Independence. *Cancer Res.* 67, 9001–9005 (2007).
 68. Guo, Z., Qiu, Y.: A new trick of an old molecule: androgen receptor splice variants taking the stage?! *Int. J. Biol. Sci.* 7, 815–22 (2011).
 69. Dehm, S.M., Tindall, D.J.: Alternatively spliced androgen receptor variants. *Endocr. Relat. Cancer.* 18, R183–96 (2011).
 70. Dehm, S.M., Schmidt, L.J., Heemers, H. V, Vessella, R.L., Tindall, D.J.: Splicing of a novel androgen receptor exon generates a constitutively active androgen receptor that mediates prostate cancer therapy resistance. *Cancer Res.* 68, 5469–77 (2008).
 71. Guo, Z., Yang, X., Sun, F., Jiang, R., Linn, D.E., Chen, H., Chen, H., Kong, X., Melamed, J., Tepper, C.G., Kung, H.-J., Brodie, A.M.H., Edwards, J., Qiu, Y.: A novel androgen receptor splice variant is up-regulated during prostate cancer progression and promotes androgen depletion-resistant growth. *Cancer Res.* 69, 2305–13 (2009).
 72. Hu, R., Dunn, T. a, Wei, S., Isharwal, S., Veltri, R.W., Humphreys, E., Han, M., Partin, A.W., Vessella, R.L., Isaacs, W.B., Bova, G.S., Luo, J.: Ligand-independent androgen receptor variants derived from splicing of cryptic exons signify hormone-refractory prostate cancer. *Cancer Res.* 69, 16–22 (2009).
 73. Lu, J., der Steen, T. Van, Tindall, D.J.: Are androgen receptor variants a substitute for the full-length receptor? *Nat. Rev. Urol.* 12, 137–144 (2015).
 74. Sun, S., Sprenger, C.C.T., Vessella, R.L., Haugk, K., Soriano, K., Mostaghel, E.A., Page, S.T., Coleman, I.M., Nguyen, H.M., Sun, H., Nelson, P.S., Plymate, S.R.: Castration resistance in human prostate cancer is conferred by a frequently occurring androgen receptor splice variant. *J. Clin. Invest.* 120, 2715–2730 (2010).
 75. Hu, D.G., Hickey, T.E., Irvine, C., Wijayakumara, D.D., Lu, L., Tilley, W.D., Selth,

- L.A., Mackenzie, P.I.: Identification of androgen receptor splice variant transcripts in breast cancer cell lines and human tissues. *Horm. Cancer*. 5, 61–71 (2014).
76. Qu, Y., Dai, B., Ye, D., Kong, Y., Chang, K., Jia, Z., Yang, X., Zhang, H., Zhu, Y., Shi, G.: Constitutively active AR-V7 plays an essential role in the development and progression of castration-resistant prostate cancer. *Sci. Rep.* 5, 7654 (2015).
77. Mediwala, S.N., Sun, H., Szafran, A.T., Hartig, S.M., Sonpavde, G., Hayes, T.G., Thiagarajan, P., Mancini, M. a, Marcelli, M.: The activity of the androgen receptor variant AR-V7 is regulated by FOXO1 in a PTEN-PI3K-AKT-dependent way. *Prostate*. 73, 267–77 (2013).
78. Hörnberg, E., Ylitalo, E.B., Crnalic, S., Antti, H., Stattin, P., Widmark, A., Bergh, A., Wikström, P.: Expression of androgen receptor splice variants in prostate cancer bone metastases is associated with castration-resistance and short survival. *PLoS One*. 6, e19059 (2011).
79. Yu, Z., Chen, S., Sowalsky, A.G., Voznesensky, O.S., Mostaghel, E.A., Nelson, P.S., Cai, C., Balk, S.P.: Rapid induction of androgen receptor splice variants by androgen deprivation in prostate cancer. *Clin. Cancer Res.* 20, 1590–600 (2014).
80. Li, Y., Chan, S.C., Brand, L.J., Hwang, T.H., Silverstein, K.A.T., Dehm, S.M.: Androgen receptor splice variants mediate enzalutamide resistance in castration-resistant prostate cancer cell lines. *Cancer Res.* 73, 483–9 (2013).
81. Watson, P.A., Chen, Y.F., Balbas, M.D., Wongvipat, J., Socci, N.D., Viale, A., Kim, K., Sawyers, C.L.: Constitutively active androgen receptor splice variants expressed in castration-resistant prostate cancer require full-length androgen receptor. *Proc. Natl. Acad. Sci.* 107, 16759–16765 (2010).
82. Cottard, F., Asmane, I., Erdmann, E., Bergerat, J.-P., Kurtz, J.-E., Céraline, J.: Constitutively active androgen receptor variants upregulate expression of mesenchymal markers in prostate cancer cells. *PLoS One*. 8, e63466 (2013).
83. Sun, F., Chen, H. -g., Li, W., Yang, X., Wang, X., Jiang, R., Guo, Z., Chen, H., Huang, J., Borowsky, A.D., Qiu, Y.: Androgen Receptor Splice Variant AR3 Promotes Prostate Cancer via Modulating Expression of Autocrine/Paracrine Factors. *J. Biol. Chem.* 289, 1529–1539 (2014).

84. Guo, Z.: A New Trick of an Old Molecule: Androgen Receptor Splice Variants Taking the Stage?! *Int. J. Biol. Sci.* 815–822 (2011).
85. Kim, J.J., Yin, B., Christudass, C.S., Terada, N., Rajagopalan, K., Fabry, B., Lee, D.Y., Shiraishi, T., Getzenberg, R.H., Veltri, R.W., An, S.S., Mooney, S.M.: Acquisition of paclitaxel resistance is associated with a more aggressive and invasive phenotype in prostate cancer. *J. Cell. Biochem.* 114, 1286–93 (2013).
86. Hayflick, L., Moorhead, P.S.: The serial cultivation of human diploid cell strains. *Exp. Cell Res.* 25, 585–621 (1961).
87. Campisi, J., d’Adda di Fagagna, F.: Cellular senescence: when bad things happen to good cells. *Nat. Rev. Mol. Cell Biol.* 8, 729–740 (2007).
88. Salama, R., Sadaie, M., Hoare, M., Narita, M.: Cellular senescence and its effector programs Cellular senescence and its effector programs. 99–114 (2014).
89. Collado, M., Serrano, M.: The power and the promise of oncogene-induced senescence markers. *Nat. Rev. Cancer.* 6, 472–6 (2006).
90. Hayflick, L.: The limited in vitro lifetime of human diploid cell strains. *Exp. Cell Res.* 37, 614–636 (1965).
91. Kuilman, T., Michaloglou, C., Mooi, W.J., Peeper, D.S.: The essence of senescence. *Genes Dev.* 24, 2463–79 (2010).
92. Gerdes, J., Dallenbach, F., Lennert, K., Lemke, H., Stein, H.: Growth fractions in malignant non-Hodgkin’s lymphomas (NHL) as determined *in situ* with the monoclonal antibody Ki-67. *Hematol. Oncol.* 2, 365–371 (1984).
93. Di Leonardo, A., Linke, S.P., Clarkin, K., Wahl, G.M.: DNA damage triggers a prolonged p53-dependent G1 arrest and long-term induction of Cip1 in normal human fibroblasts. *Genes Dev.* 8, 2540–51 (1994).
94. Di Micco, R., Sulli, G., Dobрева, M., Liontos, M., Botrugno, O.A., Gargiulo, G., dal Zuffo, R., Matti, V., d’Ario, G., Montani, E., Mercurio, C., Hahn, W.C., Gorgoulis, V., Minucci, S., d’Adda di Fagagna, F.: Interplay between oncogene-induced DNA damage response and heterochromatin in senescence and cancer. *Nat. Cell Biol.* 13, 292–302 (2011).

95. Narita, M., Nunez, S., Heard, E., Narita, M., Lin, A.W., Hearn, S.A., Spector, D.L., Hannon, G.J., Lowe, S.W.: Rb-mediated heterochromatin formation and silencing of E2F target genes during cellular senescence. *Cell*. 113, 703–16 (2003).
96. Kuilman, T., Peeper, D.S.: Senescence-messaging secretome: SMS-ing cellular stress. *Nat. Rev. Cancer*. 9, 81–94 (2009).
97. Pernicová, Z., Slabáková, E., Kharraishvili, G., Bouchal, J., Král, M., Kunická, Z., Machala, M., Kozubík, A., Souček, K.: Androgen depletion induces senescence in prostate cancer cells through down-regulation of Skp2. *Neoplasia*. 13, 526–536 (2011).
98. Acosta, J.C., Banito, A., Wuestefeld, T., Georgilis, A., Janich, P., Morton, J.P., Athineos, D., Kang, T.-W., Lasitschka, F., Andrulis, M., Pascual, G., Morris, K.J., Khan, S., Jin, H., Dharmalingam, G., Snijders, A.P., Carroll, T., Capper, D., Pritchard, C., Inman, G.J., Longrich, T., Sansom, O.J., Benitah, S.A., Zender, L., Gil, J.: A complex secretory program orchestrated by the inflammasome controls paracrine senescence. *Nat. Cell Biol*. 15, 978–990 (2013).
99. Collado, M., Gil, J., Efeyan, A., Guerra, C., Schuhmacher, A.J., Barradas, M., Benguría, A., Zaballos, A., Flores, J.M., Barbacid, M., Beach, D., Serrano, M.: Tumour biology: Senescence in premalignant tumours. *Nature*. 436, 642–642 (2005).
100. Wei, W., Hemmer, R.M., Sedivy, J.M.: Role of p14(ARF) in replicative and induced senescence of human fibroblasts. *Mol. Cell. Biol*. 21, 6748–57 (2001).
101. Mitra, J., Dai, C.Y., Somasundaram, K., El-Deiry, W.S., Satyamoorthy, K., Herlyn, M., Enders, G.H.: Induction of p21 WAF1/CIP1 and Inhibition of Cdk2 Mediated by the Tumor Suppressor p16 INK4a. *Mol. Cell. Biol*. 19, 3916–3928 (1999).
102. Chicas, A., Wang, X., Zhang, C., McCurrach, M., Zhao, Z., Mert, O., Dickins, R.A., Narita, M., Zhang, M., Lowe, S.W.: Dissecting the unique role of the retinoblastoma tumor suppressor during cellular senescence. *Cancer Cell*. 17, 376–87 (2010).
103. Sherr, C.J., DePinho, R.A., Blasco, M., Lee, H.-W., Hande, M., Samper, E., Lansdorp, P., DePinho, R., Greider, C., Bodnar, A., Ouellette, M., Frolkis, M., Holt, S., Chiu, C., Morin, G., Harley, C., Shay, J., Lichsteiner, S., Wright, W., Carnero, A., Hudson, J., Price, C., Beach, D., Chin, L., Artandi, S., Shen, Q., Tam, A., Lee, S.-L., Gottlieb, G., Greider, C., DePinho, R., Greider, C., Blackburn, E., Hanahan,

- D., Weinberg, R., Hayflick, L., Moorhead, P., Kamijo, T., Zindy, F., Roussel, M., Quelle, D., Downing, J., Ashmun, R., Grosveld, G., Sherr, C., Karlseder, J., Broccoli, D., Dai, Y., Handy, S., Lange, T. de, Kiyono, T., Foster, S., Koop, J., McDougall, J., Galloway, D., Klingelutz, A., Loo, D., Fuquay, J., Rawson, C., Barnes, D., Pantoja, C., Serrano, M., Prowse, K., Greider, C., Rohme, D., Serrano, M., Lin, A., McCurrach, M., Beach, D., Lowe, S., Todaro, G., Green, H., Westphal, C., Rowan, S., Schmaltz, C., Elson, A., Fisher, D., Leder, P., Wright, W., Shay, J., Zindy, F., Eischen, C., Randle, D., Kamijo, T., Cleveland, J., Sherr, C., Roussel, M., Zhang, S., Ramsay, E., Mock, B.: Cellular Senescence. *Cell*. 102, 407–410 (2000).
104. Passos, J.F., Simillion, C., Hallinan, J., Wipat, A., von Zglinicki, T.: Cellular senescence: unravelling complexity. *Age (Dordr)*. 31, 353–63 (2009).
105. Debacq-Chainiaux, F., Boilan, E., Dedessus Le Moutier, J., Weemaels, G., Toussaint, O.: p38(MAPK) in the senescence of human and murine fibroblasts. *Adv. Exp. Med. Biol.* 694, 126–37 (2010).
106. Macip, S., Igarashi, M., Fang, L., Chen, A., Pan, Z.-Q., Lee, S.W., Aaronson, S.A.: Inhibition of p21-mediated ROS accumulation can rescue p21-induced senescence. *EMBO J.* 21, 2180–8 (2002).
107. Gorgoulis, V.G., Halazonetis, T.D.: Oncogene-induced senescence: the bright and dark side of the response. *Curr. Opin. Cell Biol.* 22, 816–27 (2010).
108. Serrano, M., Lin, A.W., McCurrach, M.E., Beach, D., Lowe, S.W.: Oncogenic ras Provokes Premature Cell Senescence Associated with Accumulation of p53 and p16INK4a. *Cell*. 88, 593–602 (1997).
109. Grandori, C., Wu, K.-J., Fernandez, P., Ngouenet, C., Grim, J., Clurman, B.E., Moser, M.J., Oshima, J., Russell, D.W., Swisshelm, K., Frank, S., Amati, B., Dalla-Favera, R., Monnat, R.J.: Werner syndrome protein limits MYC-induced cellular senescence. *Genes Dev.* 17, 1569–1574 (2003).
110. Katakura, Y., Nakata, E., Miura, T., Shirahata, S.: Transforming Growth Factor β Triggers Two Independent-Senescence Programs in Cancer Cells. *Biochem. Biophys. Res. Commun.* 255, 110–115 (1999).
111. Nakayama, K.I., Nakayama, K.: Regulation of the cell cycle by SCF-type ubiquitin

- ligases. *Semin. Cell Dev. Biol.* 16, 323–33 (2005).
112. Wang, H., Sun, D., Ji, P., Mohler, J., Zhu, L.: An AR-Skp2 pathway for proliferation of androgen-dependent prostate-cancer cells. *J. Cell Sci.* 121, 2578–87 (2008).
113. Lu, L., Schulz, H., Wolf, D.A.: The F-box protein SKP2 mediates androgen control of p27 stability in LNCaP human prostate cancer cells. *BMC Cell Biol.* 3, 22 (2002).
114. Levine, A.J., Oren, M.: The first 30 years of p53: growing ever more complex. *Nat. Rev. Cancer.* 9, 749–58 (2009).
115. Herbig, U., Jobling, W.A., Chen, B.P.C., Chen, D.J., Sedivy, J.M.: Telomere shortening triggers senescence of human cells through a pathway involving ATM, p53, and p21(CIP1), but not p16(INK4a). *Mol. Cell.* 14, 501–13 (2004).
116. d’Adda di Fagagna, F., Reaper, P.M., Clay-Farrace, L., Fiegler, H., Carr, P., Von Zglinicki, T., Saretzki, G., Carter, N.P., Jackson, S.P.: A DNA damage checkpoint response in telomere-initiated senescence. *Nature.* 426, 194–8 (2003).
117. Alcorta, D.A., Xiong, Y., Phelps, D., Hannon, G., Beach, D., Barrett, J.C.: Involvement of the cyclin-dependent kinase inhibitor p16 (INK4a) in replicative senescence of normal human fibroblasts. *Proc. Natl. Acad. Sci. U. S. A.* 93, 13742–7 (1996).
118. Hara, E., Smith, R., Parry, D., Tahara, H., Stone, S., Peters, G.: Regulation of p16CDKN2 expression and its implications for cell immortalization and senescence. *Mol. Cell. Biol.* 16, 859–867 (1996).
119. Krishnamurthy, J., Torrice, C., Ramsey, M.R., Kovalev, G.I., Al-Regaiey, K., Su, L., Sharpless, N.E.: Ink4a/Arf expression is a biomarker of aging. *J. Clin. Invest.* 114, 1299–307 (2004).
120. Nielsen, G.P., Stemmer-Rachamimov, A.O., Shaw, J., Roy, J.E., Koh, J., Louis, D.N.: Immunohistochemical survey of p16INK4A expression in normal human adult and infant tissues. *Lab. Invest.* 79, 1137–43 (1999).
121. Brenner, A.J., Stampfer, M.R., Aldaz, C.M.: Increased p16 expression with first senescence arrest in human mammary epithelial cells and extended growth capacity with p16 inactivation. *Oncogene.* 17, 199–205 (1998).

122. Stein, G.H., Drullinger, L.F., Soulard, A., Dulić, V.: Differential Roles for Cyclin-Dependent Kinase Inhibitors p21 and p16 in the Mechanisms of Senescence and Differentiation in Human Fibroblasts. *Mol. Cell. Biol.* 19, 2109–2117 (1999).
123. Burton, D.G. a., Giribaldi, M.G., Munoz, A., Halvorsen, K., Patel, A., Jorda, M., Perez-Stable, C., Rai, P.: Androgen Deprivation-Induced Senescence Promotes Outgrowth of Androgen-Refractory Prostate Cancer Cells. *PLoS One.* 8, e68003 (2013).
124. Sadi, M. V, Walsh, P.C., Barrack, E.R.: Immunohistochemical study of androgen receptors in metastatic prostate cancer. Comparison of receptor content and response to hormonal therapy. *Cancer.* 67, 3057–64 (1991).
125. Ruizeveld de Winter, J.A., Janssen, P.J., Sleddens, H.M., Verleun-Mooijman, M.C., Trapman, J., Brinkmann, A.O., Santerse, A.B., Schröder, F.H., van der Kwast, T.H.: Androgen receptor status in localized and locally progressive hormone refractory human prostate cancer. *Am. J. Pathol.* 144, 735–46 (1994).
126. Chodak, G.W., Kranc, D.M., Puy, L.A., Takeda, H., Johnson, K., Chang, C.: Nuclear localization of androgen receptor in heterogeneous samples of normal, hyperplastic and neoplastic human prostate. *J. Urol.* 147, 798–803 (1992).
127. Mirochnik, Y., Veliceasa, D., Williams, L., Maxwell, K., Yemelyanov, A., Budunova, I., Volpert, O. V.: Androgen receptor drives cellular senescence. *PLoS One.* 7, 1–12 (2012).
128. Roediger, J., Hessenkemper, W., Bartsch, S., Manvelyan, M., Huettner, S.S., Liehr, T., Esmaeili, M., Foller, S., Petersen, I., Grimm, M., Baniahmad, A.: Supraphysiological androgen levels induce cellular senescence in human prostate cancer cells through the Src-Akt pathway. *Mol. Cancer.* 13, 1–15 (2014).
129. Taylor, R.G., Walker, D.C., McInnes, R.R.: *E. coli* host strains significantly affect the quality of small scale plasmid DNA preparations used for sequencing. *Nucleic Acids Res.* 21, 1677–8 (1993).
130. Vierbuchen, T., Ostermeier, A., Pang, Z.P., Kokubu, Y., Südhof, T.C., Wernig, M.: Direct conversion of fibroblasts to functional neurons by defined factors. *Nature.* 463, 1035–41 (2010).

131. Koushik, S. V, Chen, H., Thaler, C., Puhl, H.L., Vogel, S.S.: Cerulean, Venus, and VenusY67C FRET reference standards. *Biophys. J.* 91, L99–L101 (2006).
132. LAEMMLI, U.K.: Cleavage of Structural Proteins during the Assembly of the Head of Bacteriophage T4. *Nature.* 227, 680–685 (1970).
133. Onder, T.T., Kara, N., Cherry, A., Sinha, A.U., Zhu, N., Bernt, K.M., Cahan, P., Marcarci, B.O., Unternaehrer, J., Gupta, P.B., Lander, E.S., Armstrong, S.A., Daley, G.Q.: Chromatin-modifying enzymes as modulators of reprogramming. *Nature.* 483, 598–602 (2012).
134. Osowski, C.M., Urano, F.: Measuring ER stress and the unfolded protein response using mammalian tissue culture system. *Methods Enzymol.* 490, 71–92 (2011).
135. Jares-Erijman, E.A., Jovin, T.M.: Imaging molecular interactions in living cells by FRET microscopy. *Curr. Opin. Chem. Biol.* 10, 409–416 (2006).
136. Xia, Z., Liu, Y.: Reliable and global measurement of fluorescence resonance energy transfer using fluorescence microscopes. *Biophys. J.* 81, 2395–402 (2001).
137. Hoppe, A., Christensen, K., Swanson, J.A.: Fluorescence resonance energy transfer-based stoichiometry in living cells. *Biophys. J.* 83, 3652–64 (2002).
138. Berney, C., Danuser, G.: FRET or no FRET: a quantitative comparison. *Biophys. J.* 84, 3992–4010 (2003).
139. Eijlander, R.T., Kuipers, O.P.: Live-Cell Imaging Tool Optimization To Study Gene Expression Levels and Dynamics in Single Cells of *Bacillus cereus*. *Appl. Environ. Microbiol.* 79, 5643–5651 (2013).
140. Moullan, N., Mouchiroud, L., Wang, X., Ryu, D., Williams, E.G., Mottis, A., Jovaisaite, V., Frochaux, M.V., Quiros, P.M., Deplancke, B., Houtkooper, R.H., Auwerx, J.: Tetracyclines Disturb Mitochondrial Function across Eukaryotic Models: A Call for Caution in Biomedical Research. *Cell Rep.* 10, 1681–1691 (2015).
141. Kuo, L.J., Yang, L.-X.: Gamma-H2AX - a novel biomarker for DNA double-strand breaks. *In Vivo.* 22, 305–9.
142. Sharma, A., Singh, K., Almasan, A.: Histone H2AX phosphorylation: a marker for

- DNA damage. *Methods Mol. Biol.* 920, 613–26 (2012).
143. Haffner, M.C., Aryee, M.J., Toubaji, A., Esopi, D.M., Albadine, R., Gurel, B., Isaacs, W.B., Bova, G.S., Liu, W., Xu, J., Meeker, A.K., Netto, G., De Marzo, A.M., Nelson, W.G., Yegnasubramanian, S.: Androgen-induced TOP2B-mediated double-strand breaks and prostate cancer gene rearrangements. *Nat. Genet.* 42, 668–675 (2010).
144. Perkel, V.S., Mohan, S., Herring, S.J., Baylink, D.J., Linkhart, T.A.: Human Prostatic Cancer Cells, PC3, Elaborate Mitogenic Activity Which Selectively Stimulates Human Bone Cells1. *CANCER Res.* 50, 6902–6907 (1990).
145. Bello, D., Webber, M.M., Kleinman, H.K., Wartinger, D.D., Rhim, J.S.: Androgen responsive adult human prostatic epithelial cell lines immortalized by human papillomavirus 18. *Carcinogenesis.* 18, 1215–23 (1997).
146. Izumi, K., Mizokami, A., Lin, W.-J., Lai, K.-P., Chang, C.: Androgen receptor roles in the development of benign prostate hyperplasia. *Am. J. Pathol.* 182, 1942–9 (2013).
147. Graff, J.R., Konicek, B.W., McNulty, A.M., Wangt, Z., Houck, K., Allen, S., Paul, J.D., Hbairu, A., Goode, R.G., Sandusky, G.E., Vessellat, R.L., Neubauer, B.L.: Increased AKT Activity Contributes to Prostate Cancer Progression by Dramatically Accelerating Prostate Tumor Growth and Diminishing p27 Kip1 Expression*. (2000).
148. Sramkoski, R.M., Pretlow, T.G., Giaconia, J.M., Pretlow, T.P., Schwartz, S., Sy, M.S., Marengo, S.R., Rhim, J.S., Zhang, D., Jacobberger, J.W.: A new human prostate carcinoma cell line, 22Rv1. *In Vitro Cell. Dev. Biol. Anim.* 35, 403–9.
149. Russell, P.J., Kingsley, E.A.: *Human Prostate Cancer Cell Lines.* 81,.
150. Dehm, S.M., Tindall, D.J.: Alternatively spliced androgen receptor variants. *Endocr. Relat. Cancer.* 18, R183–96 (2011).
151. Antonarakis, E.S., Lu, C., Wang, H., Luber, B., Nakazawa, M., Roeser, J.C., Chen, Y., Mohammad, T. a., Chen, Y., Fedor, H.L., Lotan, T.L., Zheng, Q., De Marzo, A.M., Isaacs, J.T., Isaacs, W.B., Nadal, R., Paller, C.J., Denmeade, S.R., Carducci, M. a., Eisenberger, M. a., Luo, J.: AR-V7 and Resistance to Enzalutamide and Abiraterone in Prostate Cancer. *N. Engl. J. Med.* 371, 1028–1038 (2014).
152. Kong, D., Sethi, S., Li, Y., Chen, W., Sakr, W.A., Heath, E., Sarkar, F.H.: Androgen

- receptor splice variants contribute to prostate cancer aggressiveness through induction of EMT and expression of stem cell marker genes. *Prostate*. (2014).
153. Thadani-mulero, M., Portella, L., Sun, S., Sung, M., Matov, A., Vessella, R.L., Corey, E., Nanus, D.M., Plymate, S.R., Giannakakou, P.: Androgen Receptor Splice Variants Determine Taxane Sensitivity in Prostate Cancer. *74*, 2270–2283 (2014).
 154. Emadi Baygi, M., Soheili, Z.S., Schmitz, I., Sameie, S., Schulz, W.A.: Snail regulates cell survival and inhibits cellular senescence in human metastatic prostate cancer cell lines. *Cell Biol. Toxicol.* *26*, 553–567 (2010).
 155. Nishio, K., Inoue, A.: Senescence-associated alterations of cytoskeleton: extraordinary production of vimentin that anchors cytoplasmic p53 in senescent human fibroblasts. *Histochem. Cell Biol.* *123*, 263–73 (2005).
 156. Schaufele, F., Carbonell, X., Guerbodot, M., Borngraeber, S., Chapman, M.S., Ma, A.A.K., Miner, J.N., Diamond, M.I.: The structural basis of androgen receptor activation: intramolecular and intermolecular amino-carboxy interactions. *Proc. Natl. Acad. Sci. U. S. A.* *102*, 9802–7 (2005).
 157. Massey, F.J.: The Kolmogorov-Smirnov Test for Goodness of Fit. *Source J. Am. Stat. Assoc.* *46*, 68–78 (1951).
 158. van Royen, M.E., van Cappellen, W. a., de Vos, C., Houtsmuller, a. B., Trapman, J.: Stepwise androgen receptor dimerization. *J. Cell Sci.* *125*, 1970–1979 (2012).
 159. Ibraheem, A., Campbell, R.E.: Designs and applications of fluorescent protein-based biosensors. *Curr. Opin. Chem. Biol.* *14*, 30–36 (2010).
 160. Campbell, R.E.: Fluorescent-Protein-Based Biosensors: Modulation of Energy Transfer as a Design Principle. *Anal. Chem.* *81*, 5972–5979 (2009).
 161. Zaccolo, M.: Use of chimeric fluorescent proteins and fluorescence resonance energy transfer to monitor cellular responses. *Circ. Res.* *94*, 866–73 (2004).
 162. Hochreiter, B., Garcia, A.P., Schmid, J.A.: Fluorescent proteins as genetically encoded FRET biosensors in life sciences. *Sensors (Basel)*. *15*, 26281–314 (2015).

VITA

Zeynep Kaya was born in Mardin, Turkey in 1990. She attended Mardin Anatolian High School between 2004 and 2008. In 2013 she received her Bachelor of Science degree in Molecular Biology and Genetics from Middle East Technical University in Ankara, Turkey. From 2013 to 2016, she attended Molecular Biology and Genetics Master of Science Program as Research and Teaching Assistant at Koç University.